

# Robotized Lander for an Analog Mission: Design and Optimization within Experiment Constraints and Objects Integration

Master's Thesis Nr. 0207

Scientific Thesis for Acquiring the Master of Science Degree  
at the School of Engineering and Design  
of the Technical University of Munich.

<b>Thesis Advisor</b>	Laboratory for Product Development and Lightweight Design Prof. Dr. Markus Zimmermann
<b>Supervisor</b>	Laboratory for Product Development and Lightweight Design Akhil Sathuluri Johannes Soika (Second corrector)
<b>Submitted by</b>	Pedro Henrique Pavelski Connollystraße 3 M32, 80809, Munich Matriculation number: 03749749 pedro.pavelski@tum.de
<b>Submitted on</b>	Garching, 01.08.2024



---

## Declaration

I assure that I have written this work autonomously and with the aid of no other than the sources and additives indicated.

Garching, 01.08.2024



---

Pedro Henrique Pavelski

---

# Project Note

Master's Thesis	Nr. 0207
Supervisor	Akhil Sathuluri
Partners in industry/research	Deutsches Zentrum für Luft- und Raumfahrt -
Institute of Robotics and Mechatronics	
Time period	01.02.2024 - 01.08.2024

The dissertation project of Akhil Sathuluri set the context for the work presented. My supervisor Akhil Sathuluri mentored me during the compilation of the work and gave continuous input. We exchanged and coordinated approaches and results biweekly.

An accurate elaboration, a comprehensible and complete documentation of all steps and applied methods, and a good collaboration with industrial partners are of particular importance.

## **Publication**

I consent to the laboratory and its staff members using content from my thesis for publications, project reports, lectures, seminars, dissertations and postdoctoral lecture qualifications.

The work remains a property of the Laboratory for Product Development and Lightweight Design.

Garching, 01.08.2024



---

Pedro Henrique Pavelski

---

Akhil Sathuluri

---

## Abstract

Surface Avatar ISS Technology Demonstrator is a set of experiments that studies the teleoperation of a robotic team to perform complex tasks. This robotic team is composed by the humanoid Rollin' Justin, Interact Rover, the four-legged Bert, and the robotic Lander, which is the main topic of this thesis. Based on an extensive literature research about real mission and analog missions, which includes Surface Avatar, and using product development methods, this thesis shows the development of a robotic lander, focusing on these functionalities: Sample Stowage Device and its Sample Tubes, the TINA robotic arm integration, the addition of a mechanized Hands-on Tray to provide workspace for object manipulation, and the Cargo Bay area, which might serve as a space for storage and possibly future expansions. This thesis further shows the integration of each of this functionalities into a framework, and provides insights about the impact of then in the robotic teleoperation, focusing in their manipulation challenges and impact of adding flexibility to the Lander operation.

---

# Contents

<b>1</b>	<b>Introduction</b> .....	<b>1</b>
1.1	Analog Missions .....	1
1.2	Surface Avatar .....	2
1.3	Thesis Objective .....	3
1.4	Scope and Limitations .....	4
1.5	Thesis Outline .....	4
<b>2</b>	<b>Literature</b> .....	<b>5</b>
2.1	Moon Exploration .....	5
2.1.1	Apollo Program .....	6
2.1.2	Chang’e Program.....	7
2.1.3	Chandrayaan Program .....	8
2.1.4	Japanese Missions.....	9
2.1.5	Artemis .....	9
2.2	Mars Exploration .....	11
2.2.1	Viking Program .....	11
2.2.2	Mars Pathfinder .....	11
2.2.3	Phoenix .....	12
2.2.4	Mars 2020.....	13
2.3	Analog Missions .....	14
2.3.1	METERON.....	14
2.3.2	ARCHES.....	18
2.3.3	LEAD .....	20
2.4	Implications .....	21
<b>3</b>	<b>Methods</b> .....	<b>23</b>
3.1	Needs Assessment and Requirements Identification.....	23
3.2	Conceptual Phase.....	23
3.3	Preliminary Design.....	24
3.4	Detailed Design .....	24
3.5	Implementation and Validation .....	25
<b>4</b>	<b>Surface Avatar Technology Demonstration Mission</b> .....	<b>26</b>
4.1	Robotic Team .....	26
4.1.1	Rollin’ Justin.....	26
4.1.2	Interact Rover.....	27

---

4.1.3	Bert.....	28
4.1.4	Lander.....	29
4.1.5	Mission Control.....	32
4.2	Interaction Between Lander and Other Robots.....	33
4.3	Protocols.....	34
4.3.1	Protocol 1 - Seismometer Handling.....	34
4.3.2	Protocol 2 - Sample Tube Return.....	35
4.3.3	Possible Protocols involving the Lander.....	36
<b>5</b>	<b>Lander.....</b>	<b>38</b>
5.1	Sample Tube.....	38
5.1.1	Requirements.....	38
5.1.2	Conceptual Phase.....	41
5.1.3	Preliminary Design.....	44
5.2	Sample Stowage Device.....	49
5.2.1	General Requirements.....	49
5.2.2	Storage Device Requirements.....	51
5.2.3	Receptacle and Delivery Devices Requirements.....	51
5.2.4	Conceptual Phase.....	53
5.2.5	Preliminary Design.....	58
5.3	TINA Integration.....	60
5.3.1	Optimization Problem.....	61
5.3.2	TINA Simplification.....	61
5.3.3	Particle Swarm Optimization.....	63
5.3.4	Particle Swarm Optimization Implementation.....	64
5.4	Hands-On Tray.....	66
5.4.1	Conceptual Phase.....	66
5.4.2	Preliminary Design.....	68
<b>6</b>	<b>Results.....</b>	<b>70</b>
6.1	Sample Tube.....	70
6.1.1	Cone and Tube.....	70
6.1.2	Cap Mechanism.....	72
6.2	Sample Stowage Device.....	75
6.2.1	Rotational Stowage Unit.....	75
6.2.2	Extended Reachability Mechanism.....	78
6.2.3	Functionalities.....	79
6.2.4	Integration with Lander.....	79
6.2.5	Validation.....	80
6.3	TINA Integration.....	83

---

6.4	Hands-on Tray .....	86
6.5	Cargo Bay .....	88
6.6	Final Lander Design .....	88
<b>7</b>	<b>Discussion .....</b>	<b>92</b>
<b>8</b>	<b>Conclusion .....</b>	<b>93</b>
	<b>Bibliography .....</b>	<b>94</b>
	<b>Appendix .....</b>	<b>103</b>
	<b>Appendix A Sample Tube .....</b>	<b>104</b>
	<b>Appendix B Rotational Stowage Device .....</b>	<b>106</b>
	<b>Appendix C Extended Reachability Mechanism .....</b>	<b>111</b>
	C.1 Case for the Rotational Stowage Device.....	111
	C.2 ERM frame .....	113
	<b>Appendix D Particle Swarm Optimization .....</b>	<b>115</b>
	D.1 Main File .....	115
	D.2 Objective Function .....	117
	D.3 Support Functions .....	119
	D.4 Plotting Results.....	126
	D.5 Plotting the Cost .....	127
	D.6 Discretization Impact.....	128
	<b>Appendix E Height and Force for Hands-on Tray .....</b>	<b>133</b>
	<b>Appendix F Hands-on Tray Components.....</b>	<b>135</b>
	F.1 Motor Specification .....	135
	F.2 Mounting points for the Motor.....	142
	F.3 Mounting points for the Tray .....	145



---

# 1 Introduction

Space exploration has fascinated humanity since ancient times, inspiring stories, myths, and theories about the mysteries beyond the Earth. As technological advancements accelerated in the 20th century, the dream of reaching space became increasingly feasible. The competition between global superpowers during the Cold War era further fueled the ambition to explore and conquer space, leading to landmark achievements such as sending instruments and humans into orbit and eventually landing on the moon. These historic milestones marked significant triumphs for the humanity and opened the door to a new era of space exploration.

In the present day, the pursuit of space exploration has intensified, with governments and private companies investing resources in projects to explore celestial bodies such as the Moon, Mars, and asteroids. However, going into space has numerous challenges that demand intensive research and technological innovation to overcome, due to harsh and inhospitable conditions, as extreme temperatures and radiation.

To meet the challenging requirements of space exploration, testing and validation are essential to ensure the reliability and functionality of space technologies. Yet, conducting tests in outer space is impractical due to the logistical and financial constraints associated with space travel. As a result, scientists and engineers turn to analog missions as a valuable tool for simulating space environment on Earth. Analog missions provide opportunities to validate space concepts and technologies in controlled environments, helping to advance the understanding and capabilities for future space exploration efforts.

## 1.1 Analog Missions

Analog space missions are simulations or field tests conducted on Earth to mimic conditions and challenges faced during actual space missions. These tests aim to replicate multiple aspects such as the environment of a planet, mimicking its geological properties, which is a good method to test instruments and equipments, or confinement and limited resources that astronauts might encounter in space, providing a great measure for workflow and workload. Analog missions are conducted in various settings, including remote locations, underwater habitats, and simulated environments.

The importance of analog space missions lies in their ability to provide valuable insights into the physiological, psychological, and technical challenges of space mission. By subjecting participants to conditions similar to those experienced in space, researchers can study human

behavior, performance, and adaptation, as well as test equipment, procedures, and technologies in a controlled environment.

### 1.2 Surface Avatar

The goal of exploring celestial bodies on a large scale requires significant advancement in supporting missions with robots that are capable of performing various tasks within a robotic team context. To tackle the challenges of developing robots that can work together to perform complex tasks, the German Aerospace Agency (DLR) and the European Space Agency (ESA) support the Surface Avatar project. This is an ISS Technology Demonstrator that aims to further develop telerobotic operations of heterogeneous robotic teams.

Surface Avatar comprises a series of experiments from the International Space Station (ISS) to Earth. In these experiments, an astronaut in the ISS teleoperates a scalable, heterogeneous robotic team on Earth. This team performs pre-determined protocols in an analog experimental environment. The robotic team includes four distinct robots, each with different levels of autonomy. These robots are: Rollin' Justin, a highly flexible humanoid robot; Interact Rover, a four-wheeled rover equipped with two robotic arms; a Lander, which replicates a real lander and is equipped with a space robotic arm; and Bert, a small quadrupedal scout robot designed for exploring confined spaces.

Surface Avatar demands an analog environment that can simulate the conditions of Mars to support the experiment. To meet this need, a new Multi-Site Analogue Environment (MUSA) is developed. MUSA is designed to replicate larger mission scenarios and assess the robotic team's ability to effectively explore and manage expansive areas both individually and collectively. The environment layout includes multiple sites for different purposes and accessibilities, such as a lander site, a science site, and a scout site. Barriers are incorporated to create physical and visual separations. A possible layout of MUSA is shown in the Figure 1.1.

The mission's experiments require seamless integration between the analog environment and the robotic team. This can present significant challenges to teleoperation commanding, while demonstrating the capabilities of a scalable autonomy and scalable heterogeneous robotic team. Consequently, it offers insights into optimally commanding robots in future space missions.

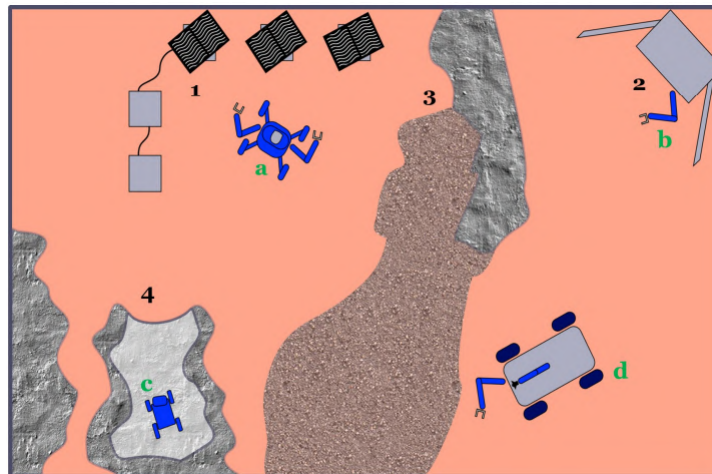


Figure 1.1: Layout of the Multi-Site Analog Environment (MUSA) includes a science site (1), a robotic lander (2), barriers (3) and scouting site (4). The robots Rollin' Justin (a), Lander with robotic arm (b), Bert (c), and Interact Rover (d), are shown. (N. Y.-S. Lii et al. 2022)

### 1.3 Thesis Objective

In order to enhance the robotic team and add value to the MUSA, a lander should be developed to perform various tasks. This lander should be designed to deliver components for surface deployment and to store sample containers for return to Earth or internal analysis. Using DLR's TINA space robotic technology, the robotic arm must allow the lander to actively participate in the transfer of these items, reducing the workload of the other robotic team members. This characteristics should provide to the Lander enough flexibility during operation.

Thus, the main objective of this thesis is to **design a ground demonstrator robotic Lander for the Surface Avatar ISS Technology Demonstration Mission**. To accomplish this need, other necessities appear. The first one is to *develop a Sample Tube that is capable to store material for robot handling*. The next one involves storing these Sample Tube, thus a *Sample Stowage Device should be designed to retrieve, store and deliver Sample Tubes*. To increase the Lander capabilities and flexibility, a *Cargo Bay must be designed in order to provide space for current and future tasks*. Finally, to enhance the equipment handling, a *Hands-on Tray must be design to provide a zone where the robots can manipulate objects*.

Given the importance of the Lander to the Surface Avatar objectives and the need to design a new one capable of performing multiple tasks, this thesis explores the process of developing a robotic mockup Lander, together with the equipment that might be required to run the experiments.

## 1.4 Scope and Limitations

Given the importance of the Lander to the Surface Avatar's objectives and the need to design a new one capable of performing multiple tasks, this thesis explores the process of developing a robotic mockup Lander, together with the equipment that might be required to run the experiments.

Initial limitations are set for the project, with physical constraints dictating the placement of the structure in the corner of the analog environment, positioned against a wall, resembling half of a typical lander. It must accommodate experimental equipment and potentially computers while. Furthermore, the overall shape has already been predetermined, imposing constraints on the design process.

Prototypes and final designs should be straightforward, not just because of time and cost constraints, but also due to the nature of an analog environment. It should resemble space conditions without being space-ready. The design should also prioritize off-the-shelf components and maintain a reasonable level of flexibility.

These factors will influence the layout and functionality of the structure, requiring careful consideration and planning to meet the specified requirements effectively.

## 1.5 Thesis Outline

This thesis starts with Chapter 2, which covers the findings in the literature regarding space missions, landers in these missions, and analog missions, providing an analysis that could aid lander development. Then, the methods are presented in Chapter 3, explaining the process used to develop the lander and its functionalities. Chapter 4 explains the Surface Avatar mission, detailing its specifics to derive the requirements for the lander development.

Next, Chapter 5 shows the development process for the lander functionalities, including the Sample Tube, Sample Stowage Device, TINA integration, Tray, and Cargo Bay. In Chapter ??, the results are presented, focusing on the detailed design of each component and its implementation and validation. Finally, the overall final design of the lander is shown.

In Chapter 7, the lander results and their impact on the Surface Avatar mission are discussed. Finally, Chapter 8 presents the conclusion of this thesis.

---

## 2 Literature

This chapter contains relevant literature results, which support the development of this thesis across various fields. It begins with a general overview of space missions that have landed on the Moon and Mars. These missions rely on landers to perform the landing procedures and to provide support for scientific experiments, bringing to the surface of these celestial bodies equipment capable of collecting valuable data. Since the focus of this thesis is developing an analog Lander for Surface Avatar, this chapter then focuses on each described mission's Lander and its functionalities, as well as the equipment used by these missions. Lastly, this chapter covers analog missions, which correspond to the type of mission that the Lander will perform during its operation. A general description and relevant information for the Lander's development are given.

### 2.1 Moon Exploration

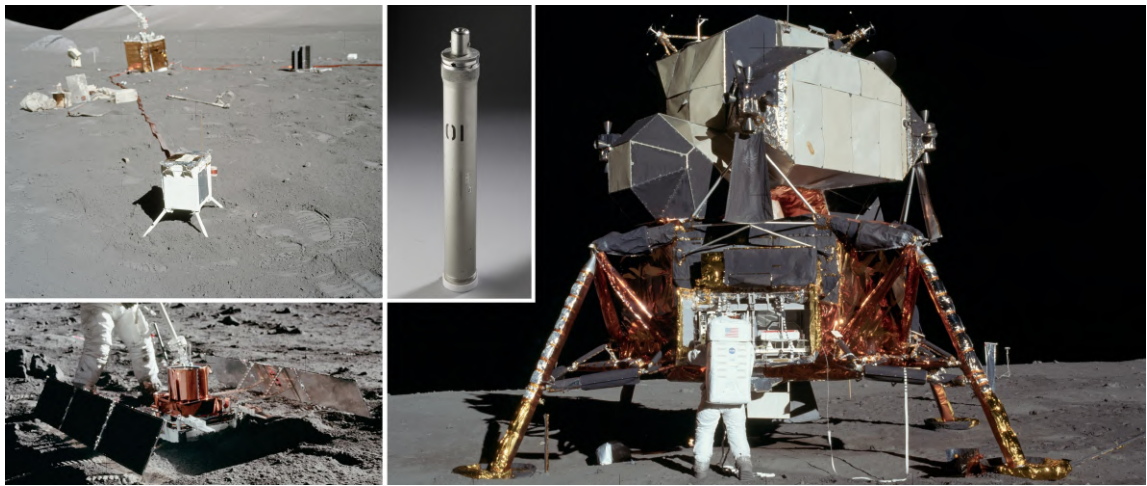
Moon exploration represents the pinnacle of human curiosity and scientific advancement. Over the decades, various nations have embarked on missions to unravel the Moon's mysteries, understand its composition, and investigate its potential for future human habitation. These missions have deepened the understanding of the Moon and furthered the boundaries of space exploration. They also serve as an inspiration for creating an analog Lander, providing information about the activities performed by equipment sent to the Moon, and what to expect from the future of exploration.

The Moon exploration started with Surveyor and Luna projects, undertaken by the United States and the Soviet Union, respectively, during the 1960s. The Surveyor program, led by NASA, involved a series of robotic spacecraft designed to soft-land on the lunar surface and gather crucial data for the Apollo missions. These spacecraft played a vital role in assessing potential landing sites and studying the Moon's soil and surface conditions. (Kloman 1972)

Conversely, the Luna focused on a series of robotic missions, including orbiters and landers, with the goal of achieving various lunar exploration milestones. Luna 2, for instance, became the first human-made object to reach the Moon in 1959, while Luna 9 achieved the first successful soft landing and transmitted images from the lunar surface in 1966. Both Surveyor and Luna projects laid the groundwork for subsequent human lunar exploration, contributing crucial insights and paving the way for future exploration. (Slyuta 2021)

### 2.1.1 Apollo Program

The next leap on the human history was the Apollo Program, which has the first mission to land a man on the Moon. Launched by NASA in 1961 and lasting until 1972, Apollo had the primary objective of landing humans on the Moon and safely returning them to Earth. The program consisted of a series of missions, with Apollo 11 making history on July 20, 1969, when astronauts Neil Armstrong and Buzz Aldrin became the first humans to set foot on the lunar surface. Over the course of six Apollo missions, a total of twelve astronauts explored the Moon, conducting experiments, collecting samples, and contributing significantly to our understanding of lunar geology. The Apollo program remains a testament to human ingenuity, determination, and the pursuit of scientific exploration on a grand scale. (Gisler and Sornette 2009)



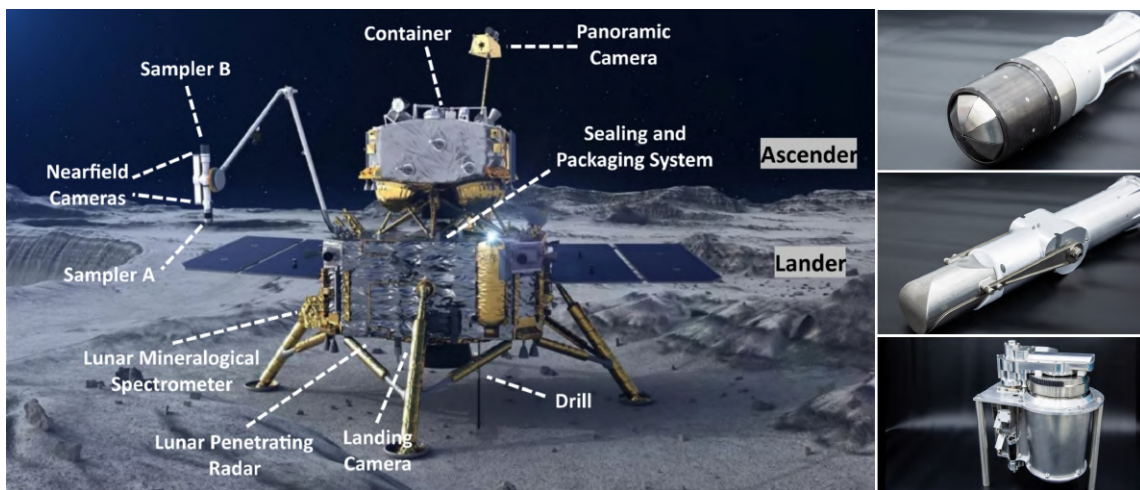
*Figure 2.1: The top-left image shows the equipment of the Lunar Ejecta and Meteorites Experiment (Jones 1995). The top-middle one shows the Sample Tube used in Apollo Missions (National Air and Space Museum 1975), while the bottom-left one shows the the Passive Seismic Experiment Package on the Moon (Jones and Glover 1995). Finally, the right image show Buzz Aldrin removing the passive seismometer from a compartment in the SEQ bay of the Lunar Lander while on the moon (Jones and Glover 1995).*

To achieve its mission goals, NASA designed an innovative Lunar Module (Figure 2.1). This two-stage spacecraft consisted of a descent and ascent stage. The descent stage housed the landing gear, radar, and scientific instruments. The four landing pads, each equipped with a crushable aluminum honeycomb structure, provided stability during lunar descent. The ascent stage was crucial for returning astronauts to lunar orbit. Certain aspects of the Lunar Module,

such as its external shape, leg positioning and structure, and the use of metal and space blankets for covering specific areas, could inspire the design of the Surface Avatar's Lander. Other equipment sent to the moon by the mission, like the scientific instruments and surface sample collection tools brought by Apollo 11 (illustrated in Figure 2.1), could inform the development of tools for the Surface Avatar's protocols. (Williamson 2006)

### 2.1.2 Chang'e Program

Chang'e 3 was a Chinese lunar exploration mission launched in December 2013. It marked China's first soft landing on the Moon and the first lunar landing since the Soviet Union's Luna 24 mission in 1976. The mission's primary objective was to deploy the Yutu rover, which, along with the lander, conducted various experiments, including analyzing lunar soil and investigating the lunar environment (Li et al. 2015). Five years later, Chang'e 4 was launched, marking the first successful landing on the Moon's far side. This mission provided valuable scientific data from this previously unexplored region. Like its predecessor, Chang'e 4 included a rover, Yutu-2, which conducted experiments and explored the lunar terrain. Additionally, Chang'e 4 featured a lander equipped with instruments to study the geology, environment, and cosmic radiation on the Moon's far side (Li et al. 2021).



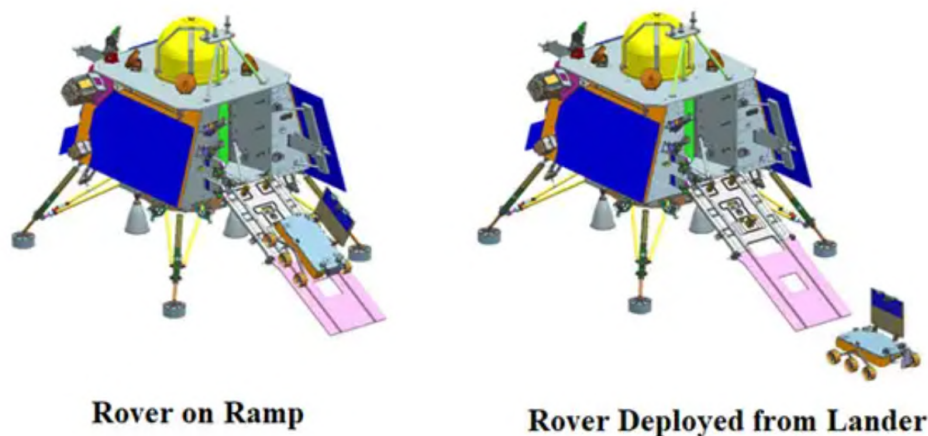
*Figure 2.2: An overview of the Chang'e-5 lander and equipment. The right images represent the tools used to collect sample from the lunar soil, with the bottom-right illustrating the device that stores the sample tubes. (Xiao et al. 2021)*

Launched in November 2020, Chang'e 5 was a significant lunar exploration mission with the aim of collecting lunar samples and returning them to Earth. It successfully landed on the moon,

collected samples, and returned them to Earth (Xiao et al. 2021). The mission utilized several spacecraft components, including a lander, an ascender, an orbiter, and a return capsule. The lander was a critical component as it was designed for the collection of lunar samples. It was responsible for landing safely on the lunar surface and deploying the equipment necessary for sample collection (Zhou et al. 2022). These equipments, such as the lander itself, the robotic arm, sample collectors, and several instruments can be seen in Figure 2.2.

### 2.1.3 Chandrayaan Program

The Chandrayaan program, supported by the Indian Space Research Organisation (ISRO), represents India's endeavor to explore the Moon through a series of missions. Chandrayaan-1, launched in 2008, marked India's first lunar probe and made notable discoveries, including the detection of water molecules and various minerals on the lunar surface. Despite losing communication in 2009, Chandrayaan-1 laid a solid foundation for subsequent missions (Goswami 2010). Chandrayaan-2, launched in 2019, aimed to explore the Moon's south pole with an orbiter, lander, and rover. Although the lander's touchdown was unsuccessful, the orbiter continues to gather valuable data from lunar orbit (Sundararajan 2018).



*Figure 2.3: 3D model of Vikram lander deploying the Prayan rover (ISRO 2024).*

In August 2023, India made a historic moon landing, becoming the fourth nation globally and the first to land on the moon's south pole with Chandrayaan-3 (Azmi et al. 2024). Following the landing, the rover Pragyan began in situ investigations, discovering various elements including sulfur, aluminum, and oxygen, while also searching for hydrogen. The lander and rover are can be visualized in Figure 2.3, whose 3D model represents the rover deployment. Simultaneously, the Vikram lander conducted experiments, such as seismography measurements and image



capture, and gathered knowledge for future missions, performing a 'hop' using its engines and moving a few centimeters (George 2024; Kanu et al. 2024).

### 2.1.4 Japanese Missions

With the Smart Lander for Investigating Moon (SLIM), Japan became the fifth country to land on the Moon. This event occurred in January 2024 and achieved its main goal of precise lunar surface landing. The landing accuracy was 100 metres, a significant improvement from the previous ranges of a few to dozens of kilometers. (Xin 2024)

JAXA and ISRO started to develop a program to investigate the presence of water on the Moon. Using the technology developed in the SLIM and Chandrayaan Programs, the missions consist of a Lander and a Rover co-operating to explore the Moon's surface. Scientific instruments and sample collectors are onboard to achieve the goal of finding water on the Moon. (Hoshino et al. 2020)

### 2.1.5 Artemis

This overview of Moon missions concludes with the most ambitious program for exploration and human presence on the Moon: Artemis. Led by NASA, Artemis aims to return humans to the lunar surface and establish sustainable operations. (Witze 2022) This will be accomplished in several steps divided in two phases. The Phase 1 of the Artemis program are named Artemis I, II, and III, begins with a series of robotic missions. It will then be followed uncrewed lunar flyby, crewed lunar flyby, and a lunar south pole landing with potential operations aboard the Gateway. Phase 2 aims to establish a sustainable human presence in cislunar space and on the lunar surface, utilizing SLS, Orion, and additional Gateway elements from commercial and international partners, while also conducting technology trials and scientific experiments to prepare for crewed missions to Mars in the 2030s. (Smith et al. 2020)

To perform all the demanded tasks, the Artemis Program involves many different parts working together, which are:

**Space Launch System (SLS):** The Artemis missions rely on the Space Launch System, NASA's next-generation heavy-lift launch vehicle, designed to transport astronauts and payloads beyond low Earth orbit. SLS serves as the primary means of launching crewed missions to the Moon and beyond. (Honeycutt et al. 2020)

**Orion Spacecraft:** The Orion spacecraft serves as the crew vehicle for Artemis missions, providing a safe and reliable means of transportation for astronauts to and from lunar orbit. Equipped with advanced life support systems, radiation shielding, and propulsion capabilities,

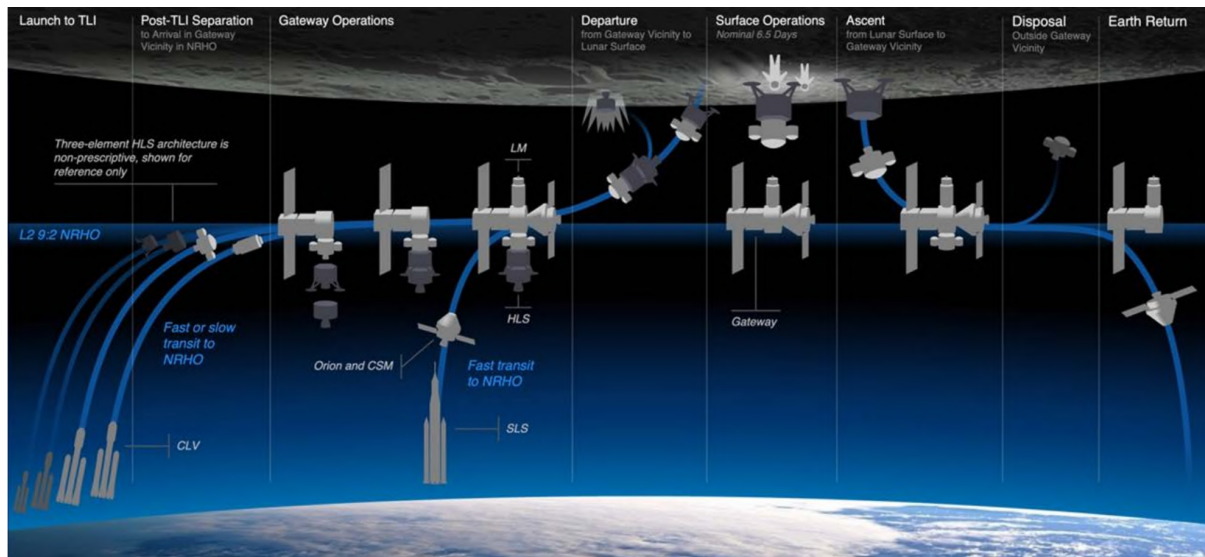


Figure 2.4: An overview of the Artemis program. (Chavers et al. 2020)

Orion ensures the safety and well-being of its occupants during extended missions. (Ehrenfried 2020)

**Lunar Gateway:** The Gateway, an international collaboration and an integral component of NASA’s Artemis program alongside the Space Launch System (SLS) rocket, Orion spacecraft, and human landing system, epitomizes a sophisticated space infrastructure designed to advance human exploration beyond Earth (Fuller et al. 2022). Positioned as a small-scale space station in lunar orbit, the Gateway will enable constant human exploration on the lunar surface while serving as a start point for deep space expeditions. Its strategic place works as a logistical facilitation for deep space transportation, sending lunar landers and spacecraft to destinations such as Mars (Lehnhardt and Connell 2023). Furthermore, the Gateway serves as a focal point for continual scientific inquiry and technological innovation, providing a platform for diverse research endeavors encompassing scientific experiments (Fuller et al. 2022).

**Human Landing System (HLS):** NASA’s Human Landing System (HLS) consists of descent, ascent, and transfer elements. It facilitates transfers between the Gateway and the lunar surface. Additionally, it provides a habitable environment for two crew members for up to eight days, regardless of pre-placed surface infrastructure (Smith et al. 2020), during which they will conduct extravehicular activities and science activities (Chavers et al. 2020). The HLS is also capable of performing automated uncrewed transfers between the Gateway and the lunar surface (Watson-Morgan et al. 2023).

All missions prior to Artemis focused on understanding the Moon's characteristics, which necessitated deploying numerous pieces of equipment to measure seismic and magnetic activities, solar winds, and to collect and retrieve soil samples for a better understanding of the Moon's composition. However, the goal of Artemis is to establish a consistent human presence on the Moon, which sets it apart from previous projects. This means that in addition to sending these scientific instruments, the lander modules need to carry other types of equipment to establish a base camp, providing the necessary conditions for human habitation on the Moon's surface. (Kessler et al. 2022)

## 2.2 Mars Exploration

### 2.2.1 Viking Program

To push further and explore beyond the Moon, NASA launched the Viking Program, which was the first spacecraft to successfully land on Mars in 1975, which featured two spacecraft, Viking 1 and Viking 2, each comprising an orbiter and a lander. The landers were designed to touch down on the Martian surface and conduct groundbreaking experiments in the search for signs of life. Equipped with a suite of instruments, the landers analyzed the Martian soil for organic compounds, measured atmospheric composition and pressure, and performed tests to detect signs of metabolic activity that could indicate the presence of living organisms. While the results did not yield conclusive evidence of life on Mars, the Viking landers provided invaluable data about the planet's geology, atmosphere, and potential habitability. (Soffen and Snyder 1976)

### 2.2.2 Mars Pathfinder

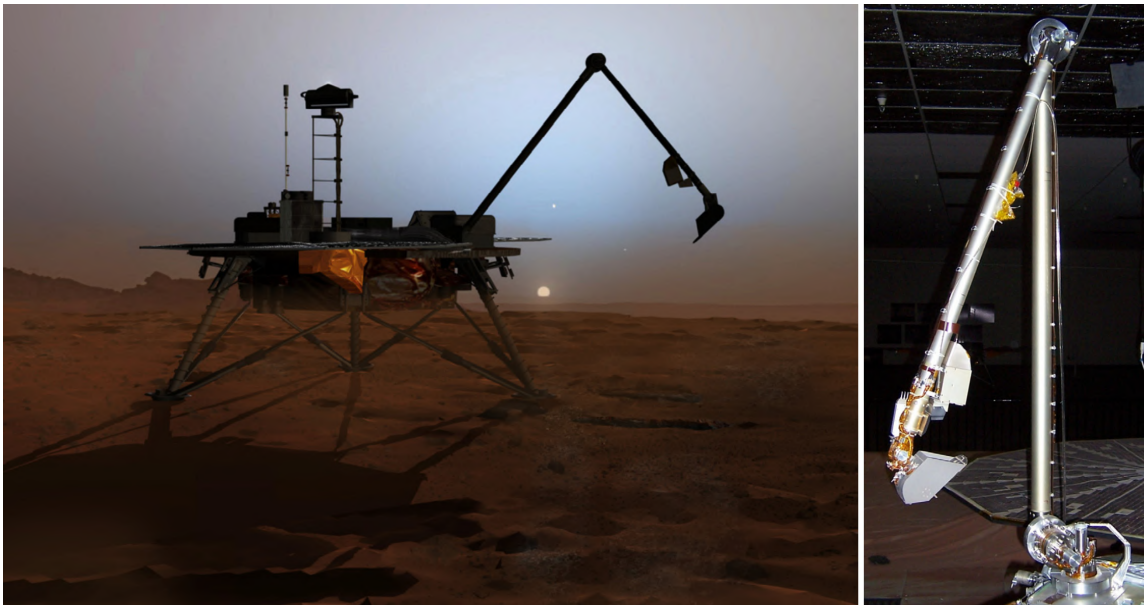
In late 90s, NASA landed again on the Red Planet with the Mars Pathfinder mission, which was the first one to deploy and operate a rover outside the Earth-Moon system. Named the "Carl Sagan Memorial Station" after the renowned astronomer, the mission's lander was equipped with a suite of scientific instruments designed to study Mars' geology, climate, and atmosphere. Its payload included cameras for imaging the Martian landscape, atmospheric sensors to measure weather conditions, and a meteorology package for studying the planet's environment. Additionally, the lander served as a base station for the deployment of the small rover Sojourner. (Golombek et al. 1999)

One of the most innovative aspects of the Mars Pathfinder mission was its landing technique. Utilizing a method known as the "airbag landing," the lander was encased in a tetrahedron-

shaped aeroshell during descent through the Martian atmosphere. Upon reaching the surface, the lander released a series of airbags that cushioned its landing, allowing it to safely touch down on the rugged Martian terrain. This successful landing demonstrated a novel approach to planetary exploration and paved the way for future missions, showcasing the feasibility of delivering scientific payloads to the surface of Mars efficiently and reliably. (Golombek et al. 1999)

### 2.2.3 Phoenix

The first decade of the XXI century is filled with many missions to space. One of them is the NASA's Phoenix mission, which sent to Mars a lander with a mounted robotic arm to collect samples from the planet's soil. Phoenix was a robotic spacecraft mission launched by NASA's Jet Propulsion Laboratory as part of the Mars Scout Program. (Shotwell 2005) Its primary objective was to study the history of water and potential habitability in the Martian arctic's icy soil (R. G. Bonitz et al. 2008). Equipped with a sophisticated suite of scientific instruments, including a robotic arm scoop, a thermal and evolved-gas analyzer, a wet chemistry laboratory, and a meteorological station, Phoenix made significant discoveries during its operational period of over five months. Overall, the Mars Phoenix lander represented a significant milestone in the exploration of Mars, contributing greatly to the understanding of the planet's past and its potential for hosting life. (Shotwell 2005)



*Figure 2.5: Phoenix Lander on the left, and the its arm on the right.(R. Bonitz et al. 2009)*

The Phoenix Robotic Arm, depicted in Figure 2.5, is a 4-degree-of-freedom manipulator with a back-hoe design. It features a forearm-mounted Robotic Arm Camera, along with a scoop and Thermal and Electrical Conductivity Probe on the wrist. The scoop is divided into two chambers. The front chamber collects material excavated by the front blade, while the rear chamber contains a rasp and a collection area for material scraped by the rasp. The scoop's front chamber is used for digging and collecting regolith, and includes a funnel to channel acquired material into a slot for improved sample delivery. (R. Bonitz et al. 2009)

### 2.2.4 Mars 2020

The Mars 2020 mission, part of NASA's ongoing exploration of Mars, is centered around the Perseverance rover, launched on July 30, 2020, and landed in Jezero Crater on Mars on February 18, 2021. The mission aims to investigate the habitability of Mars, search for signs of ancient life, collect samples for future return to Earth, and test new technologies for future human missions to Mars. (Boeder and Soares 2020) Perseverance carries advanced scientific instruments to study the geology and climate of Mars, including the capability to collect and store samples for a potential return to Earth by future missions. (Sánchez-Lavega et al. 2023). It also includes the Ingenuity helicopter, which demonstrates the feasibility of aerial exploration on Mars (Tzanetos et al. 2022).

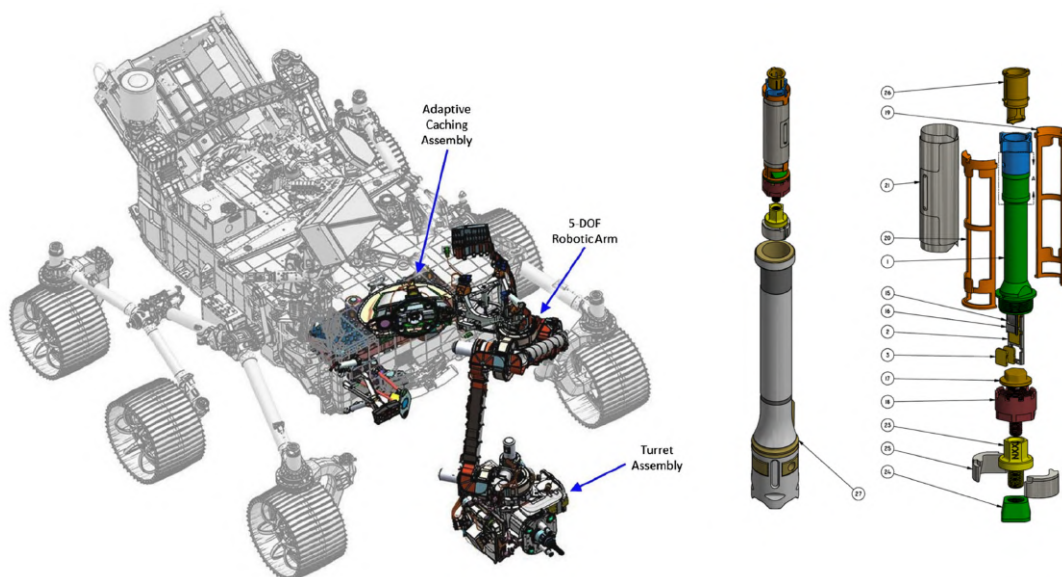


Figure 2.6: Perseverance rover on the left, highlighting its complex sample collection system, and the sample tubes used to sample the martian soil. (Moeller et al. 2020)

This mission, although not centered on a lander module, demonstrates the potential of a sample exploration task. It shows that the deployment of equipment extends beyond typical scientific tools by including the launch of a helicopter. Its sample collection and storage system (Figure 2.6) is designed to collect, seal, and cache 37 returnable samples while meeting the science-driven contamination control requirements (Moeller et al. 2020). Such a detailed description can provide inspiration for the development of Surface Avatar's equipment.

### 2.3 Analog Missions

Analog missions are multi-disciplinary exercises that test different aspects of future space missions. They provide insights into system interactions and operations. Often conducted in remote, harsh environments, these missions simulate certain features of potential spaceflight destinations. Researchers use these missions to evaluate robots, vehicle prototypes, habitats, communication systems, in-situ resource utilization, and human performance. Analog missions also validate architectural concepts, demonstrate new technologies, and address broader technical and operational challenges crucial for crewed missions beyond low Earth orbit. (Reagan et al. 2012)

Analog missions have a wide range of applications. CanMars (Osinski et al. 2019), for instance, simulated the retrieval of samples from the Martian surface and their subsequent return to Earth, in the context of Mars 2020 mission. Beyond the robotic experimentation, the analog missions can focus on human aspects, simulating the harsh conditions of space environments (NASA 2024). This thesis focuses specifically on the development of a lander in a multi-robot teleoperation environment. Thus, this section will concentrate on analog missions that involve robotic operations and activities similar to those of the Surface Avatar.

#### 2.3.1 METERON

The METERON (Multi-purpose End-To-End Robotic Operations Network) initiative, lead by ESA, aims to develop, evaluate, and demonstrate technologies for future human-robotic exploration missions. This project focuses on validating autonomous and real-time telerobotic operations from space to the ground, addressing critical questions regarding the technologies necessary for future space exploration endeavors. (Carey et al. 2012)

METERON's objectives span three primary areas: communications, operations, and robotics. Communication techniques are being tested and validated, considering disruptions, high latency, and the need for nearly real-time communications for video and haptic devices. Operations entail coordinating multiple assets, such as rovers or robots, from various operation centers, exploring

human-robot collaboration and different monitoring and control systems. The project also delves into robotics, experimenting with diverse robotic systems' concepts and functionalities, including advanced mechatronics, telepresence in space environments, human-robot interaction, and interoperability among groups of robots and control devices. (Cardone et al. 2016)

The METERON project focuses on a series of experiments in the three primary areas mentioned (Carey et al. 2022). This review will spotlight SUPVIS-JUSTIN, and ANALOG-1 experiments, which feature environments similar to the Surface Avatar objectives. This review will discuss their significance to METERON and the insights they can provide for future Lander development.

### **SUPVIS-JUSTIN**

The METERON SUPVIS-JUSTIN experiment is a collaborative effort between ESA and DLR and aimed at testing human-robot interaction in space. The experiment involves controlling Rollin' Justin remotely from the ground using the SUPVIS (Supervisory Control) interface, allowing operators to provide high-level commands and guidance to the robot for performing tasks typically carried out by astronauts aboard the ISS or similar space habitats. The primary objective of the SUPVIS-JUSTIN experiment is to evaluate the feasibility and effectiveness of using humanoid robots to support astronauts in space mission tasks such as maintenance, repairs, and scientific experiments, operators aim to determine the robot's capabilities and limitations in a space environment. Additionally, the experiment focuses on studying human-robot interaction dynamics, including communication, trust, and collaboration between astronauts and remotely operated robots. (Schmaus et al. 2018)

To run the experiments, METERON SUPVIS-JUSTIN uses the SOLar Farm EXperimental (Solex) analog environment , which serves as a realistic Martian solar farm simulation for testing and validating space robotics performance. Designed with Martian terrain and scenery, Solex provides an environment for robots to navigate and perform mechanical manipulation tasks on Solar Panel Units (SPUs) equipped with various switches and mechanisms. (N. Y. Lii et al. 2017)

### **SOLEX**

First utilized for the SUPVIS-JUSTIN, SOLEX was further developed with the aim of supporting the validation and verification of different modalities of future space robotic operations. The old METERON and the current configurations can be seen in Figure 2.7. The development of this analog environment follow three key aspects: modular design for expansion and rapid deployment, full functional interface concept and ground control for scenario management and system monitoring. (Bayer et al. 2019)

A mock-up planetary lander has been integrated into the SOLEX environment to enhance the plausibility of experiment scenarios and facilitate the delivery of infrastructure components. The lander serves as stowage for modules not yet installed on the assets within the environment. It can accommodate up to six Container Units (CUs) on a tray inside its cargo bay, with a satellite dish unit positioned above the CU-tray. Additionally, the lander can be expanded in the future to include more components, such as tools for maintenance or assembly tasks. (Bayer et al. 2019)



*Figure 2.7: The top-left image shows the METERON configuration of SOLEX, simulating a Martian environment, with the presence of Rollin' Justin and the SPUs. The bottom-left image shows the advanced SOLEX setup with the inclusion of the Lander in the right corner. The two images on the right show the SOLEX lander with its cargo bay storing the CUs and the satellite dish on the tray. (Bayer et al. 2019)*

The METERON SUPVIS-JUSTIN and SOLEX environments are crucial in the development of the Surface Avatar, as they serve as its precursor. The addition of a lander is also significant. The Surface Avatar Lander, seen as an advancement of the SOLEX's lander, can adopt some functionalities, such as acting as a cargo bay for stowing components, as a basis for its development.



## ANALOG-1

ANALOG-1 mission derives from the METERON experiments, focusing on technical implementation, UI development, autonomy, operational concepts, and scientist interaction. The mission is divided into two experiments. The first one involves performing sample return tasks with the INTERACT Rover (Figure 2.8) in an indoor analog lunar environment. Similarly to the Surface Avatar, this phase of ANALOG-1 demonstrated how an astronaut on the ISS performs when controlling robots on ground. (Krueger et al. 2020b)

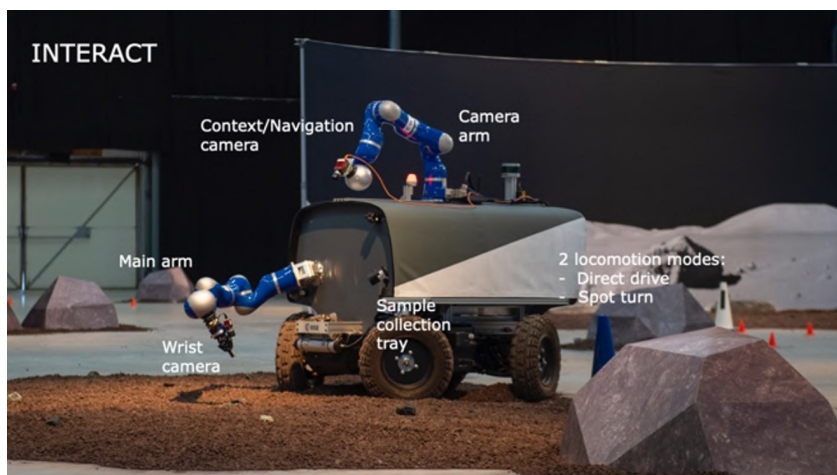


Figure 2.8: The INTERACT Rover. (Carey et al. 2022)

The results of the first ANALOG-1 experiment shows that environmental conditions, such as lighting and surface texture, posed challenges that required careful consideration and testing prior to actual missions. Camera resolution limitations affected rock and texture distinction during sample collection, impacting scientific decision-making. Greater autonomy for astronauts, combined with geology training and immersive telepresence, could have enhanced operational efficiency and scientific outcomes. Thus, this experiment gathered knowledge that can be useful when developing the MUSA, and specially the Lander for the Surface Avatar setup. (Wormnes et al. 2022)

The second ANALOG-1 experiment was conducted along with the ARCHES in the region of Mount Etna in Italy in a ground campaign aiming to complete remaining gaps in ground operations left by the first experiment. The collaboration between robotic assets, particularly the Interact rover and the Scout rover, demonstrated high reliability. AI-enabled automatic identification and collection of rock samples were successfully executed by both the crew member on the orbiter and a ground-based science support team member. Finally, having a

geologically trained astronaut significantly improved sample selection and collection efficiency, showcasing the importance of astronaut-science team interaction. (Carey et al. 2022)

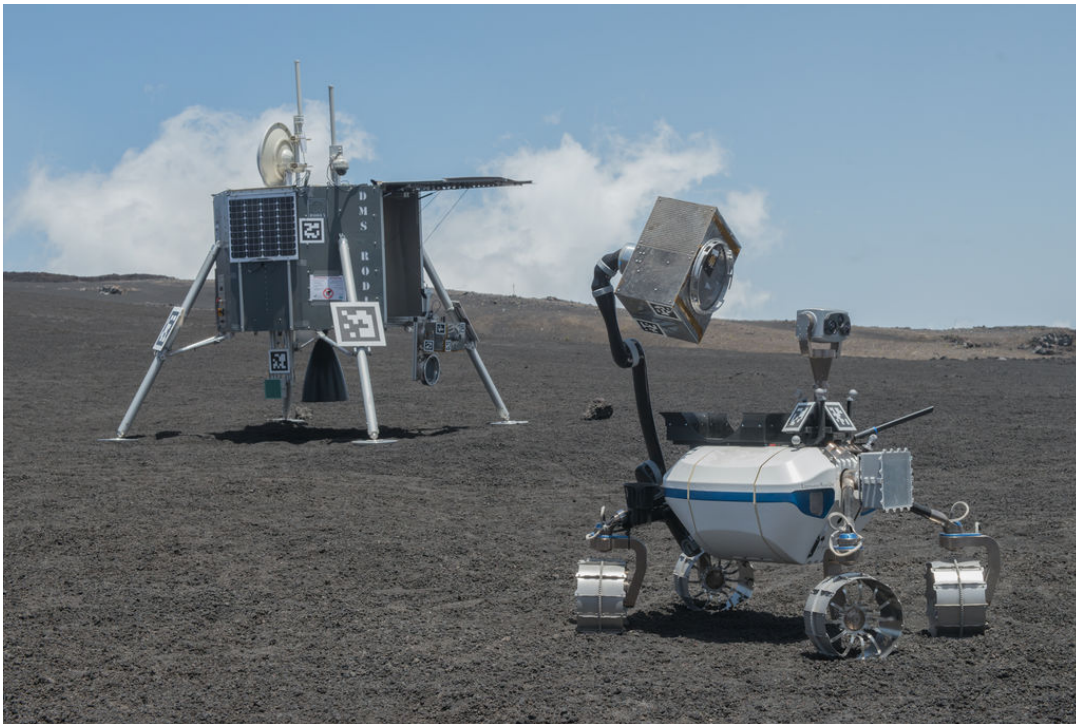
### 2.3.2 ARCHES

The ARCHES (Autonomous Robotic Networks to Help Modern Societies) project, led by the Helmholtz Association, focuses on developing heterogeneous, autonomous, and interconnected robotic systems for various applications. The project emphasizes cooperation within a diverse team of robots, including drones for scouting and rovers equipped with scientific instruments and manipulation capabilities. The experiment involved two mission scenarios: setting up a distributed radio telescope and geological exploration with sampling. (Schuster et al. 2020)

The experiment employs a diverse set of robots including ARDEA, a drone for rapid scouting, LRU1, the first planetary exploration rover for close-up inspections, and LRU2, a rover equipped with a manipulator arm for sample collection and payload manipulation. The stationary RODIN Lander serves as storage and base for scientific instruments. The experiment also included payload boxes in a standard configuration to equip various instruments. They are depicted in Figure 2.4. (Helmholtz 2018)

(Wedler et al. 2022) shows the results for all the experiments performed by ARCHES. The first one, referred to as Geo I, had both LRU1 and LRU2 rovers operating in semi-autonomy to reach, inspect, and collect targets of scientific relevance near the lander site. The first rover successfully navigated through difficult terrain to collect panoramic scans. The second one used its arm to retrieve a sample box from the Lander and navigated to the sampling sites. An analysis module was also retrieved from the Lander for analyzing the collected soil. The second experiment, known as Geo II, was basically the combination of efforts between ARCHES and ANALOG-1 explained previously.

The third mission, called LoFa, was planned to install an antenna and had several objectives. Firstly, it aimed to demonstrate the ability of a diverse team of robots to perform infrastructure installations for collecting scientifically relevant data for space exploration. Secondly, the mission sought to highlight the robots' capacity for independent and autonomous operation, with all mission-critical computations performed on their own computation stacks. Thirdly, the experiment aimed to prove the feasibility of a modular payload concept when constructing complex infrastructure at an analogue site. Additionally, the mission's goal was to validate a real-time decentralized radionavigation system for accurately localizing payload boxes, which are essential for array operations. Finally, it intended to serve as a proof-of-concept for array operations such as beamforming and signal direction of arrival estimation, enhancing capabilities vital for future space missions. (ibid.)



*Figure 2.9: RODIN Lander on the left, and LRU2 holding a payload box on the right. (Helmholtz 2018)*

The sequence of action included the rovers using the Lander to localize themselves, and collect from it boxes to perform the installation. Firstly, LRU2 took a power box from the Lander using its robotic arm and placed it in the installation site. In sequence, it returned to the Lander module to retrieve other components to continue with the installation. After the installation, both robots returned to the Lander to complete the task. During the mission, the team accomplished all goals: LRU2 installed a functional hardware unit in the LoFaR array autonomously capturing scientific data thereafter. Operations relied solely on their onboard computation stacks, with mission control setting high-level goals. The rovers stacked two payloads to create functional units, advancing modular payload installation in the array. (ibid.)

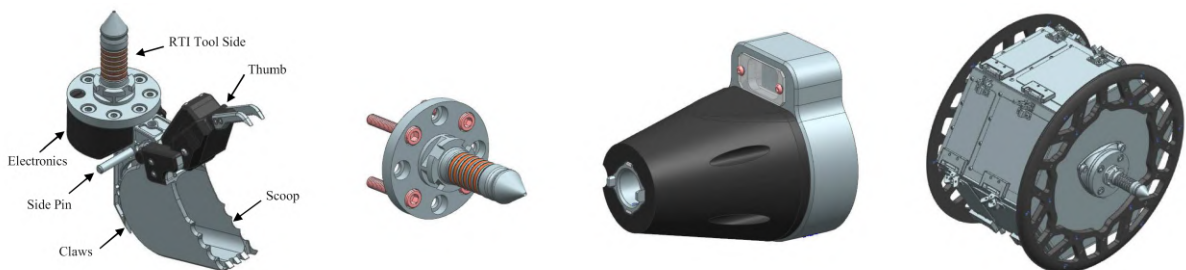
Under the ARCHES project, DLR created a modular mechatronics infrastructure for robotic planetary exploration (Fonseca Prince et al. 2021). This infrastructure includes the ENVICON Docking Interface System, payload modules, and a power and data management electronics board. These critical components enable autonomous robots to manipulate objects, conduct significant geological measurements, improve navigation and communication, and sustain the infrastructure deployed on the terrain. The successful implementation of this modularity shows

the relevance of using versatile and standard components to better explore space. (Fonseca Prince et al. 2023)

Overall, the ARCHES demonstrated the advantages of heterogeneous, autonomous, and interconnected robotic systems for diverse applications, using drones, rovers, and stationary components like the RODIN Lander. Key achievements include demonstrating autonomous infrastructure installation, validating modular payload concepts, and implementing real-time radionavigation systems crucial for future space exploration endeavors. Finally, its characteristics of possessing a lander with a major role in the experiments, and the addition of modularity components can serve as an inspiration for the Surface Avatar's Lander development.

### 2.3.3 LEAD

The Lunar Exploration Analogue Deployment (LEAD) is a program that simulates and tests technologies and procedures for lunar exploration missions. This project includes three mission simulations. The first simulation involved trained operators from the European Space Agency (ESA) and the Canadian Space Agency (CSA) conducting sample return missions. The second simulation involved six teams operating the rover along a predefined route to gather performance metrics for both manual and autonomous driving modes. The third simulation replicated rover operations under low-light conditions, similar to those in permanently shadowed lunar regions. All experiments were conducted in a rock quarry, where an analog environment environment was built. (Gingras et al. 2020)



*Figure 2.10: The first image represents the scoop mechanism. the second one contains a representation of the tool side (male) and the following image represents the master side (female). The fourth image contains a representation of the canister used to stow the collected samples. (Lamarche et al. 2020)*

To carry out these tasks, a mockup of a lander was constructed to receive the sample canisters. It also includes a scoop mechanism, allowing the rover to collect soil samples during the experi-

ments. These components have a common connector for more precise and robust manipulation. These mechanisms can be seen in Figure 2.10. (Lamarche et al. 2020)

## 2.4 Implications

Space missions, such as those mentioned above, can offer valuable insights into lander design, including appearance and functionality. For instance, the Apollo missions' lander module was extremely complex, as it had to accommodate astronauts, a rover, and a range of scientific equipment. Its distinctive visual and external shape could serve as inspiration for lander development in terms of form and materials. Analyzing the equipment used in this program could also provide insight into the likely components of the Surface Avatar's Lander. This leads to a design consideration of flexibility to accommodate any changes in equipment.

The missions from China, India, and Japan highlight the importance of certain tasks for a lander, such as deploying a rover and other equipment for surface exploration. These missions also provide insights into how a real sample return is conducted and the requirements needed to successfully collect and return rocks and soil to Earth. The presence of robotic interaction in these missions is extremely relevant to the Lander development within the Surface Avatar context, as the landing module interacts with all the robots during the experiments. The last program, likely the most relevant for near-future space exploration, is Artemis, which employs complex multi-function lander modules to support its ambitions.

The Mars exploration missions are also relevant to the Lander development and the Surface Avatar in general. The Phoenix mission, along with Chang'e 5, used a robotic arm to collect soil samples. These arms are not necessarily designed to be flexible, but they are intended to maximize their workspace, providing a larger area for soil collection and meeting other design criteria. The Lander described in this thesis includes a robotic arm for object handling. Therefore, these real missions underline the importance of having an optimized design to maximize required functionalities.

Despite not having a proper landing module, the Mars 2020 mission offers valuable insights into sample return missions. It serves as an inspiration for the design of sample tubes and the procedures for deploying these tubes and returning them to the storage system with soil inside. The mission also provides valuable information about the interaction between a robotic arm, the sample tubes, and the storage system. Therefore, important design considerations can be derived from it.

While real space missions can provide valuable insights for lander design, analog missions offer a practical implementation of an analog lander module. Therefore, these missions are crucial for gathering information for the development of the Surface Avatar's Lander. The review of

these missions focuses on those involving multi-robot operations, which are within the scope of the Surface Avatar.

METERON, for instance, is highly relevant as it used Justin in its experiments, along with several pieces of equipment that can potentially be used in the Surface Avatar. This relevance also applies to the SOLEX experiment, which included a lander with a cargo bay, an antenna, and a Container Unit. These pieces of equipment should be considered when designing the Lander, as they may be utilized in future missions. The SOLEX lander implementation featured a sliding tray that holds these pieces of equipment, thereby enhancing interaction with the robots. This design consideration emphasizes the need to account for the capabilities and limitations of other robots when designing each component of the lander, resulting in a design that is functional and optimized for robot interaction.

Analog missions also emphasize teleoperation, necessitating careful design of the Lander. The interaction between robots and the operator should be designed to reduce workload. For example, when designing the ROBEX lander, the metal surfaces had to be painted to prevent reflections that confused the operator and affected the sensors. Implementing designs, such as the standard connector from ARCHES and LEAD, has proven to enhance performance, especially in teleoperation mode. It provides a robust reference for the operator to position objects and improves grip for handling components.

The analysis of landers from other analog missions raises questions about their flexibility. They are usually limited to their initial design, making it difficult to add new functionalities. This lack of flexibility is also evident during protocol execution, as most landers are built to perform specific tasks and cannot adapt in real time to new conditions. Therefore, there is an opportunity to create a Lander design for Surface Avatar that is both flexible for future modifications and adaptable during operation. It should be able to adjust according to the task being performed and the robots and objects involved.

In conclusion, this chapter presents an extensive review of various space missions that offer valuable insights into the design and functionality of landers. Notably, the Apollo missions' lander module provides inspiration for form and materials, while missions from China, India, and Japan emphasize tasks such as deploying a rover and conducting a sample return. The Artemis program showcases the use of complex multi-function lander modules. Mars exploration missions, particularly the Phoenix mission, underscore the importance of optimized design to maximize required functionalities, such as robotic arms for soil collection. Importantly, these real missions highlight the multi-robot interaction in lander development. Analog missions, like METERON and SOLEX, stress the importance of careful design to reduce operator workload and improve performance in teleoperation mode. Finally, they show the opportunity of filling the existing technological gap by design a Lander that is flexible in terms of design and during its operation.

---

## 3 Methods

This thesis focuses on creating a robotic lander suitable for an analog environment, in accordance with the requirements of the Surface Avatar mission. Therefore, before initiating the lander's development, it is crucial to establish a product design and implementation method. To accomplish that, this section structures the work by exploring the design methodology introduced by (Pahl et al. 2006).

### 3.1 Needs Assessment and Requirements Identification

The work begins with a comprehensive description of Surface Avatar missions, which includes the analog environment, the robots, additional equipment, protocols to follow, and findings from existing literature. This is crucial for understanding the general problem addressed in this thesis and for deriving valuable information to design tasks. With this collected information, the next step involves clarifying other needs of the project and breaking down the problem into subproblems, or systems and subsystems, to effectively address various design propositions.

In parallel, the requirements are identified and documented. Whereas needs represent the broader objectives or motivations driving the product development, requirements specify the precise criteria that must be met to satisfy these needs. Aligning needs with requirements is crucial in product development. It ensures that the developed product effectively addresses user needs while adhering to technical constraints.

### 3.2 Conceptual Phase

Conceptual design is a critical phase in the design process, involving the identification of essential problems, establishment of functional structures, exploration of suitable working principles, and integration into a cohesive structure. This phase lays down the basic solution path through the elaboration of a solution principle, ultimately specifying the primary solution. This phase counts on many techniques, such as brainstorming and decision matrix. Firstly, to understand the consequences of the requirements, a function structure diagram is made to help clarify what needs to be created, and its interaction among other functionalities. Then, for each function, concepts are created by brainstorming sessions, and pre-selected. In sequence, these

concepts are merged together to form the solutions, whose the best is selected by a list of criteria to be further developed.

### 3.3 Preliminary Design

The preliminary design phase is a critical stage, often serving as a bridge between conceptual design and detailed design. According to Pahl and Beitz's framework, this phase involves transforming abstract concepts into more concrete design solutions. During this phase, key decisions are made regarding the basic structure, functions, and system architecture of a product, in this case, the Lander and its systems. It often includes creating initial sketches, design models, or CAD (Computer-Aided Design) layouts to visualize the proposed solutions. This phase is crucial in identifying the core components and how they interact within the product's structure. The goal is to establish a feasible and functional design framework that will guide subsequent stages of development.

In addition to focusing on the technical aspects of the product, the preliminary design phase also considers factors such as cost and manufacturability. This stage often involves multidisciplinary teams collaborating to assess different design options, conduct feasibility studies, and identify potential risks. Feedback from stakeholders, in this case, the Surface Avatar team, assurance, is gathered to ensure the design aligns with broader project objectives. By the end of the preliminary design phase, a well-defined design concept should be established, providing a solid foundation for the detailed design phase, where more specific design elements and components are developed and refined.

### 3.4 Detailed Design

The detailed design phase in the product development process builds on the foundation established during the preliminary design phase. It involves refining and specifying the design elements to create a comprehensive blueprint for production. According to Pahl and Beitz, this phase requires a deep dive into the specific components, materials, dimensions, and assembly processes needed to construct the product. Detailed design involves creating detailed engineering drawings, CAD models, and technical specifications that can be used for manufacturing and assembly. This phase focuses on optimizing the design for functionality, safety, and manufacturability, while also considers cost and reliability.

Additionally, this stage may also involve prototyping and testing to validate the design's performance and identify any potential issues. By the end of the detailed design phase, a



complete set of engineering drawings and technical documentation is produced, serving as the official guide for production. This phase plays a crucial role in ensuring that the product is ready for manufacturing, with all critical details meticulously planned and documented.

### **3.5 Implementation and Validation**

The implementation and validation phase, as described by Pahl and Beitz, is the final stage of the product development process, where the detailed designs are brought to life through manufacturing and assembly. During this phase, the focus shifts from design to production, ensuring that all components are fabricated according to the specifications outlined in the detailed design phase. Implementation also includes rigorous testing and validation to ensure that the product performs as intended under real-world conditions. This may involve conducting various tests, such as functional testing, stress testing, and user testing, to identify any issues that need to be addressed before the Lander is finished.

Validation is a crucial aspect of this phase, as it ensures that the final Lander design meets all the established requirements and specifications. Pahl and Beitz emphasize the importance of continuous feedback and iterative improvements during this stage. Any discrepancies or issues discovered during testing and validation are addressed through corrective actions, which may involve redesigning certain components or adjusting manufacturing processes. The goal is to achieve a product that not only meets the functional and performance criteria but also adheres to safety, reliability, and cost-effectiveness standards. By the end of the implementation and validation phase, the Lander should be fully functional, ready for use, and capable of fulfilling the mission's needs and expectations.

# 4 Surface Avatar Technology Demonstration Mission

This chapter exposes the Surface Avatar Technology Demonstration Missions (N. Y.-S. Lii et al. 2022; Schmaus et al. 2022), focusing on the analog experiments. It provides detailed analysis and extracts crucial information to guide the development of the Lander. An outline of the robotic team and their operational characteristics is also included. The chapter provides detailed information about MUSA, including descriptions of each piece of equipment. It then describes the Lander and its expected capabilities. Finally, it presents consolidated and potential protocols.

## 4.1 Robotic Team

The Surface Avatar's robotic team consists of four robots, each with unique features. Together, they form a diverse team with a high capacity for flexible task performance. These robots are designed for autonomous operation and teleoperation.

### 4.1.1 Rollin' Justin

Rollin' Justin (Ott et al. 2006) is a dexterous humanoid robot equipped with two DLR Light Weight Robot III (LWR) arms (Hirzinger et al. 2002), each with seven degrees of freedom (DoF), and two DLR-Hand-II (Butterfass et al. 2001), each with four fingers and a total of 12 DoF.

Justin also features a 2-DoF head with cameras that provide visual feedback from its surroundings. This feature is crucial for navigating the environment and performing tasks with precision. The cameras can also identify Apriltags in the environment, allowing the robot to recognize which object it is observing and understand the object's position and orientation in space. Additionally, the cameras can serve as support for other robots by providing a secondary view of a scene. (N. Y.-S. Lii et al. 2022)

Justin has a 3-DoF torso, which enhances its reachability, and a four-wheeled mobile platform with eight DoF for movement. In total, Justin has 51 DoF, making it incredibly versatile for performing a range of tasks, from simple to complex. (Borst et al. 2009; Fuchs et al. 2009)

During the Lander development, design consideration must be taken regarding the Justin features and limitations. One key aspect is the reachability of Justin's arms and hands, which are important for objects that could be transferred between the Lander and the robot. Thus,

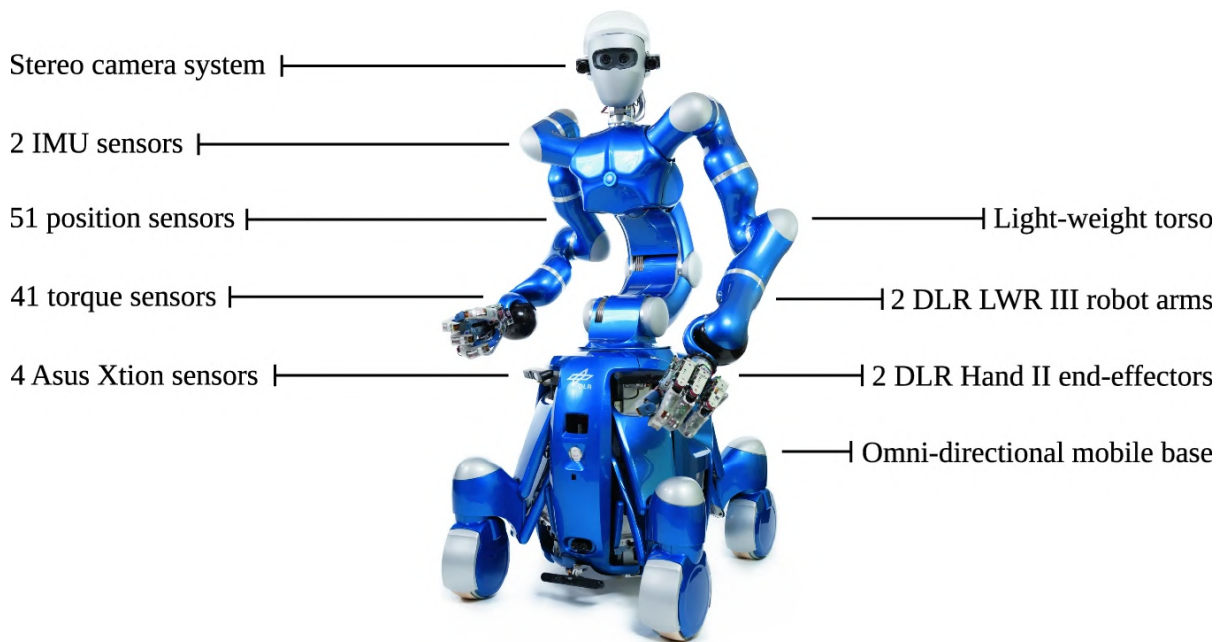


Figure 4.1: Image of Rollin' Justin with its main components. (Leidner 2019)

the Lander design should include components that make the interaction with Justin easier and design additions should not compromise the robot's reachability. Another component of interest is the hand, since Justin uses it to handle objects, taking into account its requirements for size, shape, and weight. Finally, it is interesting to notice that, when relying on teleoperation, the capability of placing objects precisely might decrease.

#### 4.1.2 Interact Rover

The Interact Rover is an on-ground robotic system, designed to be controlled by an astronaut from space. This platform is an assembly of numerous off-the-shelf systems into one highly modular and robust framework. The AMBOT GRP-4400 system provides locomotion, offering four-wheel drive and independent steering. Atop the platform, there is a structure built from modular 30mm aluminum profile struts. This structure accommodates space for mounting components such as power distribution units, target computers, control devices, and networking devices. The internal components are protected from weather and dust by a custom fabric cover. The system also includes two KUKA Light Weight Robot (LWR) manipulators. For outdoor weather conditions, these robots can be fitted with custom water and dust-proof sleeves. To

facilitate object grasping, the Rover employs a Robotiq 2F-85 gripper, which is mounted to the arm at the front of the robot. (Krueger et al. 2020a)



*Figure 4.2: Image of interact rover used in the Surface Avatar. (Krueger et al. 2020a)*

### 4.1.3 Bert

Bert is a four-legged robotic system designed to study biological locomotion and translate these insights into robotics. It is equipped with series elastic actuators (SEA) to provide passive compliance, which is crucial for traversing rough and slippery terrains. This compliance enables Bert to maintain stability and grip without depending on high-bandwidth torque control. Moreover, the system's foot design includes a passive adaptive planar joint, further enhancing its adaptability to variable ground conditions. (Raffin et al. 2023)

Bert's legs, each with a hip and knee joint, attach to the main body via the hip axis. The motors driving these joints reside within the body and connect to the legs via belt drives. The springs in Bert have relatively low stiffness, allowing for energy storage during routine movements. This



Figure 4.3: Image of Bert during a terrain exploration. (Raffin et al. 2023)

stored energy can later be released to generate additional kinetic energy. The compact size of Bert ( $0.40 \text{ m} \times 0.30 \text{ m} \times 0.25 \text{ m}$ ), coupled with its unique features, enhances its agility and efficiency, providing enough flexibility to navigate challenging terrains, surpass larger obstacles, and climb steeper slopes up to 30 degrees. (Seidel et al. 2020)

#### 4.1.4 Lander

This thesis explores the concept of constructing a Lander capable of performing various tasks to support Surface Avatar experiments. As mentioned in Chapter 1, the Lander should adhere to the protocols of the Surface Avatar experiment, leading to the development of four main characteristics: a Sample Tube and a Sample Stowage Device, TINA integration, a Hands-on Tray, and a Cargo Bay. The development of these systems, along with future improvements and capabilities, hinges upon a deep understanding of the Lander's concept. This section presents the Lander's initial state and the expectations surrounding it.

### Physical Description

The Lander has a predefined shape, with a frame built from off-the-shelf 40x40 aluminum construction profiles. These profiles not only simplify construction but also add flexibility to the project. They allow for the addition of new components and quick modifications without needing to alter the structure, thus saving cost and time. Figure 4.4 displays the Lander frame, illustrating half of an octagonal Lander used in real missions as described in Chapter 2. It has three usable vertical surfaces - two lateral surfaces, each at a 45-degree angle relative to the front one. The Lander features two legs, providing stability alongside the support at the bottom. The Lander's dimensions, which act as constraints for objects designed to fit inside it.



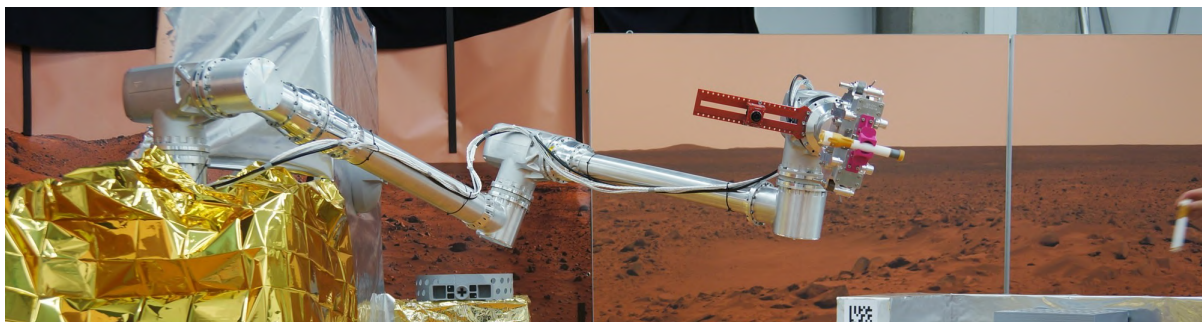
*Figure 4.4: Representation of the Lander frame.*

### TINA

TINA (This Is Not an Arm) is a system designed for space missions where cost and complexity demand optimized solutions. Unlike traditional robotic arms, TINA is a collection of torque-controlled joints that can be configured according to specific requirements. This modular approach allows flexibility in how these joints are used, enabling customization for different tasks and needs. The joints can be configured to meet different kinematic requirements, such

as varying joint numbers, configurations, and limb lengths. This adaptability makes TINA versatile for a range of space-related activities. The shoulder component, one of the main modules of TINA, contains two robotic joints and an electronic box, which can be repositioned to accommodate various limb distances, allowing for compact configurations when space is limited. (Maier et al. 2019)

The TINA used in Surface Avatar is a 7 DoF robotic arm. It comprises three shoulder elements, a connection element between the shoulders, a base, and a gripper. Figure 4.5 illustrates the TINA for Surface Avatar. The base needs to be attached to the Lander structure, and connects to the first shoulder. This shoulder is then linked to a cylindrical component with a rotational. Subsequently, the middle shoulder connects to both the previous and the following cylindrical components. The final shoulder links to the cylindrical component and a Robotiq 2F-85 gripper.



*Figure 4.5: Tina used in Surface Avatar. Note that the gripper of this Image differs from the one used during the experiments.*

### **Sample Tube and a Sample Stowage Device**

One important task of Surface Avatar is sample handling and storage. Thus, a Sample Tube must be created in order to safely transport materials between the mission's sites. The Sample Tube will be manipulated by all robots, thus its design must comply with their characteristics. To mimic the Stowage of the samples, a device must be created to retrieve, store and deliver them. This device will mainly interact with TINA during its operation.

### **Cargo Bay**

The Lander must have a space dedicated to store other devices, such as a seismometer and mechanical and electrical devices that could be part of the experiment in the future. It must also provides a flexible space to add new components as needed.

### **Hands-on Tray**

To provide a area where TINA can pick and place objects, such as the Sample Tubes or components from the Cargo Bay, the Lander must have a Hands-on Tray in front of it that can be reached by the TINA and other robots.

### **Spacial distribution of the onboard Systems**

As previously mentioned, the Lander must include four onboard systems: a Sample Tube, a Sample Stowage Device, TINA integration, a Hands-on Tray, and a Cargo Bay. Allocating the left side for TINA enables the Hands-on Tray to be placed at the Lander's front, and turns the arm operation safer, because the Lander is placed in the corner of the analog environment, which limits the overall space available in the right side. The proposed placement of the Cargo Bay and the Sample Stowage Device not only provides sufficient space for device development but also enhances the Lander's flexibility by offering a larger volume for the Cargo Bay. All the equipment requires computers, which must be installed inside the Lander. If the existing space, which exclude the Cargo Bay area, is not enough, the space below the structure can be used.

#### **4.1.5 Mission Control**

The 3-DOF RCT joystick allows roll, pitch, and yaw inputs. It features six additional programmable buttons and an enable button, which also serves as a dead man's switch. The sigma.7 has 6-DOF movement and an extra pincer DOF, all with force-reflection functionality. This characteristic is especially beneficial for the telepresence operation of robotic arms with grippers for object grasping. The RCT notebook computer is a standard HP ZBook used on the ISS. The GUI program on the notebook serves as the command center of the RCT. It manages all input devices and offers a wide range of visual and textual information, as well as command options. The astronaut issues commands via the Multimodal Robot Command Terminal on the ISS, shown in Figure 4.6.

When teleoperating Justin, for instance, his arms are controlled via the sigma.7, which allows the astronaut to feel the height of an object or how much force something required to be moved. The hands are also controlled via the sigma.7, but using the pincer device. This allows the operator to control the fingers' position and applied force.



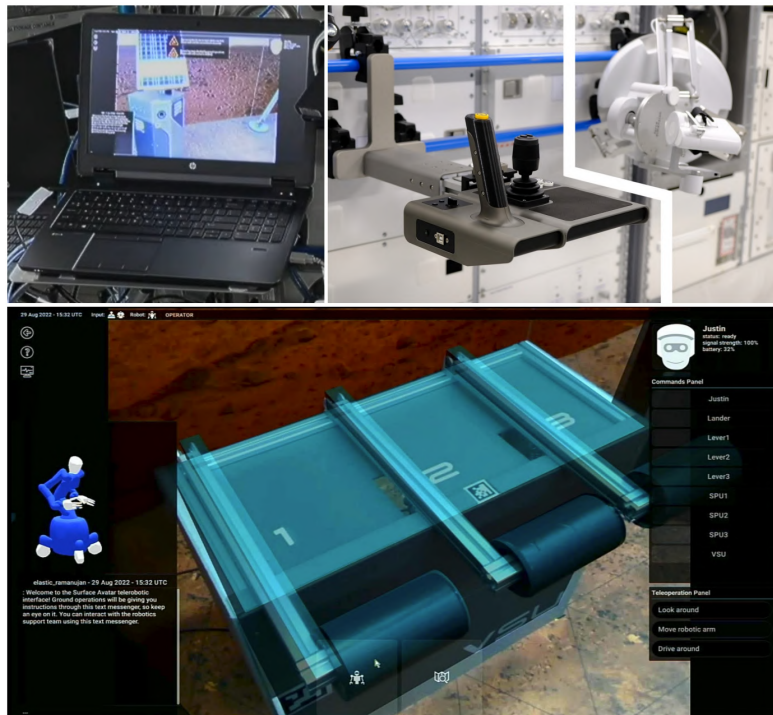


Figure 4.6: Surface Avatar’s RCT features a notebook computer (top left) with a GUI program (bottom), an open-loop joystick (top center), and a force-reflection sigma.7 input device (top right). The GUI serves as the ISS crew’s command center, offering functions like viewing the robot’s pose, texting ground control, accessing the robot’s camera, and selecting input devices. (N. Y.-S. Lii et al. 2022)

## 4.2 Interaction Between Lander and Other Robots

This document details how Justin’s arms, torso, and mobile platform, as well as the general features of the Interact Rover, can interact with the Lander. A workspace approximation was conducted to illustrate this, with results shown in Figure 4.7. To determine Justin’s reach, we considered the capabilities of the arms, torso movements, and the height of the mobile platform. For the Interact Rover, we took into account the arm capabilities and the position of the arm base.

The results indicate that Justin should not have any issues interacting with the Lander and its objects. However, the design of the Hands-on Tray for the Interact Rover must consider height restrictions to ensure the robot can handle objects and operate in the space above the tray.

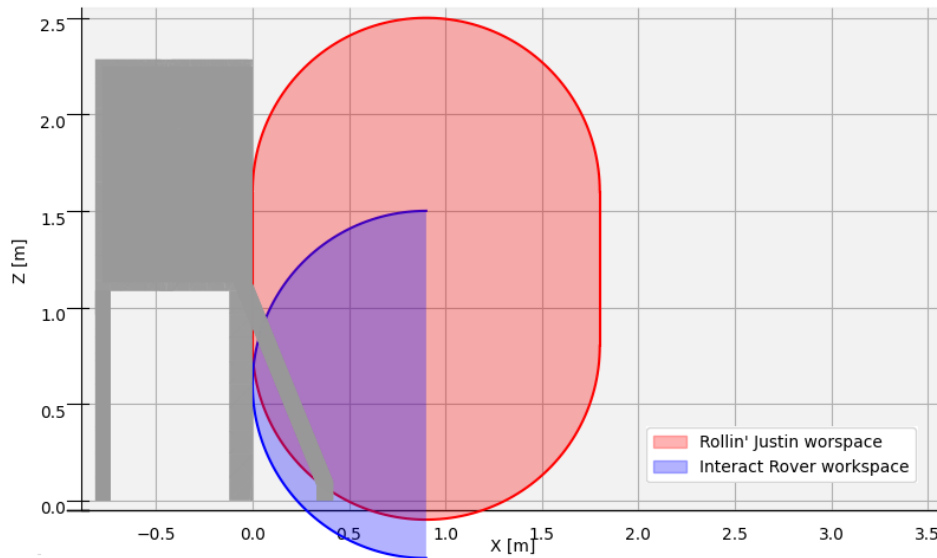


Figure 4.7: Workspace of Justin in red and Interact in blue

### 4.3 Protocols

The mission follows some pre-defined protocols, whose tasks must be performed by the robots and the astronaut in command. The first session of Surface Avatar includes two main protocols, which requires the integration between the the robots and the Lander.

#### 4.3.1 Protocol 1 - Seismometer Handling

In the initial Surface Avatar protocol, the goal is to transfer a seismometer from the Lander to Justin, who will then position it at a specific site. Here's a breakdown of the actions involved:

1. TINA retrieves the seismometer from the Lander.
2. TINA sets the seismometer on the Hands-on Tray in front of the Lander.
3. Justin moves toward the Lander.
4. Justin picks up the seismometer.
5. Justin transports the seismometer to its designated placement location and places it on the ground.

6. Justin moves away from the site.

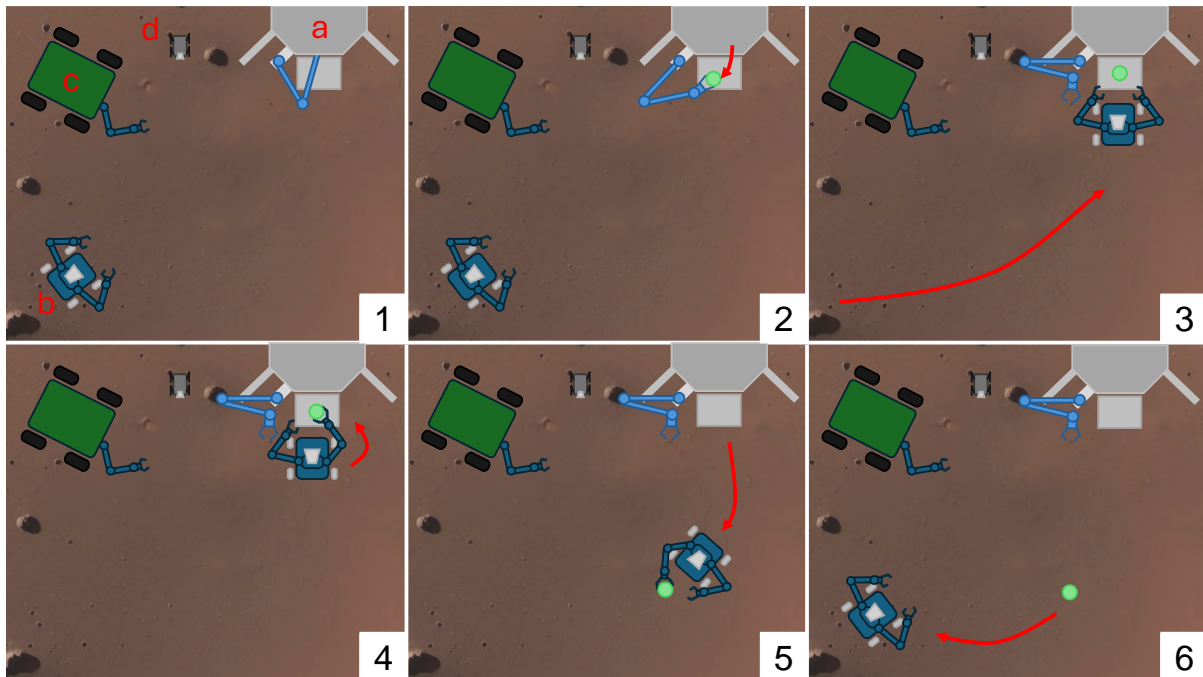


Figure 4.8: Sequence of action for the Protocol 1 - Seismometer Handling. (a) represents Lander; (b) represents Rollin' Justin; (c) represents Interact Rover; (d) represents Bert.

The first protocol involves interaction between Justin, the TINA arm, and other Lander components. The first step requires consideration of the Cargo Bay design, from which the Seismometer is taken. Subsequent procedures involve interaction between the robots and the Tray. Therefore, the design should ensure the tray's size and height are suitable for TINA and Justin's operations. Additionally, when integrating TINA, it is vital to guarantee that her position does not interfere with other robots' operations when she is not in use.

#### 4.3.2 Protocol 2 - Sample Tube Return

The second protocol involves placing a sample tube in a designated location using Justin and TINA's coordinated efforts. Here's the action sequence:

1. Interact Rover holds the Sample Tube.
2. Justin moves to the Interact Rover, which transfer the Sample Tube to Justin.

3. Justin moves to the Lander carrying the Sample Tube.
4. Justin places the Sample Tube on the Hands-on Tray and then moves away.
5. TINA picks up the sample tube.
6. TINA inserts the sample tube into the Sample Stowage.

The second protocol demands special attention to the Sample Tube Development, managed by three distinct robots using two different grasping tools: the Robotiq 2F-85 and DLR Hand II. It also necessitates the Sample Tube to be stowed, prompting the creation of a stowage device that interacts with both the Sample Tube and TINA.

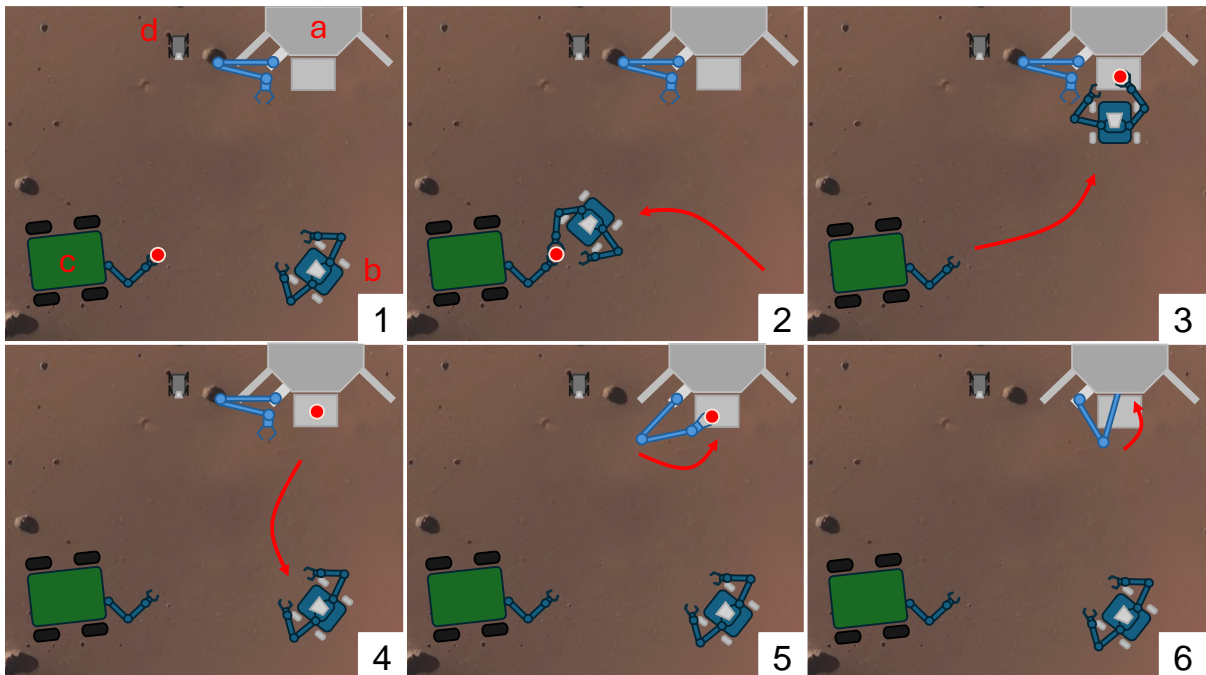


Figure 4.9: Sequence of action for the Protocol 2 - Sample Tube Return. (a) represents Lander; (b) represents Rollin' Justin; (c) represents Interact Rover; (d) represents Bert.

#### 4.3.3 Possible Protocols involving the Lander

It is possible to establish many more protocols that could be used by the mission. The following protocols are example of that.

##### **Bert deployment:**

- TINA retrieves Bert from the Cargo Bay.
- TINA sets Bert on the Hands-on Tray.
- TINA unboxes Bert.
- The Hands-on Tray lowers to get closer to the ground.
- Bert walks out of the tray to explore the environment.

## 5 Lander

In Section 4.1.4, the Lander was presented and its expected functionalities were introduced. This Chapter continues on the Lander, but now detailing the development of each of these functionalities, following the design methodology of Chapter 3. Therefore, this Chapter is devoted to the development process of Sample Tube, Sample Stowage Device, TINA integration, Hands-on Tray and Cargo Bay.

### 5.1 Sample Tube

The Sample Tube works alongside the Sample Return Unit, providing a safe and controlled means of transporting samples in the analog environment. It aids in moving materials from the collection point to the Lander for future storage. Additionally, it offers a reliable method to test the robots' object handling capabilities, which also results in a unique experience for astronauts when teleoperating the robots.

Following the description of the mission and the needs to be tackle regarding the Surface Avatar, this Section presents the design development of the Sample Tube. Starting with the requirement in Section 5.1.1. Overall, the sample tube design should take considerations of geometry, kinematics, forces, material, signals, quality control, operation, and maintenance to meet the functional requirements of robot handling, identification, and operational efficiency within the context of space exploration missions.

In Section 5.1.2, the Concept Phase is presented and described. A function diagram is created based on the list of requirements. Following this, concepts are developed for each required function. Selection criteria are then defined, resulting in the final selection of concepts.

Section 5.1.3 is dedicated to the development of the preliminary design, which was created using Design Thinking methods such as designing, prototyping, learning, and improving. Therefore, this part of the thesis describes the evolution of the Sample Tube's design through various successful and unsuccessful attempts to refine the concepts.

#### 5.1.1 Requirements

When creating Sample Tubes for Surface Avatar, it is essential to follow a comprehensive set of design requirements, which covers various factors such as shape, movement, forces, materials,

communication, quality checks, operation, and maintenance. Every requirement is critical in ensuring the sample tube performs efficiently, reliably, and aligns with the mission's objectives and conditions. Therefore, this section explores these design requirements for a sample tube. They are influenced by a range of factors, from the manner in which robots handle the tube, the material's property, to its communication with the mission control. By following these guidelines, the design development can create a Sample Tube that not only meets the mission's requirements, but also integrates well with robotic systems, facilitates sample handling, and is easy to maintain throughout the mission.

### Functional Requirements (FR)

The first set of requirements are dedicated to the functional ones.

**FR01 - Sample Tube shall have a open/close mechanism:** The robots should be able to open and close the sample tube during the protocol execution to pour sample material into.

**FR02 - Sample tube must communicate the ID with the stowage and analysis unit:** The sample tube should be able to transmit its ID to the stowage and analysis unit.

**FR03 - Sample Tube should self-orient when placed on a surface when it involves TINA handling:** Regarding the limitations of TINA operations, an object that is constantly handled should be placed in the same orientation on a surface for later handling by TINA.

### Non-Functional Requirements (FR)

**NFR01 - Sample Tube size should be between 30x30x100mm and 40x40x200mm (LxWxH):** This requirement arises from the need to balance between the appearance and the ease of handling. A notable example is the sample tube used by NASA in its Perseverance mission, as shown in Figure 2.6. The decision to use a larger tube than the one in NASA's mission is influenced by the handling abilities of the robots, particularly those with Justin hands. The TINA and Interact rovers use a gripper that can hold components no larger than 85mm, while Justin struggles to securely handle small objects. As such, the current requirement proposes a sample tube size that is both suitable for all robot capabilities and aligned with the dimensions used in real missions.

**NFR02 - Sample Tube must have at least two flat surfaces:** This requirement is added due to the localization tag used by the mission and the fact that Justin achieves greater stability when pinching between two parallel flat surfaces, as compared to round or irregular shapes.

**NFR03 - Sample Tube should have a volume for sample material greater than 30 cm<sup>3</sup>:** This requirement relates to the fact that the sample tube is made to carry sample material, thus it must contain an internal capacity.

**NFR04 - Sample Tube should have a minimum opening of 10mm:** The design should allow the storage of spherical shapes with a maximum diameter of 10mm.

**NFR05 - Sample Tube should be lighter than 200g:** This requirement is based on Justin's capabilities when handling objects smaller than 40x40mm. Given this size constraint, Justin must use a pincer pose to hold the object, which means the robot can't hold heavy items with its fingertips. Justin was tested with a 40x40mm square-shaped object 3D printed in PET-G, resulting in a weight limit of approximately 2kg. To account for variations in material and surface finish that could affect the grip, and to accommodate for the addition of sample material inside the tube, a maximum weight of 200g was chosen for safety.

**NFR06 - Any Sample Tube operation must be performed using a force less than 10N:** The same consideration about the weight of the Sample Tube applies here. This 10N should account for all forces exerted on the device.

**NFR07 - Sample Tube should have a transparent body:** This requirement stems from a need for visual appeal. It would enhance the visualization if it were possible to see inside the tube during operation, especially when pouring sample material into it.

**NFR08 - Sample Tube shall have no magnets:** The sensors embedded in Justin's hand can be affected by magnets. Therefore, the Sample Tube must not contain any material or device that generates magnetic fields.

**NFR09 - Sample Tube must contain ID:** The mission must be able to identify each Sample Tube unit.

**NFR10 - Sample Tube must have a localization tag on its exterior surface:** This would allow the robots to detect and localize the Sample Tube, inferring the object type, position and orientation on space.

**NFR11 - All Sample Tube shall have similar handling characteristics:** The characteristics of weight, inertia, and required forces should be consistent across all Sample Tubes.

**NFR12 - Sample Tube must be operated just with one arm:** Given the teleoperation characteristics, which allow controlling only one arm of Justin at a time, or considering other robots that only have a single arm for object handling, it's necessary to use all the features of the Sample Tube with just one arm.

**NFR13 - All parts should be replaceable:** All parts of the Sample Tube should be replaceable.



### 5.1.2 Conceptual Phase

Before presenting the concepts itself, this section presents the function structure of the Sample Tube, in order to guide the concept creation and further merge to formulate solutions and select the best according to the determined criteria.

#### Function Structure

The Sample Tube has a simple and straightforward set of required functionalities, which can be translated into the Function Structure in the Figure 5.1. The first and third functions are based on requirement FR01, which is divided into an open function and a close function. This division provides enough abstraction for creating a mechanism that can perform both functions or two different mechanisms each performing a specific function. The second function involves communication with mission control, which needs to receive the ID of the addressed Sample Tube when interacting with the Sample Stowage Device System. Consequently, the Sample Tube must receive energy and a signal, and in return, provide its ID and a signal.

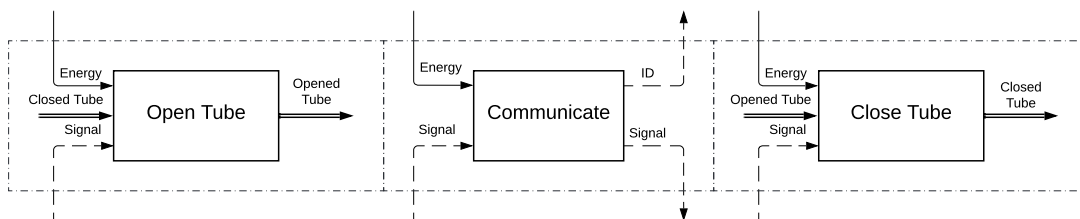


Figure 5.1: Functional Structure of Sample Tube.

#### Concepts for Communicate

The communication of its ID, which fulfills requirement F02, will be discussed in tandem with the development of the Sample Stowage Device. This is because the ID communication functionality largely depends on the Stowage definitions and the Surface Avatar's communication decisions. The communication concept involves having a passive sensor installed on the Sample Tube, with the active part handled by the stationary Stowage, which may also contain support components like a power source.

### Concepts for Open and Close Tube

The concepts for the Open and Close functions are divided into two categories: mechanism and actuator. The mechanism relates to the component that provides the opened or closed state, allowing samples to enter the tube when open and securing them inside when it is closed. Its concepts can be seen in Figure 5.2. The actuator concept pertains to the mechanism that provides the transition between the opened and closed states. The concepts' illustrations are in Figure 5.3.

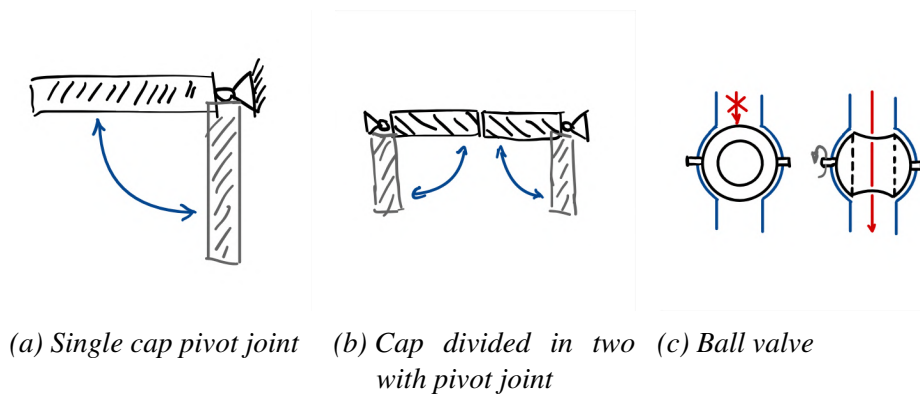


Figure 5.2: Concepts for the open and close mechanism for the Sample Tube

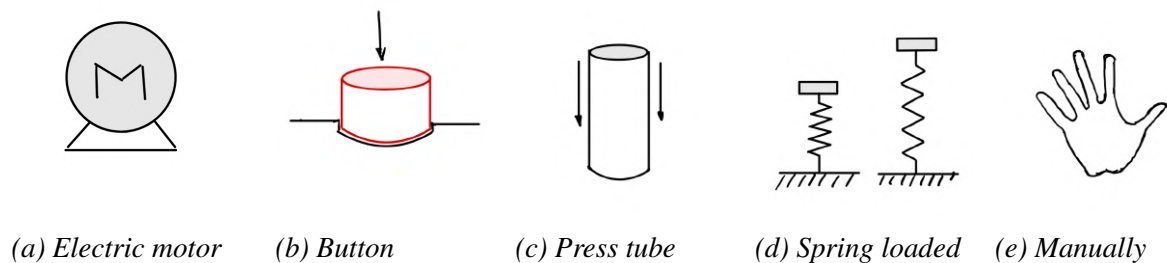


Figure 5.3: Concepts for the actuator that provides the open and close functionalities

### Solutions

Several design concepts were created to address the sample tube's functionality. By strategically combining these concepts, six unique solutions emerged. The list below provides details of these solutions.

- **Solution 1:** Single cap pivot joint + open manually + close manually
- **Solution 2:** Single cap pivot joint + open press tube down + close spring loaded
- **Solution 3:** Cap divided in two with pivot joint + open manually + close spring loaded
- **Solution 4:** Cap divided in two with pivot joint + open press button + close release button
- **Solution 5:** Ball valve + open electric + close electric
- **Solution 6:** Ball valve + open manually + close manually

### Selection Criteria

The solution criteria can be divided into three main categories, in which the criterias are breakdown. The Figure 5.4 shows depicts the weight of each category, as well as the relative and absolute weights for each criteria. **Geometry:** size (NFR01); volume (NFR03); opening size (NFR04). **Force:** weight (NFR05) required forcen(NFR07). **Operation:** simple (NFR11 and NFR13); one arm operation (NFR12)

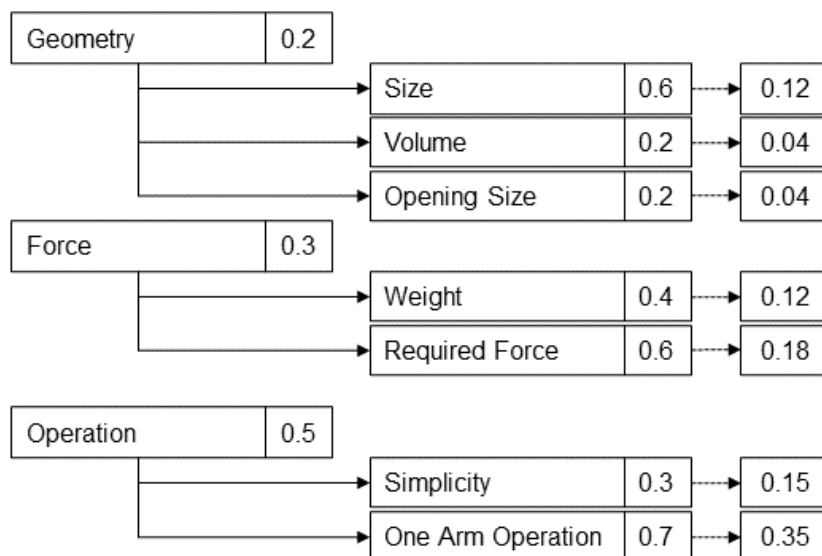


Figure 5.4: Criteria for the Sample Tube solution selection. The weight distribution is shown for each category and then for each criteria.

## Solution Selection

To choose the solution for further development, a decision matrix was created. It consists of the solution and various criteria, each with its respective weight. A solution could score 1 for each criterion, indicating a negative impact, 2 for a neutral impact, and 3 for a positive impact. Once all scores are assigned, the weights are applied. The solution with the highest overall score is selected. Table 5.1 shows the score assigned to each criterion for the corresponding solution. The chosen solution was **Solution 2**. It combines the concepts of a single cap pivot joint, which opens when the tube is pressed down and closes using a spring-loaded mechanism.

Criteria	Wieght	Solutions					
		1	2	3	4	5	6
Size	0,12	3	2	3	2	1	2
Volume	0,04	2	2	3	3	1	1
Opening Size	0,04	3	3	2	2	2	2
Weight	0,12	3	3	3	3	1	3
Required Force	0,18	1	2	1	2	3	2
Simplicity	0,15	3	2	3	2	1	2
One Arm Operation	0,35	1	3	1	2	3	1
Total		1,9	2,0	1,9	1,9	1,4	1,6
Rakinng		2	1	2	2	6	5

Table 5.1: Best solution selection for the Sample Tube.

### 5.1.3 Preliminary Design

The development of Solution 2 was iterative, involving cycles of design, prototyping, learning, and improvement. Initially, a detailed design was proposed, specifying the components and their potential interactions. Each component was then created and prototyped, and the Sample Tube was assembled to test and validate the concept. The model was subsequently analyzed, and the insights gained informed the design of the next prototype. This cycle was repeated until the final product was ready.

### First Prototype

The initial prototype consists of two concentric tubes, a spring, two pins, a rod, and a cap. The cap is connected to the inner tube by a cylindrical pin through a pivot joint, and to the outer tube by a rod. The working principle involves pressing the inner tube against a surface, causing it to

slide downward inside the stationary outer tube. As the inner tube moves, the cap moves with it and the rod causes the cap to rotate around the pivot joint, opening the Sample Tube. Once the inner tube is released, a spring returns the system to its closed position, moving the inner tube upwards while the outer tube remains stationary. Additionally, a pin is attached to the bottom of the inner tube and runs along a path carved on the outer tube. This prevents relative rotation between the two tubes. Figure 5.5a shows a CAD design with the first prototype assembled, next to an exploded view, showing each of the mentioned components. It also presents the prototype result. All plastic parts were 3D printed using PET material colored in black, the rod was made by bending a steel wire, and the pivot cap's pin was also made with a steel wire.

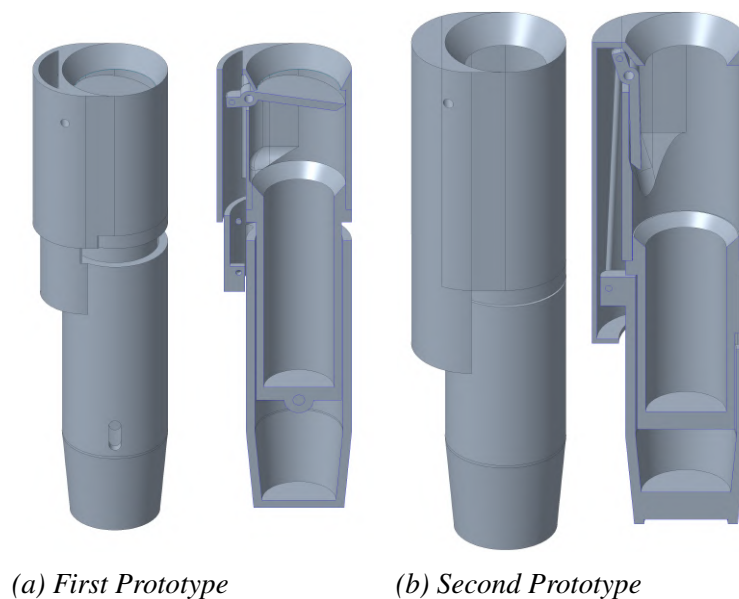


Figure 5.5: First and Second Prototypes in an assembly view.

The main characteristic given by this prototype was the diameter of the Sample Tube, which was defined as 36 mm. This was considered a good size because it follows the NFR01 and leaves room to expand the top of the tube to accommodate the cap mechanism. The concept of the opening and closing mechanism proved valid and functioned as expected, with one major consideration: the design of the Sample Tube's top part should facilitate access to the rod. Lastly, the pin locking the rotation between the two tubes needs modification, as it is difficult to keep it in place.

## **Second Prototype**

The modifications made to the second prototype addressed two issues of the first one: the accessibility of the rod and the anti-rotational pin. The rod accessibility issue was resolved by exposing the entire mechanism and adding a removable cover. The anti-rotational pin problem was addressed by removing the pin and replacing it with a cam. This cam, attached to the inner tube, slides in a rail carved into the outer tube, thus preventing relative rotation. Finally, a cutout was added to the bottom of the Sample Tube to accommodate a PCB design for communication. Figure 5.5b illustrates the second prototype.

The second prototype highlighted the difficulty in achieving good tolerances with 3D printed components. The rough surface finish and tolerances caused the anti-rotation mechanism to lock up, preventing the cap from moving. The cap itself was also problematic, as the material around its joint hole became less resistant, increasing its susceptibility to breakage. Finally, assembling and reaching the spring of the Sample Tube, located between the tubes on the bottom part, was challenging.

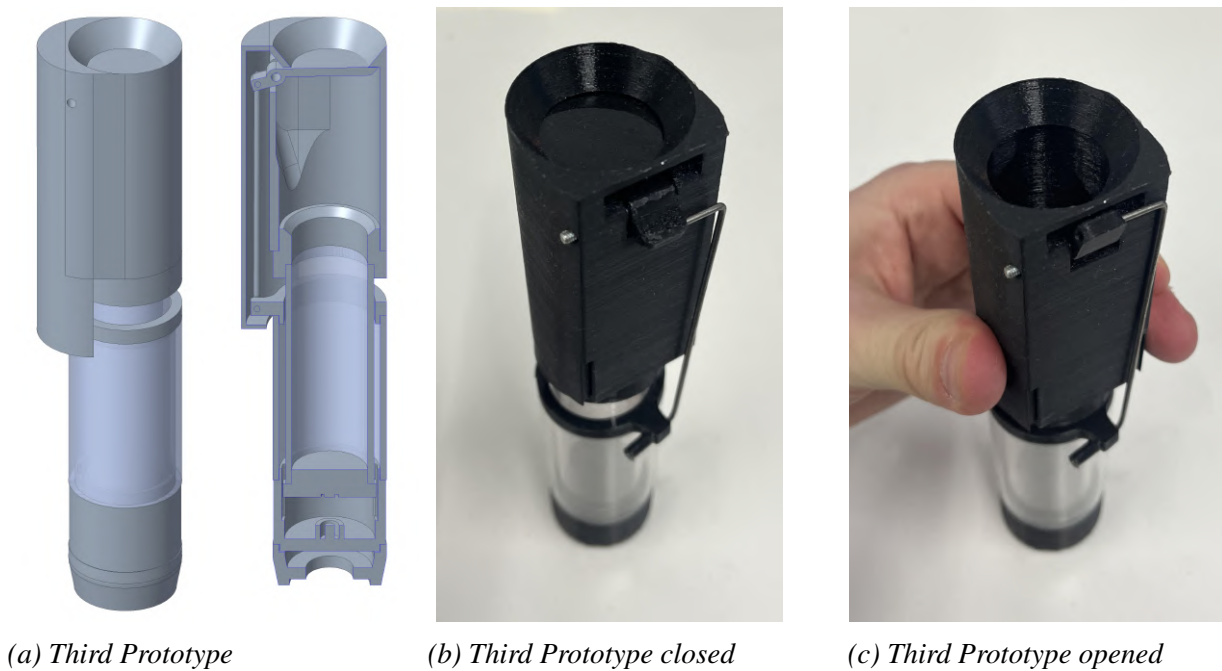
## **Third Prototype**

The third prototype focuses on incorporating the transparent tube requirement NFR07. Two tubes were chosen: one with an outer diameter of 36 mm, and another with 28 mm, both with a thickness of 2 mm. Acrylic was selected as the material. New parts were designed to foster the interface between key elements. The spring region components were modified for easier access, and the cone shape at the bottom was redesigned to fit the stowage slot designed in parallel. This part was also separated from the rest of the Sample Tube, allowing it to be replaced if there is a need to modify only this component. The tolerances involving the cam were optimized. Figure 5.6 illustrates the third prototype.

This prototype was the first to offer satisfying operational characteristics. However, it still had some issues, particularly the complexity of the two sliding tubes mechanism and the exposed sliding interface, despite the rod mechanism cover. This makes them susceptible to failure. But the major flaw in these three designs relies on its format. The rounded shape makes a pincer grasp hard to perform and does not allow the installation of tags to its surface.

## **Fourth Prototype**

The fourth prototype represents a significant change to the opening and closing mechanism. The new prototype design changes are based on moving the spring from the top to the bottom, eliminating the need for two sliding tubes along the entire Sample Tube, and simplifying



*Figure 5.6: Third Prototype.*

assembly. Figure 5.7 presents the new design. As one can see, the Sample Tube now has a square shape, which allows the installation of a tag on each lateral surface. The Sample Tube is now divided into two parts: the stationary and sliding systems.

The stationary system is composed of the cone with a self-orienting surface. This design stems from an initial requirement of the Sample Stowage Device that was incorporated into the Sample Tube as part of the mechanism. The design process will be detailed in the next chapter. The cone is attached to the acrylic tube, which is connected to the upper component that provides a contact surface for the sliding mechanism, attachment of the rod, and base for the two springs.

The sliding system has an upper part, which provides a funnel shape for better insertion of sample material, and support for the pivot pin of the cap. The cap itself was redesigned to be more robust. The upper part is connected to the middle part, which secures an inner tube used as a sliding interface, and the two springs. Finally, a cover is added to the middle part and serves as a way to prevent rotation, eliminating the need for a dedicated anti-rotation mechanism.

This Sample Tube version proved superior to the previous one in many aspects. It is the first one that is fully operational, undergoing tests with the robots. Justin is now able to grasp it with a pincer pose. He is also capable of opening the cap properly. The main point to improve is related to the characteristics of the 3D printing method used. It does not have satisfactory

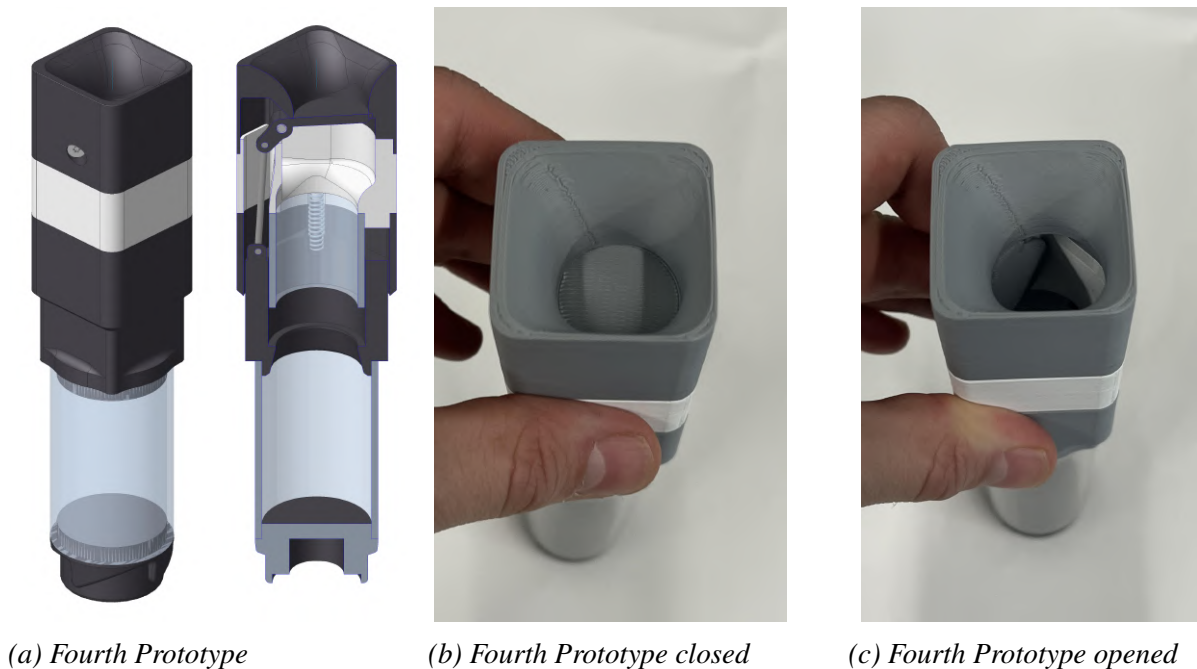


Figure 5.7: Fourth Prototype.

precision and the tolerances are not good, causing all the 6 units manufactured to have different handling characteristics, especially related to the force needed to open the cap. Another problem is that the parts are held together by friction, and extensive use shows that some tubes become loose, causing the Sample Tube to disassemble during use. Finally, the robots often drop the Sample Tube during tests, and the fact that it relies on friction to hold the parts in place causes it to completely disassemble when it hits the ground, leading to delays in the experiments.

### Fifth Prototype

The fifth prototype was designed to address two issues: lack of precision and reliance on friction to secure parts. The problem of precision and tolerances was resolved by altering the material type and 3D printing technique. The parts were printed using PA12 via the HP Multi Jet Fusion process. This new method resulted in parts with improved tolerances and surface finish. Bushings were added to the sliding interfaces. The cap pivot joint is secured by a pin, held in place by a screw, and its interface with the cap is facilitated by bushings, ensuring smoother operation. The reliance on friction to secure parts was eliminated by using screws, enhancing the overall robustness of the assembly. The steel wire rod was replaced with a 3D printed model, providing the Sample Tube with more consistent characteristics, as it no longer



depends on a bent wire. Both rod joints consist of bushings and pins secured by rings. The cover and the upper component of the stationary system in the previous prototype functioned to prevent rotation. However, when torsional forces were applied, the friction between these two components often caused the Sample Tube to lock up. To circumvent this issue while still preventing rotation, two sliding pins inside the springs were incorporated into the design.

Due to similarities with the final design, the Fifth Prototype will be shown with the Detailed Design in Section 6.1.

## 5.2 Sample Stowage Device

Sample stowage in the context of the Surface Avatar refers to a designated location where all the collected samples will be stored and secured. This area serves as a crucial repository for the samples, ensuring their preservation and protection during a real mission. The collected material, whether soil, rocks, or other specimens, can be safely stored in the sample stowage for subsequent analysis, experimentation, and potential transport back to Earth.

Following the description of the mission and the needs to be addressed regarding the Surface Avatar, this Section presents the design development of the Sample Stowage Device system. Starting with the requirement in Sections 5.2.1, 5.2.2, and 5.2.3. Overall, the design of the Sample Stowage Device system should take considerations of geometry, kinematics, forces, material, signals, quality control, operation, and maintenance to meet the functional requirements of receiving, stowing, delivering and communicating with the mission command.

In Section 5.2.4, the Concept Phase is presented and described. A function diagram is created for each device to be developed, and is based on the list of requirements. Following this, concepts are developed for each required function. Selection criteria are then defined, resulting in the final selection of concepts.

Section 5.2.5 is dedicated to the development of the preliminary design, and describes the evolution of the Sample Stowage Device system's design through the development process.

### 5.2.1 General Requirements

The initial set of requirements provides a broad overview of expectations for the Sample Stowage Device. Similar to the Sample Tube case, these requirements are divided into functional and non-functional categories. These general requirements form the basis for two distinct lists: Storage Device requirements, and Receptacle and Delivery Device requirements.

### Functional Requirements (FR)

**FR01 - The Sample Stowage Device shall communicate with the mission command:** The system should provide real-time information about its status, which includes currently executed commands, the position of key mechanical components, and the presence of sample tubes. It should also allow mission command to input instructions for initiating and terminating tasks.

**FR02 - The Sample Stowage Device shall communicate with the Sample Tube:** The system should be able to retrieve information about the Sample Tube, such as the ID, and sense the presence of it.

### Non-Functional Requirements (NFR)

**NFR01 - All the equipment shall fit inside the lander:** All the parts related to the Sample Stowage Device must be inside the lander.

**NFR02 - All the equipment should be hidden when not in use:** All the parts should be hidden inside the lander when the mission is not operating the protocols related to the Sample Tube.

**NFR03 - The Sample Stowage Device should possess a storage device for the Sample Tubes:** the system should contain a device to keep the Sample tubes stored.

**NFR04 -The Sample Stowage Device should feature a receptacle device to receive the Sample Tube:** The system should contain a mean to add new Sample Tubes to the storage.

**NFR05 - The Sample Stowage Device should include a delivery device for dispensing the Sample Tube:** The System should contain a mean to retrieve the sample tubes from the storage device

**NFR06 - The Sample Stowage Device shall be electrically powered:** Due to limitation on other types of energy carriers, like pneumatic one, the Sample Stowage Device should run exclusively with electrical power.

**NFR07 - The Sample Stowage Device should use off-the-shelf components:** As previously explained, to keep development cost and time low, the system should utilize as many off-the-shelf parts as possible.

### 5.2.2 Storage Device Requirements

The need for a storage device comes from the general requirement NFR03. It states that the Sample Stowage Device should have a mechanism to store the sample tubes. Thus, this Section presents the requirements for the Storage Device.

#### Functional Requirements (FR)

**FR03 - The storage device should make an empty slot reachable for the receptacle device.**

**FR04 - The storage device should receive the Sample Tubes from the receptacle device.**

**FR05 - The storage device should stow the Sample Tubes in a slot:** The device should be able to store a set of sample tubes.

**FR06 - The storage device should provide the Sample Tubes to the delivery device.**

**FR07 - The storage device should be able to identify whether these slots are used or not:** This requirement is essential for operating the device correctly. It involves knowing where to position the tubes and informing mission control about the number of tubes stored in the device.

#### Non-Functional Requirements (NFR)

**NFR08 - The storage device should be able to store a minimum amount of 8 sample tubes at once:** With this configuration, the mission can mimic a situation where some storage slots are filled with used and unused sample tubes, as well as empty slots which are available for receiving tubes delivered by robots.

### 5.2.3 Receptacle and Delivery Devices Requirements

The need for a receptacle device comes from the general requirement NFR04. It states that the Sample Stowage Device should be able to receive the sample tubes. The requirement NFR05 demands a delivery device, which should be able to deliver sample tubes. Their requirements are similar, thus, this Section presents the requirements for both Device, highlighting possible differences that they might have.

### Functional Requirements (FR)

**FR08 - The receptacle device should move to the transfer point:** The receptacle device should be able to reach the transfer point.

**FR09 - The receptacle device shall receive the Sample Tube from TINA:** The receptacle device should provide means to receive securely the Sample Tube from TINA.

**FR10 - The receptacle device should move from the transfer point to the storage device area:** The receptacle device should be able to reach the transfer point.

**FR11 - The receptacle device should transfer the sample tube to the storage device:** The receptacle device should provide means to transfer securely the Sample Tube to the storage device.

**FR14 - The delivery device should retrieve the sample tube from the storage device:** The device should provide a method for retrieving sample tubes from storage.

**FR15 - The delivery device should move to a transfer point:** The delivery device should be able to reach the transfer point.

**FR16 - The delivery device shall ensure that the Sample Tube has always the same orientation upon reaching the transfer point:** Given the characteristics of TINA mentioned earlier, the delivery device must consistently position the Sample Tubes in the same orientation. This ensures correct grasping by TINA's gripper.

**FR17 - The delivery device shall deliver the Sample Tube to TINA:** Once the device consistently reaches the transfer point in the same position and orientation, it should provide a method to transfer the Sample Tubes to TINA.

**FR12 - The receptacle and delivery devices should communicate its state to the mission control:** The devices should be able to communicate the status of each possible operation they might have.

**FR13 - The receptacle and delivery devices device should identify the presence of a Sample Tube:** The device should detect the presence of the Sample Tube to confirm its correct receipt and communicate as necessary.

### Non-Functional Requirements (NFR)

**NFR09 - The receptacle and delivery devices must provide a minimum clearance of 30mm around the sample tube for the robotic gripper operation.**

**NFR10 - The receptacle and delivery devices should be at a transfer point to receive or deliver the Sample Tube** To aid understanding, the location where sample tubes are received or delivered to TINA is referred to as the transfer point.

**NFR11 - The transfer point should be within a reachable point of TINA:** Since the process of retrieving or delivering Sample Tubes from the Sample Stowage Device involves TINA, the transfer point should be accessible by the robotic arm.

**NFR12 - The transfer point should be always in the same position:** each TINA's motion planning tasks is done offline for the first two sessions. To facilitate the protocols involving the Sample Tubes, they must be delivered and retrieved always in the same position.

**NFR14 - The receptacle and delivery devices should be mechanically or electrically operated:** The operation could be provided by either purely mechanical motions without any motors or actuators, or by electrical mechanical means.

#### 5.2.4 Conceptual Phase

This section firstly presents the function structure of the Sample Stowage Device, in order to guide the concept creation and further merge to formulate solutions and select the best according to the determined criteria.

##### General Function Structure

With the list of requirements clearly defined, it becomes possible to construct functional structures that represent the tasks the system is required to perform. Figure 5.8 depicts a general functional structure. In this structure, the flow of material symbolizes the Sample Tube, signals represent commands and state communication, and energy signifies electrical power. Note that other types of energy, such as heat, are disregarded as these can vary depending on the specific design adopted. Each general function is further subdivided into a sub-function structure, enabling a more detailed representation of each task that the Sample Stowage Device system is expected to execute.

##### Storage Device Function Structure

In order to construct the functional structure for the Storage Device, some assumptions are made. Firstly, a component called 'slot' is defined to better represent what should hold and store the Sample Tubes. The Storage Device directly interacts with the Receptacle and Delivery Devices, which allows for a complete cycle of receiving and delivering Sample Tubes.

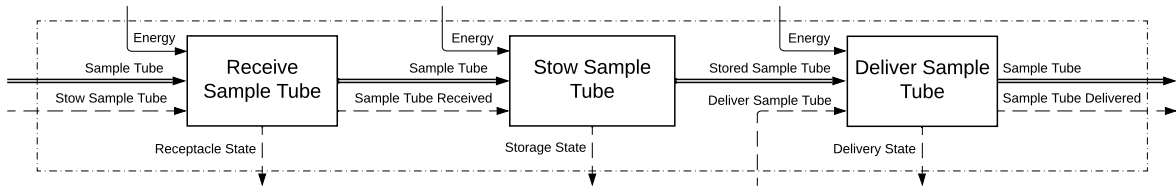


Figure 5.8: General Functional Structure of Sample Stowage Device.

Figure 5.9 illustrates the expected functionality of the Storage Device. To meet the communication requirements, the system indicates its states, revealing the availability of storage and providing the ID of stored Sample Tubes. The material flow represents the Sample Tube, which acts as an input when received for storage, and as an output when delivered for external use. The 'slot' is also an important material flow component, as its physical state changes with each step of the storage procedure. Lastly, as stated in the general functions, energy only represents electrical power.

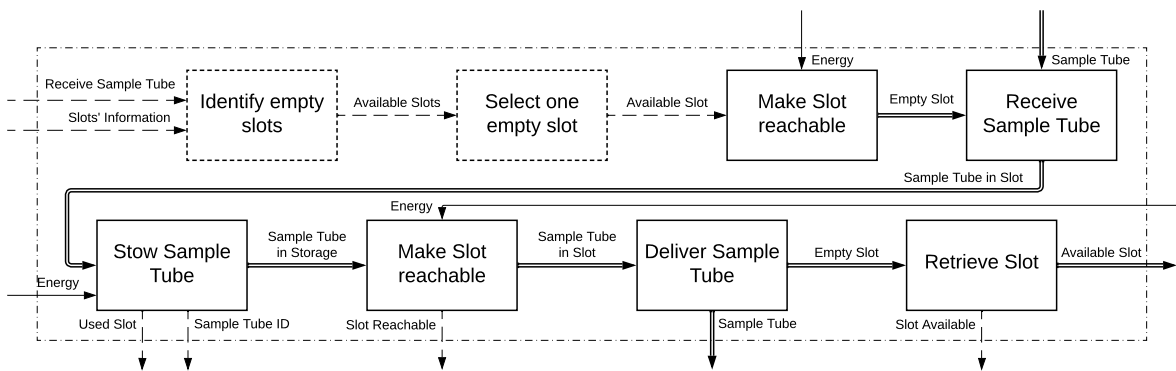


Figure 5.9: Storage Device Functional Structure of Sample Stowage Device.

### Receptacle Device Function Structure

In the function structure of the Receptacle Device, a component called 'slot' is also defined. However, it differs from the slot in the Storage Device function representation. Here, the 'slot' serves as a component that moves the Sample Tube through the space, providing the necessary interface between the storage location and the transfer point.

Figure 5.10 shows the function structure. It has internal signals that provide the controller with important information about the states of the receptacle device. It also has external signals,

which include inputs representing commands to execute specific tasks, and outputs, which communicate the device's states to mission control. The function structure represents the slot and the Sample Tubes as material flow, and electrical power as energy flow.

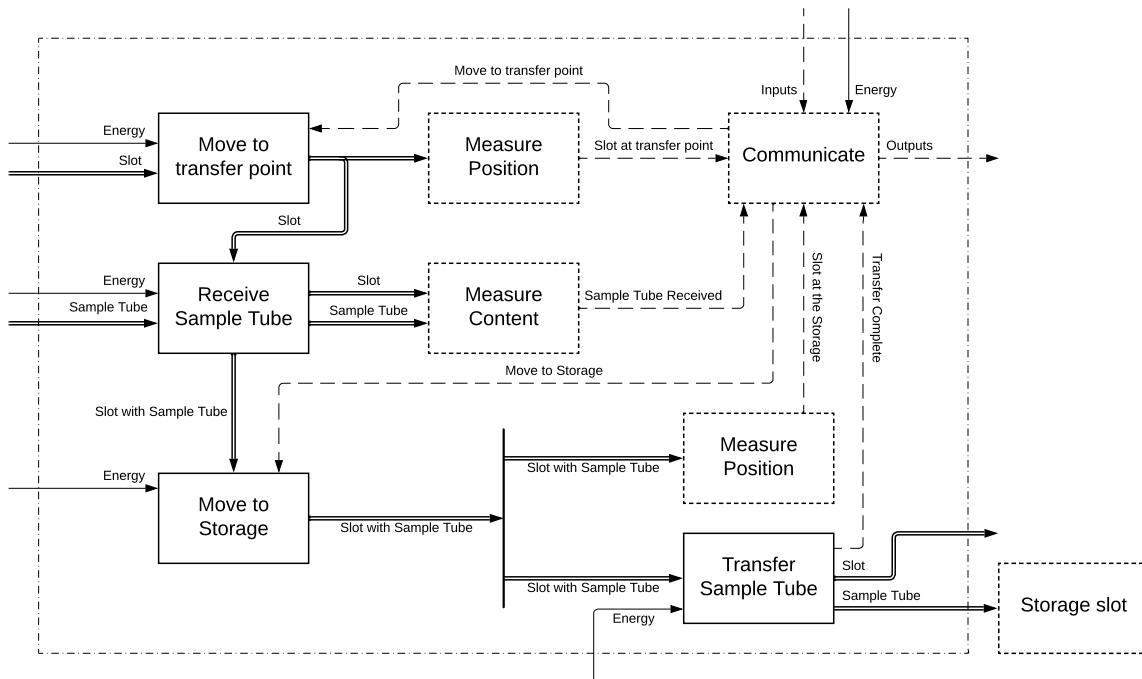


Figure 5.10: Receptacle Device Functional Structure of Sample Stowage Device.

### Delivery Device Function Structure

The last function structure represents the delivery device, which is similar to the receptacle one. The only difference is due to the requirement **FR16**. This requirement necessitates not only delivering the Sample Tube to the transfer position but also ensuring its correct orientation. Figure 5.11 shows how this requirement influences the functional structure.

### Concepts for Storage Device

During the concept development for the Storage Device, many possibilities were considered. This report discusses two concepts and explains the selection of the optimal one. These concepts were created based on the functional structure displayed in Figure 5.9.

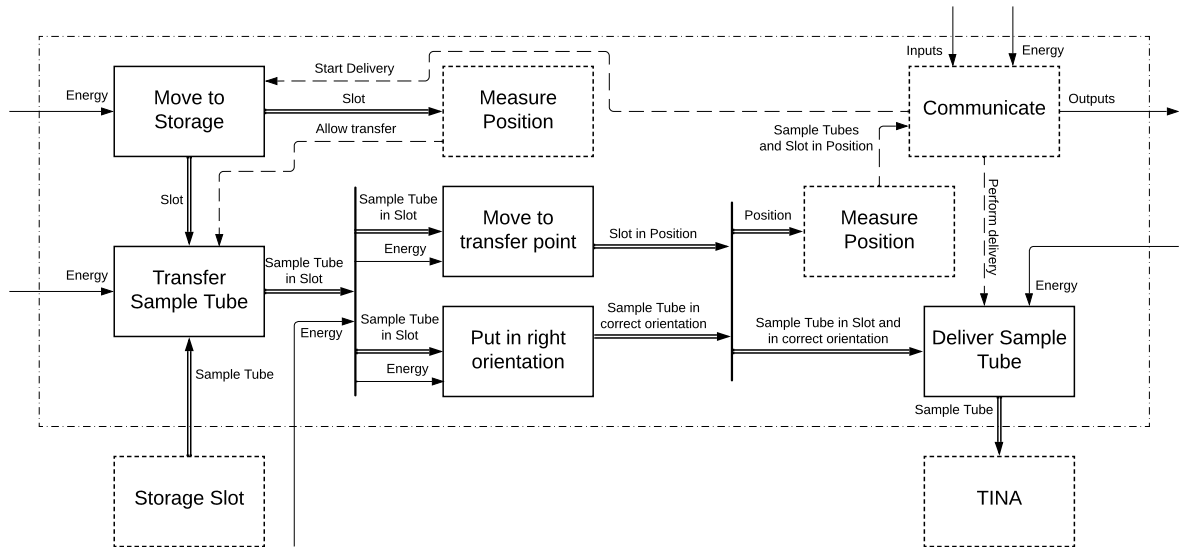


Figure 5.11: Delivery Device Functional Structure of Sample Stowage Device.

The two primary functions of the Storage Device are to stow the Sample Tube and to transport it to a position accessible by the robot. To fulfill the first function, we conceived a slot in a cup format where the Sample Tube can be placed and held securely. This concept is illustrated in Figure 5.12.

To address the second function, we devised two mechanisms. The first is a rotating plate with fixed slots. When a specific slot is required, the entire storage rotates to position the slot for use by the Receptacle and Delivery Devices. This rotating concept is shown in Figure 5.12a.

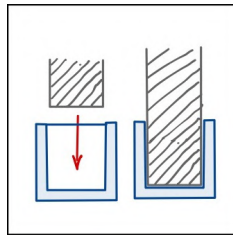
The second concept, shown in Figure 5.12b, involves a continuous loop where the slots slide on a track, following a straight line, and curving 180 degrees at each end. This allows the slot to travel to the desired position.

The rotating concept was chosen over the continuous loop for its simplicity in design, operation, and maintenance. While the continuous loop offers better space optimization, it has a more complex mechanism, involving many more moving parts to achieve the same goal as the rotating mechanism.

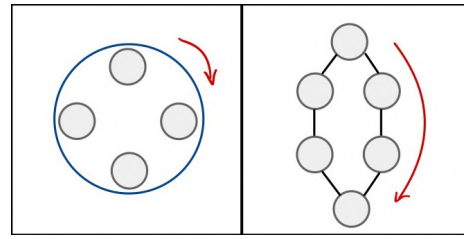
### Concepts for Receptacle and Delivery Devices

Three concepts for Receptacle and Delivery Devices were created. The first concept involves a drawer-like mechanism where the rotating stowage is installed. When transferring a Sample





(a) Sample Tube Slot concept.



(b) Concepts for moving the Sample Tube to the transfer point.

Figure 5.12: Concepts for Storage Device.

Tube between the Stowage Device and TINA is needed, the drawer opens, revealing the Storage Device and positioning the slot for transfer. A sketch of this mechanism can be found in Figure 5.13.

The second concept involves a mechanism that grasps the slot with the Sample Tube and brings it to the transfer point. This could be achieved by a pantograph mechanism which, during its extension, detaches the slot from the Storage Device. During contraction, it reattaches the slot, thereby providing delivery and retrieval functions.

The third concept involves leaving the slots inside the lander near its lateral wall, creating a window that provides direct access to the Sample Tubes.

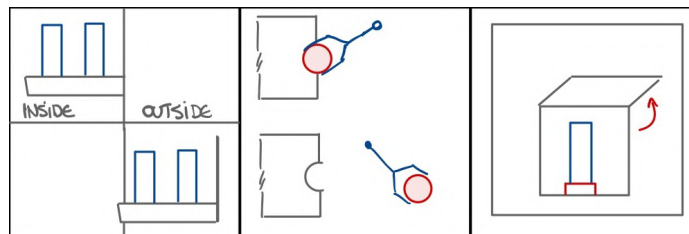


Figure 5.13: Concepts for the Receptacle and Delivery Devices.

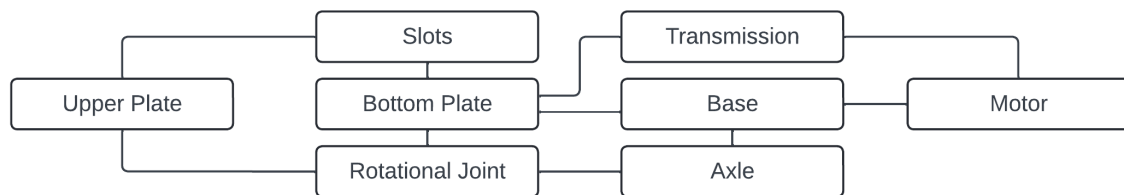
The first concept was chosen because of its simplicity in implementation, and its increased reachability and efficient use of space. The pantograph mechanism is feasible, but the drawer mechanism can be designed to be more robust and, consequently, more reliable. Designing the Storage Device with a detachable slot is more complex. Though the first concept is more complex than the third, it offers better reachability and more efficient use of space inside the lander. This is because TINA needs space inside the lander to grasp and remove the Sample Tube, which is not required when using the drawer mechanism.

### 5.2.5 Preliminary Design

The selected solution consists of a system divided into two subsystems. The first is the Rotating Device, which encompasses all functions of the Storage Device and some aspects of the Receptacle and Delivery Devices. The second subsystem, known as the Translating Device, is tasked with reaching the transfer point. The Rotating Device should be encased and connected to the Translating Device. A surface cover will be designed to conceal the mechanisms and integrated into the Lander to improve its aesthetics. It's also worth noting that the diameter of the Sample Tube is defined as 36 mm.

#### Rotational Stowage Unit

The design for the Rotating Device consists of slots between two circular plates, a fixed axle connecting them to the base via a rotational joint, and a motor and transmission for rotational movement. By understanding the interaction between each component, we can determine their design order. As shown in the interaction map in Figure 5.14, the Bottom Plate interacts with four other components, followed by the Base and Rotational Joint, each with three interactions. These three components were therefore designed first.



*Figure 5.14: Tina used in Surface Avatar. Note that the gripper of this Image differs from the one used during the experiments.*

Due to space limitations within the Lander, a maximum diameter of 250 mm was set for the circular plate. This determined the number of slots for the Sample Tubes, which, considering the clearance required for the robotic grippers (requirements NFR09 and NFR15), was six. The slots, designed to accommodate the tubes, need circular holes in both the top and bottom plates. The slots should have an internal diameter of 36mm, with a tolerance allowing the tube to slide inside.

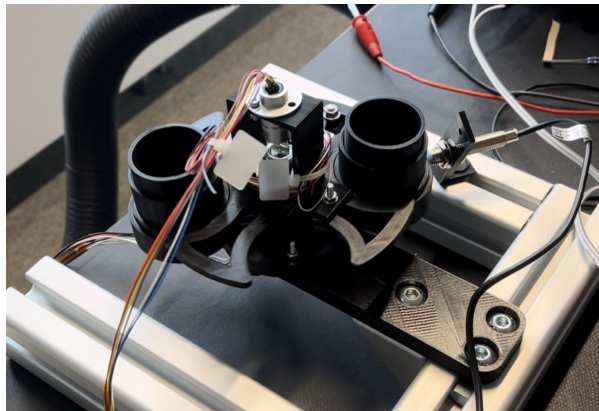
The assembly of plates and slots is compressed against the base by the axle, which also allows for rotation around the fixed axle. To enable this rotation under compressive force, an axial roller bearing was chosen. As the axle diameter is 10mm, the roller bearing should be compatible.

Assumptions about rotational inertia informed the selection of the motor and transmission. We set a maximum acceleration of  $0.5 \text{ U/s}^2$  and speed of  $0.25 \text{ U/s}$  to ensure operation time is less than 30 seconds (NFR13 and NFR16). This led to the choice of the brushless DC-Gearmotors with a transmission ratio of at least 5:1. A 6:1 internal transmission gear was chosen due to availability and compliance with the minimum transmission ratio. The motor allows precise position control but requires a full rotation for calibration, handled by an inductive proximity switch.

The selection of the motor and transmission initiated the base design, considering its interface with the roller bearing and housing.

Finally, considering internal sensors to detect a Sample Tube and retrieve its ID, cabling is critical. As the slots rotate but the base and electronics remain stationary, a rotating interface is needed to prevent cable damage. A slip ring was chosen to fulfill this requirement.

To prove the solution concept, a prototype was built to test the rotation mechanism and its integration with the motor and sensors. The Figure 5.15 shows the equipment built with 3D printing techniques. This prototype proved that the concept worked as expected, but with a few modifications needed. First one regards the inductive proximity switch position, which should be attached to the base to better future integration with the housing. The base should be better designed to enhance the interface between components.



*Figure 5.15: RSU prototype developed to prove the concept.*

### **Extended Reachability Unit**

The Extended Reachability Unit is part of the assembly that includes the housing for the Rotational Stowage Unit. The housing needs to have support to secure its base, and there should

be a rail on which the housing can slide. The assembly should also include a rack and pinion mechanism, as well as a motor. All these components are mounted on a base structure, which is then assembled into the frame of the Lander.

The housing is connected to the base of the Rotational Stowage Unit and is built from off-the-shelf structures with a 20mm profile. It is designed to provide clearance for Tina, but it should be completely hidden when retracted. The housing is covered with laser cut plates that are fixed with screws, and it is connected to the slide rails.

The slide is a telescopic rail with 300 mm of travel. It is connected to the housing and the base structure. The rack, which is an extension of the housing, is positioned on the bottom side of the housing. It has a length of 450mm, offering the possibility for future extension if the slide is modified.

The pinion is attached to the base structure, and it is driven by the motor. The system does not require a position sensor, as the motor can precisely determine its position. The system is calibrated by sliding off and determining the position when it hits the full retrieved position.

### 5.3 TINA Integration

TINA, a robotic manipulator, plays a crucial role in the Lander's objectives. Her capabilities include delivering objects worldwide, retrieving items for the Lander's internal equipment like the Sample Stowage Device, and performing manipulations such as assembling equipment. To ensure the most efficient performance, her installation should be done in a manner that maximizes the workspace.

Another key aspect of its operation is the ability to operate using only pre-defined motion planning, i.e., without relying on vision or object identification for navigation. Therefore, the installation of TINA must be precise, and the connection between TINA's base and the Lander should be rigid enough to prevent significant torsion or bending when manipulating objects far from its attachment point.

The description above leads to the TINA integration requirements:

**NFR01 - TINA arm shall be installed in a base:** the base should also utilize off-the-shelf components, preferably using the same construction profile as the Lander's frame.

**NFR02 - Base should be part of Lander structure:** the base must guarantee a satisfying integration with the Lander's frame.

**NFR03 - TINA and base should be installed in front left side of the Lander.**

**NFR04 - Base should be installed in a position to maximize the TINA's workspace.**

**NFR05 - Base should be installed in a position that minimizes the distance between TINA's base and and base attachment point.**

### 5.3.1 Optimization Problem

To determine the optimum position of TINA's base, an optimization problem was defined. The design variables are the  $(x, y, z)$  position in space regarding the geometrical center of the TINA's base. There are two objective functions, each one derived from the requirements NFR04 and NFR05. Finally, the inequality constrain given by the requirement NFR03, which specifies the region that TINA must be installed.

### 5.3.2 TINA Simplification

The particle swarm algorithm, used to solve this optimization problem, requires a large number of particle, in which it must assess the objective function value. Thus, using the complex design and assessing TINA workspace via Inverse Kinematics is too costly to compute. Therefore, a simplification of the problem is required and depicted in Figure 5.16.

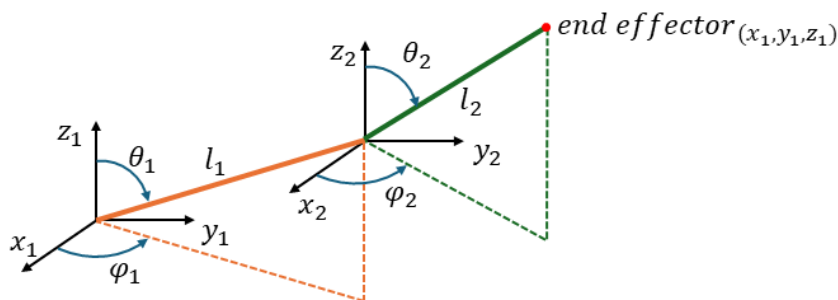


Figure 5.16: Representation of TINA using polar and azimuthal angles.

To simplify the problem, TINA is considered as a robot composed of two line segments, with the start of the first at the base position. The end of the first segment is connected to the beginning of the second. The endpoint is considered the end of the second segment. To define the pose of the arm, polar and azimuthal angles are used:  $\theta_1, \varphi_1, \theta_2, \varphi_2$ . This simplification results in a problem with four degrees of freedom, which is considerably faster to compute than TINA's 7 DoF. Simplifying to straight lines also makes it easier to compute collisions between the arm representation and the Lander.

**Objective Function: TINA's workspace**

The first objective function relates to TINA's workspace. Based on the  $(x_b, y_b, z_b)$  position of the base, this function outputs a score indicating the number of points TINA can reach without colliding with the Lander or the floor. These points are defined by the polar and azimuthal angles of each segment of the arm according to Figure 5.16. If a given point is inside the box of interest and the arm pose is not colliding with anything, it is considered valid. For a given  $k$  number of points, the following equation mathematically represents the described objective function.

$$f_1(x_b, y_b, z_b) = \sum_{i=0}^k \frac{p_i}{k}, \quad p_i = \begin{cases} p_i = 1 & \text{if is in the box and not colliding} \\ p_i = 0 & \text{otherwise} \end{cases} \quad (5.1)$$

**Objective Function: distance between TINA's base and the attachment point**

The proposed base is susceptible of two relevant deformation means. The first one is due to bending moment. Considering that the problem can be simplified as a cantilever beam of a length  $L$  and with a load  $P$  concentrated at the free end, the slop  $\theta$  at free end and the maximum deflection  $\delta_{max}$  can be determined as:

$$\theta = \frac{PL^2}{2EI}, \quad \delta = \frac{PL^3}{3EI}. \quad (5.2)$$

Another relevant mean of deformation comes from torsional forces. Thus, given a torque  $T$  applied in the direction of the beam main axle, and the beam length  $L$ , the twist angle can be defined as:

$$\varphi = \frac{TL}{GI_p} \quad (5.3)$$

It is possible to determine the  $L$  by calculating the distance between the plane formed by the front left surface of the Lander and the point where the base is attached. Given a plane  $ax + by + cz + d = 0$ , the distance is

$$L(x_b, y_b, z_b) = \frac{|ax_p + by_p + cz_p + d|}{\sqrt{a^2 + b^2 + c^2}}. \quad (5.4)$$

Since the strongest dependency comes from the maximum deflection  $\delta_{max}$ , the second objective function can be determined as:

$$f_2(x_b, y_b, z_b) = L^3 \quad (5.5)$$

### Unified Objective Function

To create a single function for minimization, the inverse of  $f_1$  is combined with  $f_2$ . Each function is normalized individually by factors  $n_1$  and  $n_2$ , producing values between 0 and 1. Then, each function is assigned a weight ( $w_i$ ) to represent its importance in the position optimization. The weight  $w_1$  for the TINA's workspace function is set at 0.7, and  $w_2$  at 0.3. The first function is given a higher weight because reachability is deemed more important than rigidity. In other words, it is acceptable to sacrifice rigidity to enhance the workspace, but the reverse is not true. The Equation 5.6 shows the final objective function.

$$f(x_b, y_b, z_b) = w_1 n_1 f_1^{-1} + w_2 n_2 f_2 \quad (5.6)$$

#### 5.3.3 Particle Swarm Optimization

In order to optimize the positioning of TINA, the Particle Swarm algorithm (Banks et al. 2007; M. Shami et al. 2022; Poli et al. 2007) was chosen. One of the primary reasons behind this choice is that the algorithm does not necessitate the use of the function gradient. This quality proves to be highly beneficial in this context, particularly because determining the function gradient for  $f_1$  presents its own set of challenges. Consequently, the use of the Particle Swarm algorithm simplifies the process of optimizing TINA's positioning, making it a more efficient and effective solution for this task.

Particle Swarm Optimization (PSO) is a computational method that optimizes a problem by iteratively trying to improve a candidate solution with regard to a given measure of quality, or 'fitness function'. It solves a problem by having a population of candidate solutions, or 'particles', and moving these particles around in the search-space according to simple mathematical formulae. These movements are guided by the particle's own best known position in the search-space as well as the entire swarm's best known position. When optimized, the swarm's position should represent the best solution.

PSO is initialized with a group of random particles and then searches for optima by updating generations. It has two main operators: velocity updating and position updating. Velocity on each dimension is influenced by the distance between the current particle position and pbest and gbest positions. PSO is expected to move the particles toward the best solutions.

Advantages of PSO include the fact that its concept is relatively easy to understand, and that it often works effectively with continuous nonlinear functions. Furthermore, PSO is more efficient than other evolutionary algorithms in terms of computer memory and computational time.

### 5.3.4 Particle Swarm Optimization Implementation

The code implementation was done in Python using the PySwarms (Miranda 2018) package to perform Particle Swarm Optimization. The process starts with a simple function that transforms the polar and azimuthal angles of each section into their start and end points. This is later used to determine if the segments are colliding with the Lander and to identify the reached point, which can be inside or outside the box of interest.

The implementation of the first objective function is more complex compared to the second. Firstly, the code takes the Cartesian coordinates of the end tip of the arm and checks if it is in the box of interest. If it is inside, it then verifies if the segments are colliding with the Lander. If free of collisions, the point is valid, increasing the base position score.

The second objective function is simpler to compute. It requires the arm's base position to infer the distance between the arm base and the plane of attachment. The code takes the Cartesian coordinates of the arm base and computes the distance to the given plane. The result is then divided by the maximum allowed distance, normalizing the result.

There is an overall objective function that combines both functions into one. This function creates an array of values for each angle with a predefined discretization, then computes the first objective function value. Next, it computes the second objective function. Finally, it returns the final score, which is the weighted sum of the results from both objective functions.

The score is then used by the PySwarms algorithm to compute the best base position. The algorithm allows full control of the optimizer parameters, including the number of particles and iterations, addition of bounds, and choosing the  $c_1$ ,  $c_2$ ,  $w$  parameters that dictate the particles' behavior.

With the main functions created, the code was tested to confirm that it correctly computes the collisions and the end tip position. The code was then parallelized, and its results were compared with the non-parallelized code, showing similar outcomes. The entire code can be seen in Appendice D and a representation of it in Algorithm 5.1.

The code requires input for some optimization hyperparameters. One of these is the discretization of the polar and azimuthal angles, which significantly impacts the running time. A test was conducted to verify the consistency of the cost function for different discretizations using the same base positions. Figure 5.17 shows the results, indicating that discretization doesn't



*Algorithm 5.1: Simplified Objective Function for Collision Detection***Require:** *start\_points*, *options***Ensure:** Collision scores for each starting point

```

1: Rotate start_points
2: Load options from options
3: Initialize score array
4: for all start_point in start_points do
5:   Initialize collisions and tasks
6:   for each combination of angles do
7:     Create task with current angles and start_point
8:     Add task to tasks
9:   end for
10:  Compute collisions using parallel processing
11:  Calculate collision_rate
12:  Calculate distance to attachment plane
13:  Update score with weighted sum of collision_rate and distance
14: end for
    return score

```

significantly impact cost computation. Therefore, for optimization, a lower discretization can be used to speed up the code.

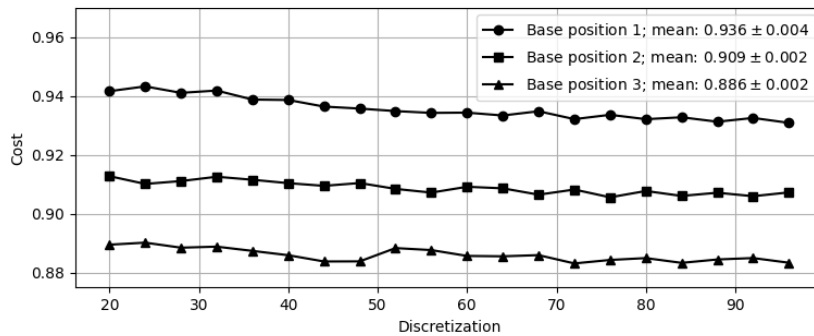


Figure 5.17: For the same three base positions, the cost of function was computed changing only the discretization.

## 5.4 Hands-On Tray

The necessity for a work and handling space near the lander derives from the requirement to facilitate the transfer of objects between the robot and the lander or between multiple robots, and provide a space to manipulate equipment. In response to this need, a Tray positioned in front of the lander serves as a solution by offering a designated space for seamless object manipulation and exchange. To ensure efficiency in its design, several key aspects must be considered, which are explained in this Section.

Firstly, the Tray must provide a stable base for secure object handling, ensuring that objects can be manipulated and transferred reliably. Secondly, the Tray should accommodate the operational requirements of the robots. It must be designed to offer a workspace specific to each robot, enabling them to perform their tasks without degrading the workspace of the other robot. This consideration is crucial for maintaining operational independence and efficiency, allowing robots to work in their optimum way without interference.

Therefore, the Tray needs can be summarized into these two requirements:

**NFR01 - The tray should provide space for secure object handling.**

**FR01 - The tray should adapt itself to fulfill the robot's capabilities.**

**FR02 - The tray should adapt itself according to the object being handled.**

By addressing these aspects in the Tray's design, the mission can ensure a smooth and effective workflow for object transfer and robot operations in the proximity of the lander. This guarantees a higher level of flexibility for the Lander during its operation.

### 5.4.1 Conceptual Phase

Before starting the conceptual phase description, it is necessary to understand the limitations that bound the Tray development. The main functionality is already defined, which is moving the tray up and down to adapt to the operation, fulfilling requirements FR01 and FR02. Therefore, many components were previously defined by availability and must be included in the Tray design.

The tray itself is a 1000 x 800 mm metal plate, supported by a 40 x 40 mm aluminum construction profile. This setup uses a linear guide, which is attached to a rail. An electric motor provides vertical motion to the tray. With these limitations, the conceptual phase can focus on the mechanism layout, using the motor and the linear guide as needed. Sensor integration can also be addressed here.

## Function Structure

To clarify the requirements for the conceptual phase, Figure 5.18 shows a Function Structure of the Hands-on Tray. The main function is to move the tray. This is supported by a sensory system that detects the tray's position and communicates this information to the controller. The controller then decides where the tray should be positioned based on this information.

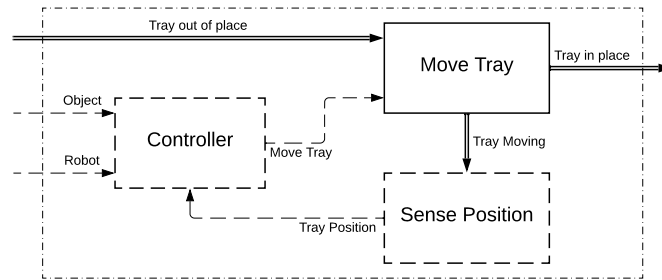


Figure 5.18: Functional Structure of Hands-on Tray.

The function structure indicates that the Tray system interacts with the object and robot involved. However, this can vary based on the Tray's development. Other options may include receiving the required tray position directly or implementing a way to detect the robot and the object, then deciding where to move without needing complex information from the mission command.

## Concepts

The concepts considered are shown in Figure 5.19. Both are similar in construction, using predefined components. The first concept has a motor installed under the tray, while the second one has the motor located above the tray.

To select the best concept for the Hands-on Tray development, the height range was considered. The first concept can reach a high height, at the same level as the Cargo Bay floor, but it can't reach a low height due to the motor's location. The second concept can reach the MUSA floor by having the motor above it, but it can't reach the Cargo Bay floor level.

Due to limitations regarding the operation of Interact Rover and Bert, the selected concept is the second one. It is more useful for the mission because it allows the Tray to reach both lower and higher heights.

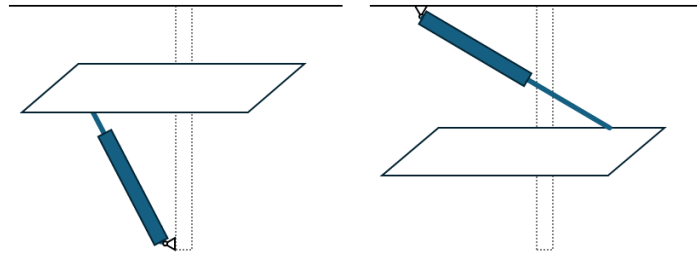


Figure 5.19: Concepts for the Hands-on Tray. On the left: motor installed under the tray; on the right: motor installed above the tray.

#### 5.4.2 Preliminary Design

The preliminary design of the Hands-on Tray involves deciding the placement of each component and analyzing which configuration provides the best height range. Figure 5.20 shows a simplification of the Tray mechanism, which is defined as:

$$\max(h(d)) = H - \sqrt{(L+l)^2 - (P_x + d)^2} \quad (5.7)$$

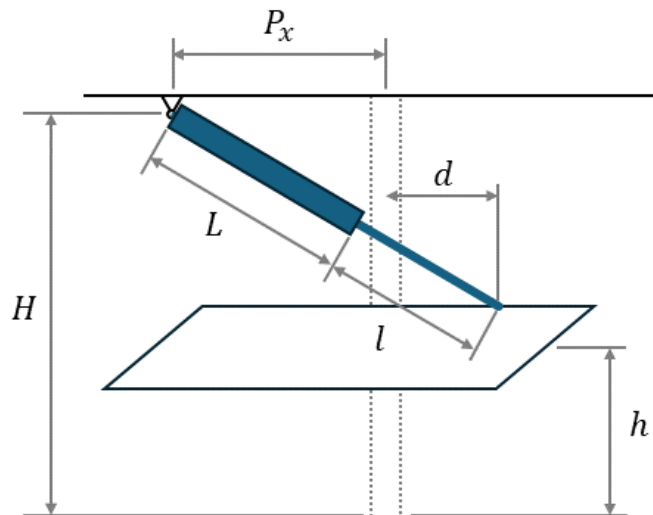


Figure 5.20: Functional Structure of Hands-on Tray.

The geometrical parameters are given by  $H$ ,  $P_x$ ,  $L$ , and  $l$ , with values in meters.  $H = 1.050$  represents the height of the motor joint attached to the bottom of the Lander.  $P_x = 0.400$  represents the distance between this joint and the symmetry plane of the Lander, where the linear rail guide is installed.  $L = 0.770$  represents the length of the motor when fully retracted.  $l$  represents the extension of the motor and can range from  $0.0 \leq l \leq 0.502$ . Finally,  $d$  represents the design variable and is the distance between the symmetry plane and the joint where the motor connects to the Tray structure.

A constraint for  $d$  can be defined by imposing that when  $l = 0.480$ , the height should be  $h = 0.000$ , avoiding the need to fully extend the motor to reach the ground. This should represent the minimum height possible with the proposed mechanism. Thus, the following equation is obtained:

$$0.000 \geq 1.050 - \sqrt{(0.770 + 0.480)^2 - (0.400 + d)^2} \Rightarrow d \leq 0.276 \quad (5.8)$$

By design,  $d$  should also have a minimum value due to the installation of the anchor point in the tray. Thus,  $0.100 \leq d \leq 0.276$ .

To calculate the maximum height, the extension length should be set as minimal as possible, thus  $l = 0.000$ . This implies that the maximum height is obtained when  $d = 0.276$ . Therefore,  $h_{max}(d = 0.276, l = 0.000) = 0.681$  m.

## 6 Results

This chapter is divided into six sections. The first section shows the final design of the Sample Tube, developed from the previous chapters. Next, the final solution for the Sample Stowage Device is presented, focusing on its two major components: the Rotational Stowage Unit and the Extended Reachability Mechanism. The integration with the Sample Tube and its validation are also described.

In the third section, the results of the Particle Swarm Optimization for TINA's base position are shown and described. The following section explains the Hands-on Tray design, including a geometrical description and kinematics analysis. Next, the Cargo Bay is briefly explained. Finally, the chapter presents the final design of the entire Lander, along with the integration of systems and their validation.

### 6.1 Sample Tube

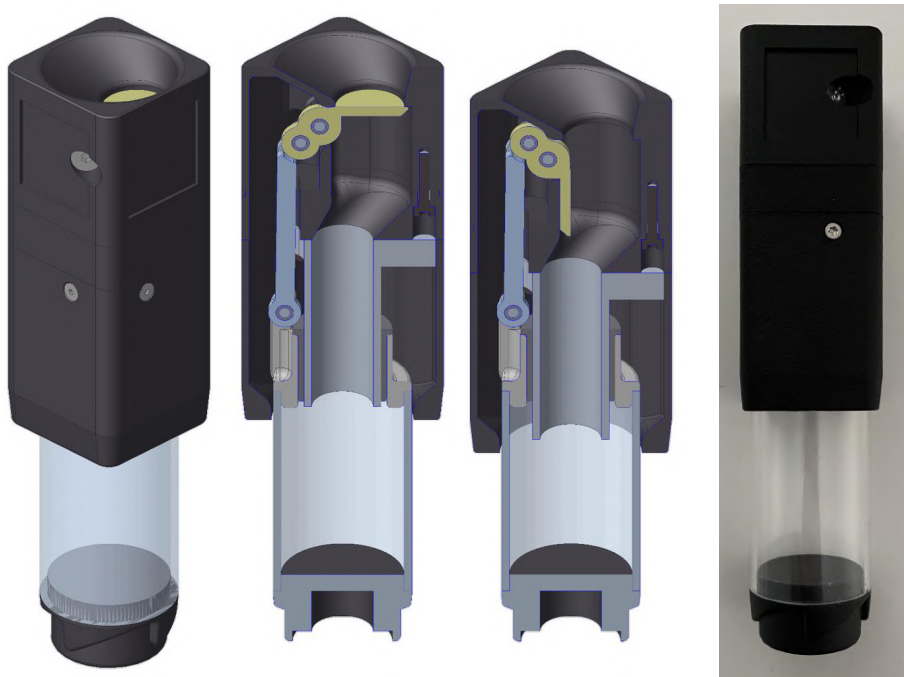
This section provides information about the detailed design, evaluation and validation of a Sample Tube. The details include the materials used, dimensions, and the specific design choices made to optimize the functionality of the Sample Tube. Also, it discusses the experiments conducted to test the efficiency and reliability of the tube in various conditions. The results from these tests provide a thorough understanding of the performance characteristics of the Sample Tube.

Figure 6.1 shows an 3D model of the final design, including a section view exposing the internal parts. Sample Tube can be divided into two major components: Cone and Tube, and Cap Mechanism.

#### 6.1.1 Cone and Tube

The Sample Tube is composed by a transparent acrylic tube with 36 mm of external diameter. The internal diameter is 32 mm, and combined with a useful height of 45 mm, the Sample Tube has an internal volume of  $36.3 \text{ cm}^3$ . These characteristics fulfill the requirements NFR03 and NFR07.

The bottom of the sample tube features an auto-centering cone (Figure 6.2a), connected to the tube by friction. This cone offers a flat surface, allowing the sample tube to stand upright. The



*Figure 6.1: Final design of the Sample Tube. The left image shows the sample tube in the closed position. The middle ones show a section of it in the opened and closed positions revealing its internal components. The right one shows the real Sample Tube assembled.*

cone also contains a circular PCB (Figure 6.2b), part of the Sample Tube ID system's passive sensor. The cone's design prevents the sensor from touching the flat surface where the sample tube is placed, yet ensures the Sample Stowage Device's active sensor can reach the Sample Tube PCB. This feature matches the requirement FR02 and NFR09.

Moreover, the cone also serves to auto-center the Sample Tube. This capability is achieved by the interaction between the cone and a centering ring, which mirrors the cone's design. Consequently, the sample tube can only be placed in four possible orientations on this centering ring. Regardless of its initial orientation, the weight of the Sample Tube and the inclined contact surfaces of the cone and ring cause the Sample Tube to rotate into a pre-defined position. Given the Sample Tube's square cross-section, this auto-centering system ensures the tube's lateral surfaces remain consistent for future handling. Figure 6.2a illustrates the cone with its auto-centering system, as well as the centering ring, which fits inside any compartment matching the Sample Tube's diameter. The auto-centering mechanism was design to fulfill the requirement FR03.

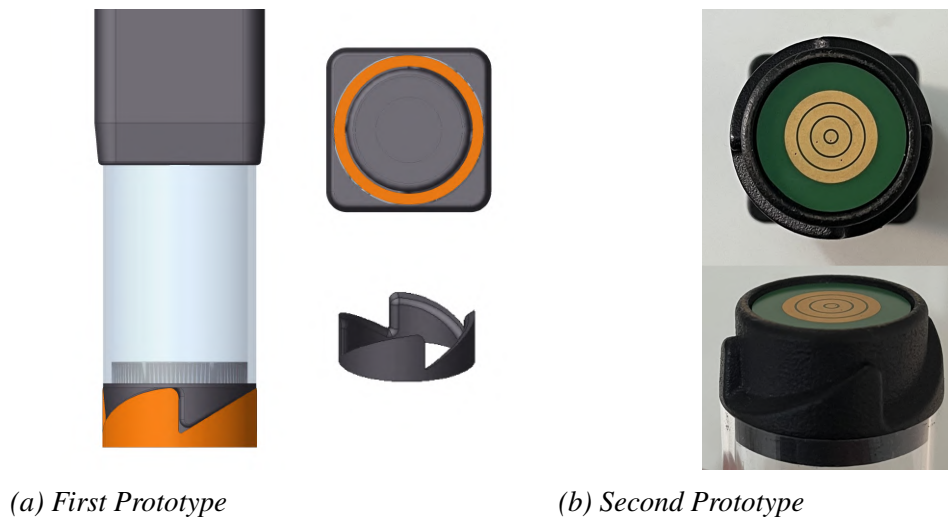


Figure 6.2: First and Second Prototypes in an assembly view.

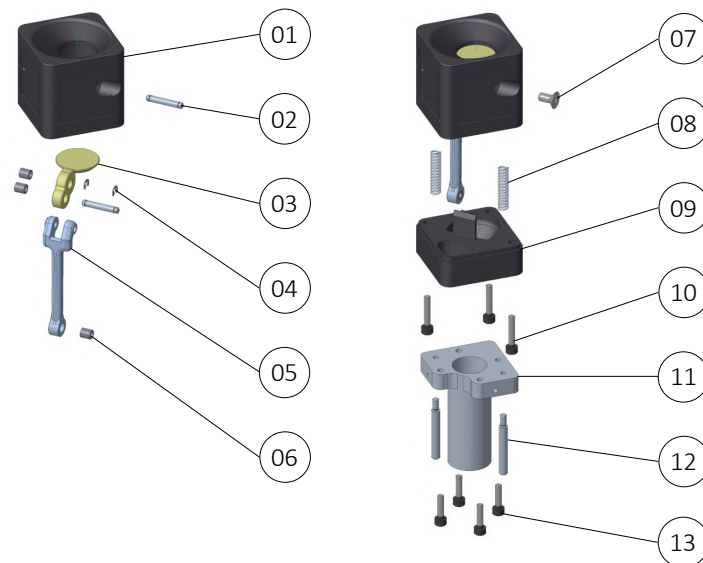
### 6.1.2 Cap Mechanism

To accomplish the requirement FR01, the cap mechanism was developed. It provides a mechanism that opens the cap when the Sample Tube is pressed down against a surface and closes it when the Sample Tube is released. The explanation of this design will be made with the aid of four exploded views of the Sample Tube.

Figure 6.3 displays the head (component 01), which contains an opening hole of 16 mm. This allows the sample to enter the tube and exceeds the required diameter of 10mm (NFR04). It is also a crucial component of the Cap Mechanism that serves as an anchor for the cap. This top part also includes a funnel to facilitate the introduction of samples into the tube. Finally, the head contains dedicated space for localization tags (NFR10). The cap (component 03) is connected to the head by a rotational joint, which consists of an axle (component 02) and a bush (component 06) to minimize friction and increase accuracy. The axle is secured by a screw (component 07) in the lateral part of the Sample Tube, and on the opposite side, there's a small hole for inserting a wire to remove the cap axle if necessary.

A rod (component 05), installed in the cap using the same rotational joint, pushes the entire top part of the Sample Tube down when pressed, causing the cap to rotate and open due to its connection to the head. The middle component (component 09) acts as an interface between the head and the sliding tube (component 11 detailed in Appendix A, and isolates the rod chamber from the canal where the samples will travel. The sliding tube, made of aluminum, provides a sliding interface between the top part and the tube, and houses the sliding pins (component 12). These pins guide the spring (component 08) installed around them, preventing rotational

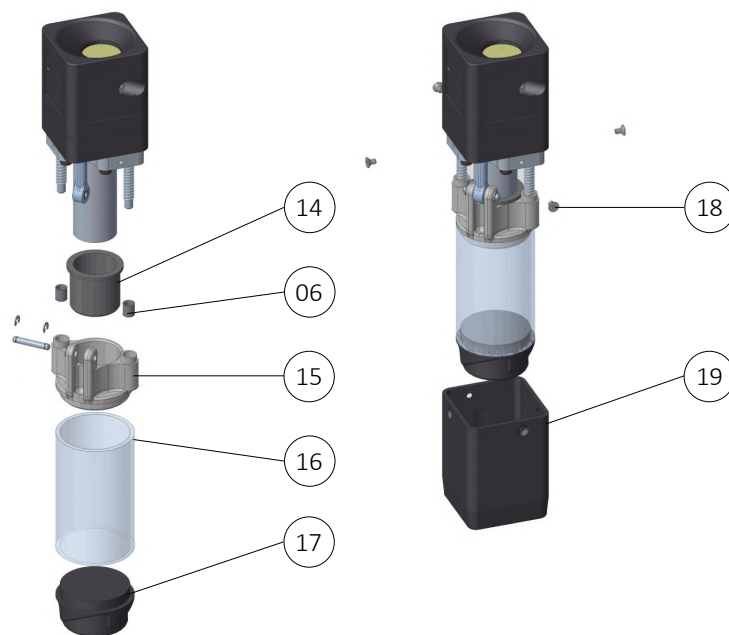




*Figure 6.3: First and second exploded view of Sample Tube.*

movement between the top part and the acrylic tube. The head, middle component, and sliding tube are all connected by screws (components 10 and 13), ensuring accuracy in the assembled mechanism.

Figure 6.4 displays the assembled upper part of the cap mechanism. It highlights the bush (component 15) that offers a suitable surface for the sliding tube's upward and downward movement. Moreover, a pair of bushes (component 6) forms a sliding joint with the anti-rotational pins. The Holder (component 15) component, which serves as the foundation for the bushes, secures all elements together. These bushes are installed in a way that they remain in place due to friction. The Holder includes a rotational joint for the rod and also functions as a spring seat. Finally, the Holder connects to the acrylic tube (component 16) via friction. Figure 6.4 also reveals the cover (component 19) that shields the mechanism and provides an increased area for gripping the Sample Tube. This cover is secured in place by four screws (component 18).



*Figure 6.4: Third and fourth exploded view of Sample Tube.*

### **Validation**

The Sample Tube measures 40x40x172mm when closed, fulfilling requirement NFR01. The final design melds the head, middle component, and cover, forming a solid structure with four flat surfaces which accommodate robotic handling, thereby meeting requirement NFR02. The Sample Tube is designed for one-handed operation, conforming to requirement NFR12. Moreover, the tube can be fully disassembled, allowing for the replacement of any damaged parts as per requirement NFR13, or for cleaning procedure in case the mechanism eventually get stuck due to dust. Finally, the Sample Tube is free of magnets, eliminating interference with Justin's hands and satisfying requirement NFR08.

A total of 12 Sample Tubes were assembled, with an average weight of  $150 \pm 3$  g. The force needed to fully open the cap averages  $7.68 \pm 0.35$  N. These results demonstrate that the design is consistent, providing similar handling characteristics across all Sample Tubes. These characteristics meet the requirements NFR05 NFR06 NFR11.

As tested with the fourth prototype and confirmed with the final Sample Tube, the design provides a solid grip for any robots required to handle the Sample Tube. For example, Justin

can firmly grasp the square-shaped top part using a pincer pose with his fingers. Meanwhile, TINA and Interact can hold it by the top part or the acrylic tube, allowing for numerous grasp positions.

The auto-centering mechanism functions as intended, allowing precise placement of the Sample Tube. In all cases, the Sample Tube can be placed with any rotation in the surface normal direction, as the mechanism ensures it rotates to the desired position. Occasionally, if the Sample Tube doesn't reach the desired position by getting stuck, this can be resolved by lifting and releasing it again.

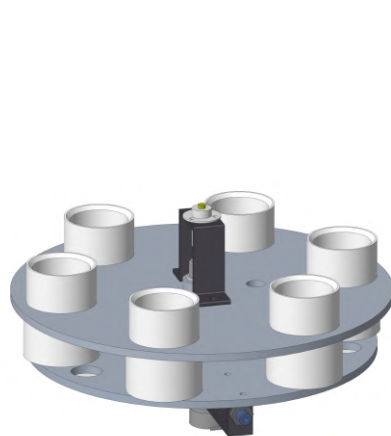
When the ring is placed on a surface alone, the mechanism allows only a small margin for error in offsetting or tilting the Sample Tube. It can tolerate an offset of 4 mm and the angle between the surface normal direction and the tube axle cannot exceed 5 degrees. To enhance the auto-centering capabilities, auxiliary devices could be designed to reduce the tilting angle and offset distance as the Sample Tube approaches the centering ring.

## 6.2 Sample Stowage Device

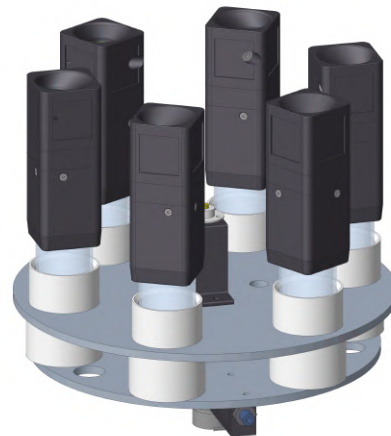
This section presents the final design of the Sample Stowage Device, its integration with the Lander, and its validation process, in line with the Surface Avatar protocol. The Sample Stowage Device comprises the Rotational Stowage Unit (RSU) and Extended Reachability Mechanism (ERM). Each device's dimensions, materials, mechanisms, motorization, and sensing are described in detail. Next, an in-depth explanation of how both devices integrate is provided, including information about the necessary mechanisms and electronics. Lastly, details on how the devices integrate with the Lander are outlined, as well as the tests conducted to validate the required functionalities and the interaction with the Sample Tube.

### 6.2.1 Rotational Stowage Unit

The final design of the Rotational Stowage Unit is shown in Figure 6.5a and 6.5b and further detailed in Appendix B. Figure 6.6 contains an exploded view with an identification for each component, and thus will guide the explanation of the mechanism. The Rotational Stowage Unit consists of two circular 5mm thick aluminum plates (components 05 and 09), the Upper and Bottom Plates, which sandwich the Sample Tube Slots (component 07) in between. The current design includes six slots, but the Bottom Plate has cutouts for up to eight slots, requiring a replacement of the Upper plate.



(a) *Rotational Stowage Unit.*



(b) *Rotational Stowage Unit with Sample Tubes*

*Figure 6.5: Rotational Stowage Unit.*

The Plates and Slots are held together by an M10 screw (component 02), which presses the plates against each other. This screw is then fixed to a base (component 15). As the Plates and Slots need to rotate around the fixed screw, their interface is a rotational joint, supported by two axial ball bearings (component 04).

A motor (component 13) located under the base provides the necessary rotational movement. The connection between the motor and the Bottom Plate is achieved through an internal geared transmission with a ratio of 6:1. The internal gear (component 14) is fixed under the Bottom Plate, while the driving gear (component 17) is mounted on the motor's axle.

A proximity sensor (component 12) installed in the base, paired with a small screw (components 10 and 11) fixed in the Bottom Plate, helps to determine the device's position. The sensor only needs to detect the screw's position once.

Each slot includes a centering ring (component 06) for the automatic alignment of the Sample Tube, as well as an active sensor for Sample Tube detection and ID retrieval. The sensor has three pins that contact the sensor under the Sample Tube. As each Tube has a sensor with a unique resistance, the active sensor can identify the resistance value, thus retrieving the Sample Tube's ID.

To connect the rotating slots, which contain the Sample Tube sensor system and the position sensor, to a stationary board, a slip ring (component 01) is installed on top of the Upper Plate

with the aid of a support (component 03). This provides the necessary interface. Finally, all the components are connected to the plates by M3 screws.

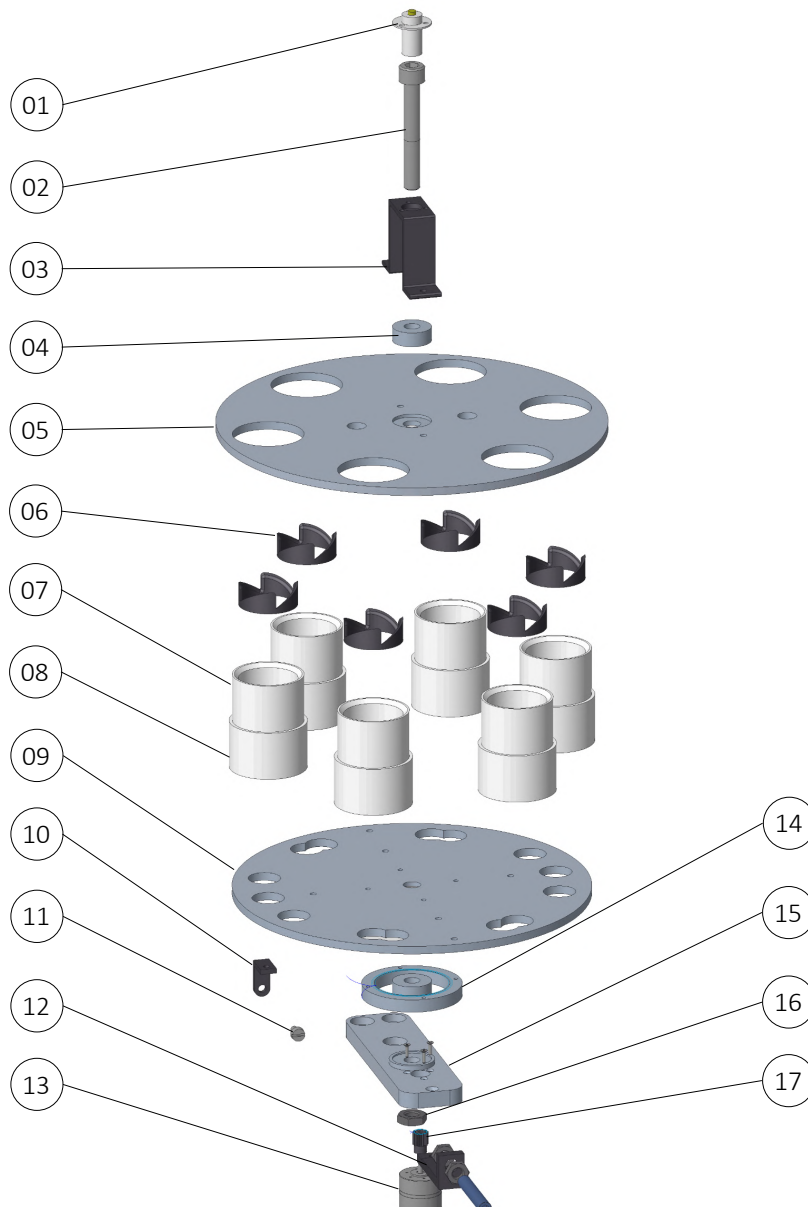


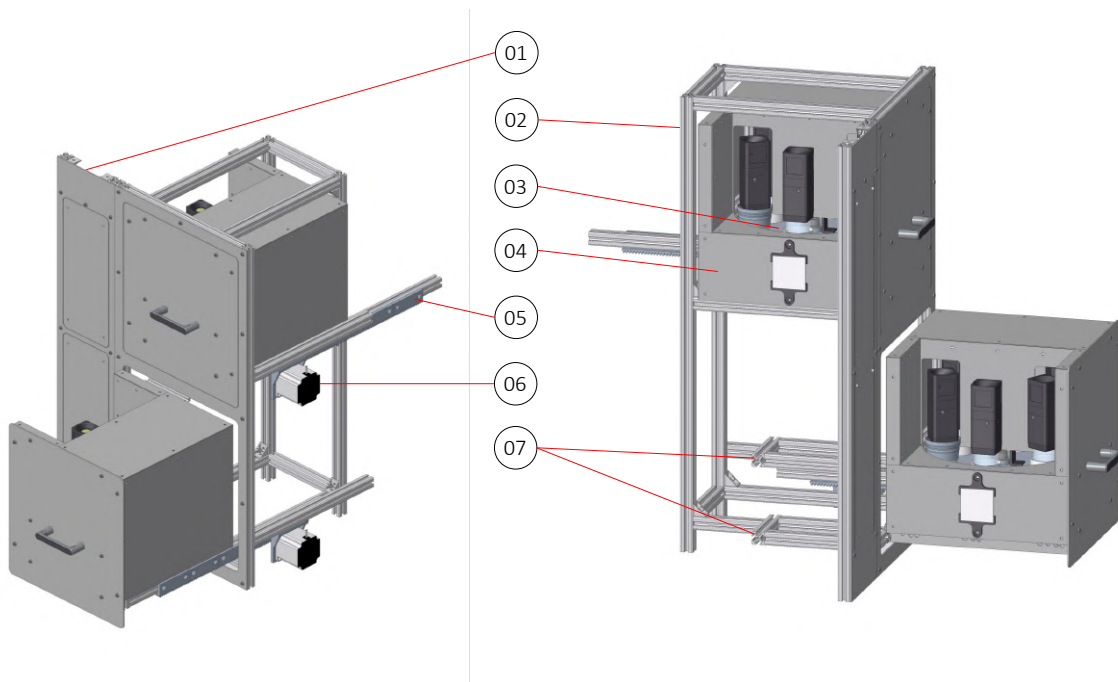
Figure 6.6: Exploded view of Rotational Stowage Unit.

### 6.2.2 Extended Reachability Mechanism

The Extended Reachability Mechanism consists of two main components: the Drawer (component 04 represented in Appendix C.1) and the Frame (component 02 represented in Appendix C.2). The Drawer houses the RSU, constructed from a 20mm profile, with covers made from 1mm thick stainless steel sheets. The RSU connects to its housing via its base using M4 screws, and all cables feed through an opening at the back of the Drawer. The Drawer then attaches to the Frame via a telescopic rail with 300mm of travel.

To achieve the necessary transnational motion, a rack and pinion actuator was designed. The rack (component 05), an extension of the housing, is positioned on the housing's bottom side. It measures 450mm in length, allowing for possible future extensions if the slide is modified. The pinion attaches to the base structure and is driven by the motor (component 06). The system doesn't need a position sensor because the motor can determine its position accurately.

Lastly, there's a dedicated space (component 07) for the controller board. The Frame is covered by 2mm thick stainless steel sheets (component 01).



*Figure 6.7: Exploded view of Rotational Stowage Unit.*

### 6.2.3 Functionalities

The electronic board of the Sample Stowage Device requires the following connections for normal operation: Revolver Motor Encoder, Drawer Motor, Reference Position Sensor, Sample Tube Detection, Power Supply (12V), Revolver Motor Output, Communication and Control Board Logic Power Supply. The electronics are powered via the 12V connector and the power supply must be capable of delivering at least 1 Amp of current. For device control, connect the computer via the Micro-USB connector.

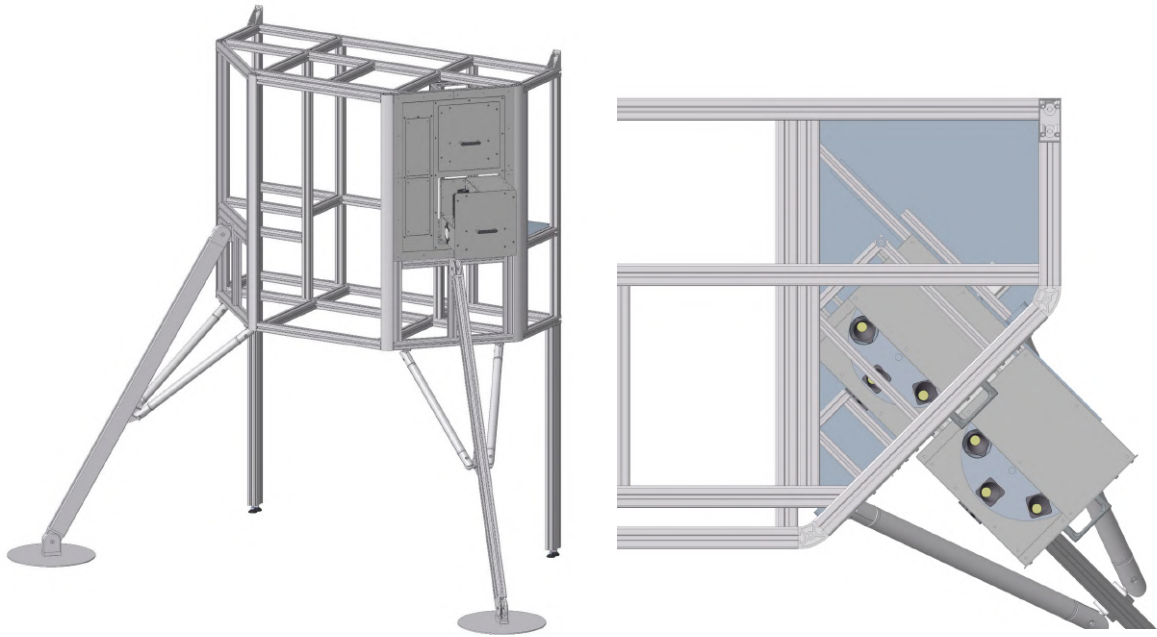
The controller logic of the device (the ESP32 Board) is also powered via USB. The Sample Stowage Device accepts several commands which include:

- Move to Slot (MS): This command targets a slot within the interval (1 to 6). Acceleration and angular velocity of the Revolver should not exceed  $3.14 \text{ rad/s}^2$  and  $3.14 \text{ rad/s}$  respectively.
- Get Slot state(s) (GS): This command returns the state of the desired slot or the slot states of all slots as an ASCII string.
- Drawer Homing (DH): This command initiates the homing procedure of the drawer.
- Drawer Open (DO): This command moves the drawer into its OPEN position.
- Drawer Close (DC): This command moves the drawer into its CLOSED position.
- Drawer Acknowledge (DA): This command resets the drawer from an error state.

The drawer requires a homing procedure before being able to send the open or close commands. During homing, the drawer extends slightly before retracting until it hits the endpoint.

### 6.2.4 Integration with Lander

The Drawer and Frame were designed with the location's space limitations in mind. The Sample Stowage Device is secured to the lander by its lateral frame (Figure 6.8). After installation, all the necessary electronic connections are made, and the power supply is connected to a hub beneath the Lander. The compact design of the drawer and the space provided by the lander allow for the inclusion of two drawers. This increases the Lander's capability to handle 12 Sample Tubes simultaneously. Figure 6.8 presents a top view of the Lander with the Sample Stowage Device installed, illustrating the position of the Drawers when they are open and closed.



*Figure 6.8: Integration of Sample Stowage Device into the Lander.*

### **6.2.5 Validation**

The validation of the Sample Stowage Device (SSD) is a thorough process that confirms the device meets all necessary requirements for Surface Avatar protocols. The process includes several stages: component testing, integration testing, functional testing, system integration testing, and sample tube interaction testing. Each stage verifies the SSD's reliability, accuracy, and robustness, ensuring it can operate seamlessly under Surface Avatar conditions and integrate effectively with the Lander. Successful validation proves the SSD's readiness for use and its ability to handle, store, and retrieve sample tubes.

#### **Component Testing**

First, the mechanical components were tested during the assembly of the RSU. The rotational joints were examined and the M10 screw was tightened to adjust the rotation characteristics, resulting in a stable and smooth rotation. The transmission was then successfully tested to ensure that the driving gear can rotate the RSU without any interference due to small assembly tolerances.



Next, sensors were installed to confirm the correct positioning of rotating components 10 and 11 as shown in Figure 6.6. The sensors inside the slots and the slip ring were also installed, followed by the cabling. A manual rotation was performed to confirm that all components were working without interference. Some adjustments were made to increase the gap between the cables under the Bottom Plate and the position sensor, ensuring safe operation.

Once all RSU components were installed and tested, the sensors and motor were connected to the controller. Six sample tubes filled with sample were placed in slots with extra weight, and rotation was initiated. The rotation was successful, and the Sample Tubes sensor system was found to be working as expected. The homing procedure also performed as expected, with the RSU rotating until the proximity sensor detected the screw. This allowed the RSU to define its position.

After validating the RSU, it was mounted inside its housing. A manual rotation was performed to check for any interference between the RSU components or Sample Tubes and the housing walls. The Drawer was then installed in the frame and connected by the telescopic rail, ensuring the coupling between rack and pinion.

Following installation, the cables from the RSU and the motor that drives the pinion were unified. The Drawer's opening and closing procedure was manually tested to ensure smooth sliding on the rail. At this stage, one of the rack segments was replaced and the rail was adjusted to ensure smooth operation. After these adjustments, the control board was fixed into the frame and all cables were connected. Finally, the Drawer motor was tested, confirming that the mechanism can successfully open and close the Drawer.

### **Integration and Functional Testing**

After verifying the function of each component of the Sample Stowage Device (SSD), a comprehensive test was conducted to confirm the overall operation. This confirmed that all functionalities, as described in Section 6.2.3, were functioning properly. The SSD proved capable of ensuring that the selected slot is in the exact position, as well as the Drawer when opened. It was concluded that the integration between the drawers and the frame did not impact any functionality.

### **System Integration Testing**

With the confirmation that the SSD was working as expected, it was integrated into the lander. Once installed, the drawer's open and close functionalities were tested again. Due to the position of a camera (shown in Figure 6.9), a modification in the Lander setup was required. The camera

was moved down to prevent collision with the drawer. With all functionalities working correctly, the integration of the Sample Stowage Device into the Lander was successful.



*Figure 6.9: Sample Stowage Device in use during a dry run test. The mission was simulating the return of a Sample Tube to the Sample Stowage Device using TINA.*

The interface between the mission command and the SSD controller was established. This ensures that the Surface Avatar mission command can effectively control all SSD functionalities and access its states.

### **Sample Tube Interaction Testing**

All the tests and validation of functionalities with respect to the interaction between the Sample Tubes and the Sample Stowage Device was conducted during the final stages of the SDD and Sample Tube development. Thus, the SSD can recognize the presence of a Sample Tube, as well as retrieving its ID. The Slots position ensures that the Robotiq Gripper used by TINA has enough room between Tubes to grasp it securely.

## Validation Outcomes

The Sample Stowage Device was extensively tested during the dry runs. Minor failures were encountered during operation, mainly due to the lack of performing the homing procedures. Sometimes, during tests, TINA offsets the Sample Tube placement by millimeters, which is enough to cause the placement procedure to fail. The validation process verified that the Sample Stowage Device (SSD) satisfies all requirements within the Surface Avatar protocols. Rigorous testing at each phase ensured the SSD's robustness, precision, and seamless integration with the Lander. The Sample Tube Return protocol could be performed during the Prime Session. In this session, the astronaut in control commanded the Drawer to open, executed the TINA procedure to pick up the Sample Tube and place it inside the SSD, and finally, closed the Drawer. The device performed all the commands as expected.

## 6.3 TINA Integration

In the Particle Swarm Optimization used to find the best placement of TINA's base, the parameters  $c_1$ ,  $c_2$ , and  $w$  set the dynamical behavior of the particles, influencing how the algorithm searches for the best position in space. The parameter  $c_1$  is set to 0.5, indicating a moderate inclination for the particles to follow their own best positions. This balance suggests that particles are guided by their individual past experiences without being overly reliant on them. Conversely, the parameter  $c_2$  is set to a lower value of 0.3, reflecting a lower tendency for particles to follow the global best position. This means the influence of the best-known position among all particles is not as strong in directing their movements.

The inertia weight  $w$  is set to a high value of 0.9, which significantly impacts this configuration. With a high inertia weight, the particles' current velocities play a substantial role in determining their next moves. This results in particles maintaining a significant amount of momentum, potentially leading to a smoother and faster convergence as they traverse the search space.

In summary, this configuration emphasizes the importance of particles' historical velocities while balancing their tendencies to explore both personal and global best positions, fostering a dynamic and potentially efficient search process.

The number of particles used in this optimization is 50, providing good results without being computationally expensive. The number of iterations is set to 20, which is sufficient for convergence based on tests. Finally, the chosen discretization is 20, yielding a good objective function score.

The best position for the TINA arm base according to the Particle Swarm Algorithm is (0.449 – 0.4280.535). Figure shows a representation of the arm in its best base placement. It also shows

the bounds for the particle in blue, and the box of interest in red. Figure 6.10 shows the cost function curve, which converges in 8 iterations to the best final position. Several runs were executed using the same parameters, yielding similar results. The ones shown in Figure 6.11 are the best among them.

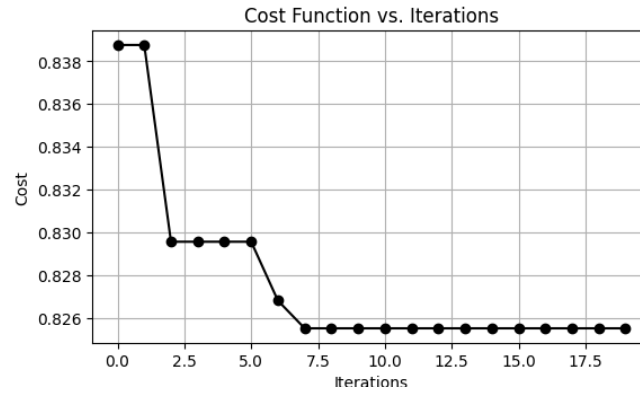


Figure 6.10: Cost evolution of TINA base position optimization.

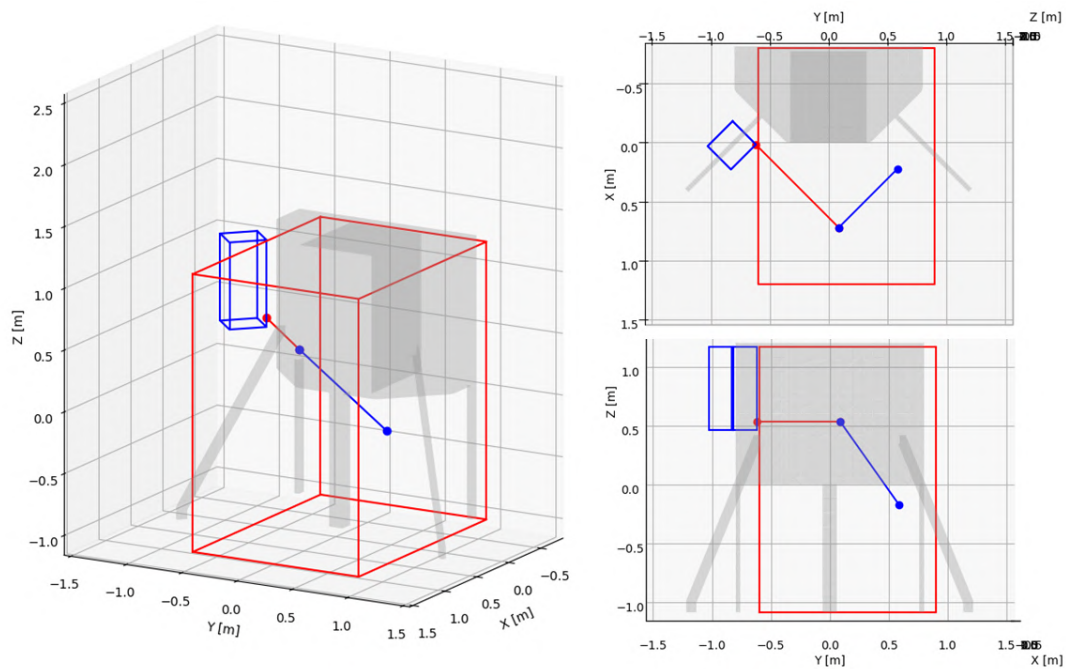


Figure 6.11: TINA final position represented by the simplification.

Figure 6.12 shows the technical execution of this result. The arm base is mounted on a standard profile construction, which is fixed in the Lander frame. This new position for TINA provides a good workspace and reach while offering more robustness to the base installation, reducing torsional displacements. One issue with the previous position was that the structure of the arm and the arm itself were above the Hands-on Tray, potentially interfering with the operation of other robots and limiting the Tray's usability. This issue is resolved with TINA's new base position, which has been moved to the left of the Tray, leaving it free of obstacles. Finally, this base position allows TINA to reach all the required places for the Protocols execution, such as the Sample Tubes inside the Sample Stowage Device, or the Seismometer inside the Cargo Bay.

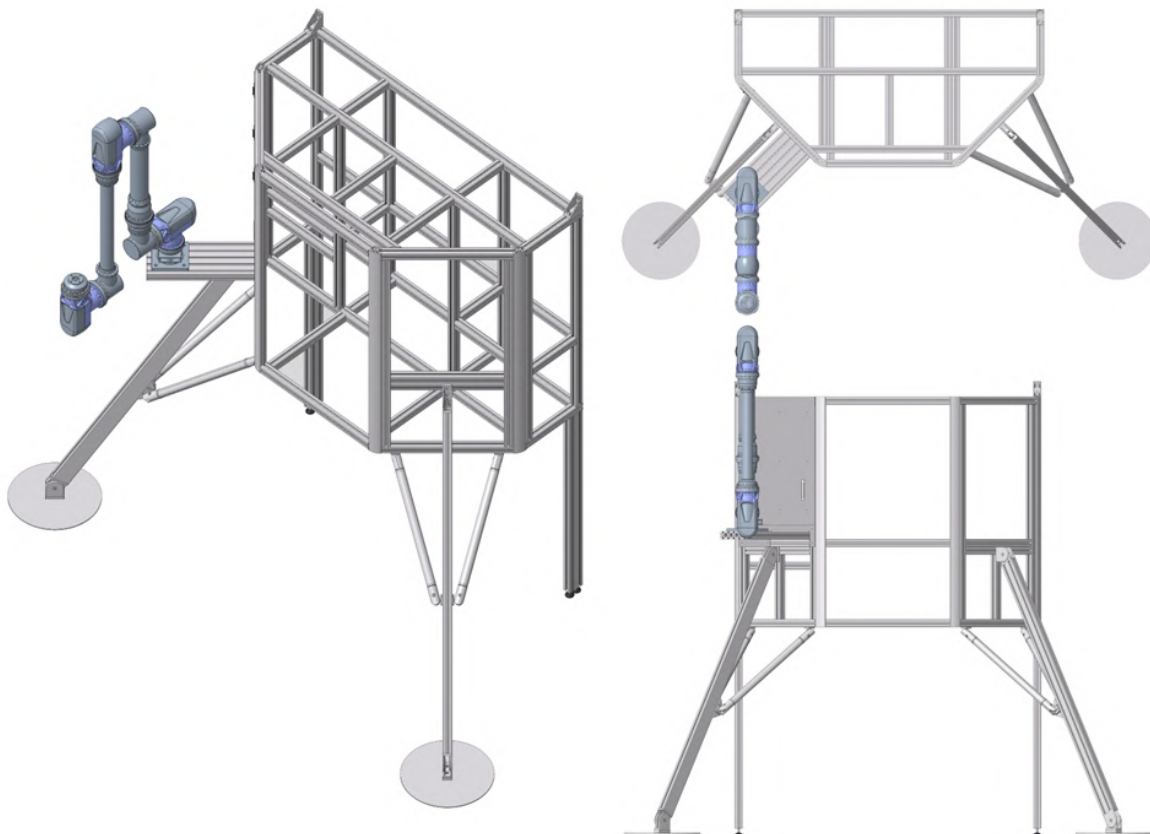


Figure 6.12: TINA final position represented in CAD.

## 6.4 Hands-on Tray

The Hands-on Tray, shown in Figure 6.13, consists of a 1000 x 800 mm metal plate supported by a 40 x 40 mm aluminum profile. This setup is connected to a linear guide, which is attached to a rail. An electric motor provides vertical motion to the tray, with one end fixed to the Lander's bottom surface and the other to the tray. Special connectors ensure a secure joint between the motor and Lander components. The mechanism operates by extending or retracting the motor; when the motor retracts, the tray moves upwards, and when it extends, the tray moves downwards. The component description can be seen in Appendix F.



Figure 6.13: Hands-On Tray and its mechanism.

Since the joint between the motor and the Tray is located 0.120 m under the tray surface, the height can be determined according to the following equation:

$$h = 1.050 - \sqrt{(0.770 + l)^2 - (0.400 + 0.276)^2} + 0.120 \quad (6.1)$$

To further analyze the feasibility of installing the mechanism with the described configuration, an approximation of the forces applied by the motor on the Tray structure can be made. Figure 6.14 shows a simplification of the forces. Considering that the Tray needs a vertical force of approximately  $F_y = 100N$ , the force in the horizontal direction can be obtained with the following equation:

$$F_x(h) = \frac{(P_x + d)F_y}{H - h} = \frac{(0.400 + 0.276)100}{1.050 - h} \quad (6.2)$$

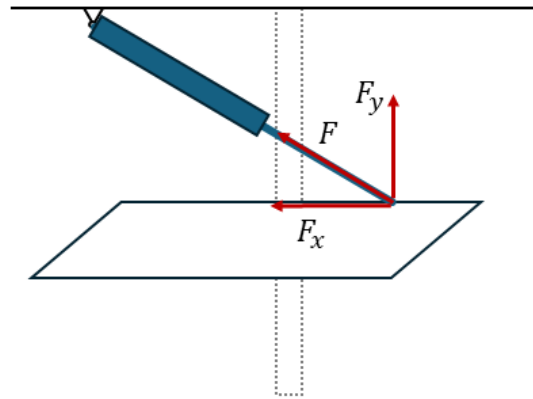


Figure 6.14: Forces and height involved in the Hands-on Tray operation.

Figure 6.15 shows the plot for the height and forces according to the extension length of the motor. One can conclude that the height range  $[0.120, 0.801]$  is fully operational, with the forces not exceeding the limits of the motor or the Tray structure. The code source is Appendix E.

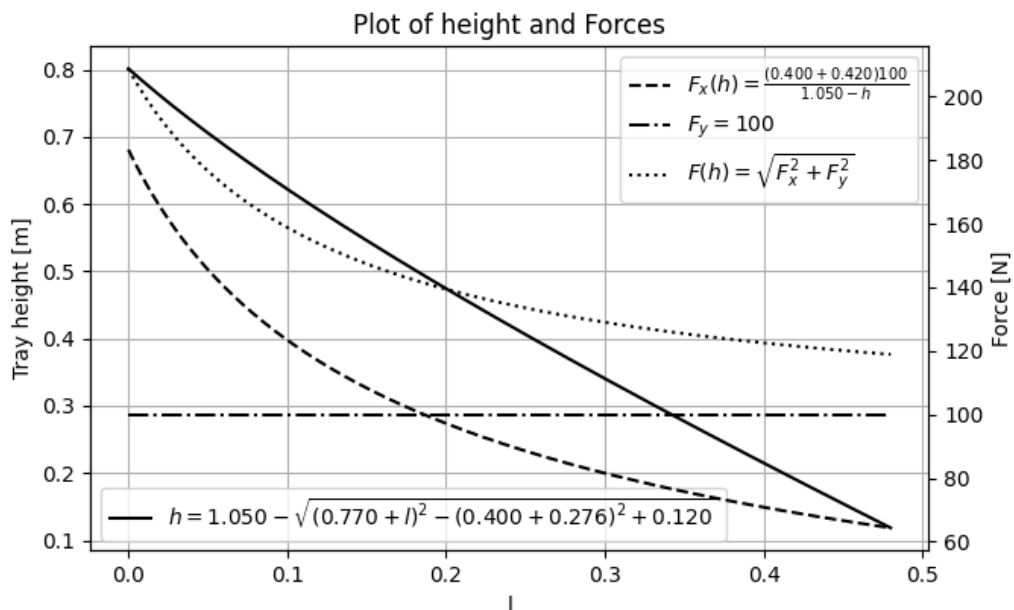
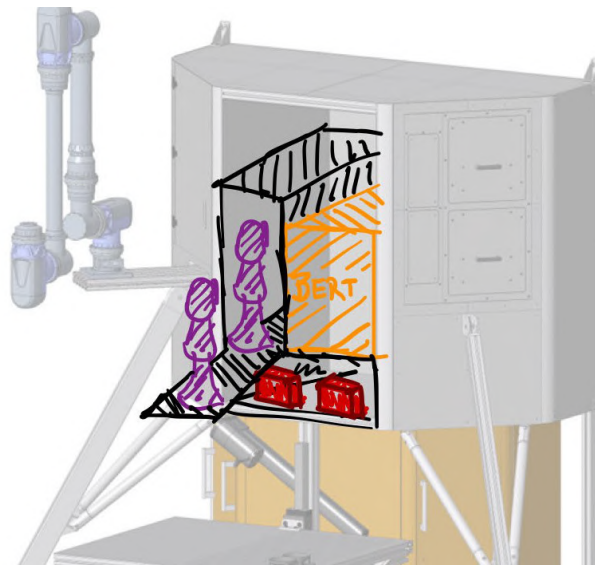


Figure 6.15: Forces and height involved in the Hands-on Tray operation.

Currently, the tray is mounted to the lander by its linear guide, which works as intended. During the Prime Session, the tray demonstrated its ability to serve as an exchange area for the Seismometer and the Sample Tube. However, its functionality of moving up and down still needs further development. The motor needs to be implemented and validated to operate correctly in the Surface Avatar experiments. Using a sensor to measure its position and provide closed-loop feedback is also encouraged. Finally, the addition of components that can facilitate the placement of equipments on the Tray can be installed.

### 6.5 Cargo Bay

The Cargo Bay is an internal space created in the middle section of the Lander. It has a dimension of 775x646x1115 mm, which is enough for Seismometer handling in Protocol 1. The main structure uses the construction profile from the Lander frame as support for the metal plates that form the walls, roof and floor. Light equipments can be attached directly to the metal plates, while the heavier ones must use the frame for fixation.



*Figure 6.16: A sketch of a possible use of the Cargo Bay. In purple, the Seismometer, that could be installed in a rack. Next to it, in orange, a box that could contain Bert. In red, the electronic modules placed on a drawer.*

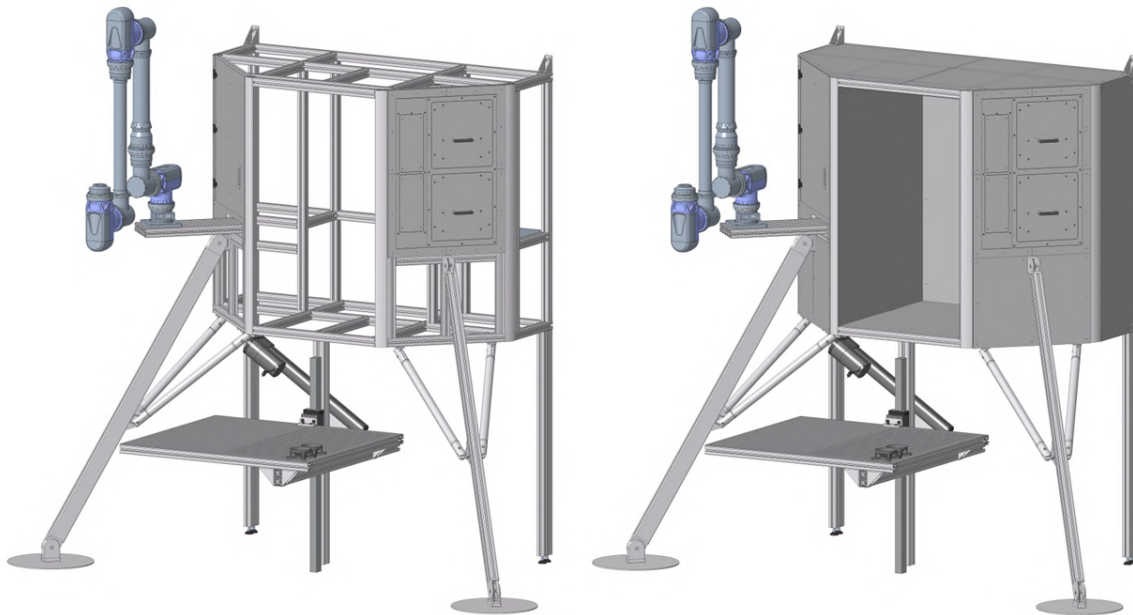
Despite its simplicity, the Cargo Bay adds flexibility to the mission by allowing for future functionalities. For instance, a drawer system inspired by the Sample Stowage Device can



be created to increase the number of seismometers stored in the Cargo Bay while enhancing equipment accessibility. Another possibility is adding a case for Bert, who would be stored inside. When needed, TINA could pull it out, place it on the Tray for unboxing, which can be aided by other robots. Finally, the Tray can move down to the floor for Bert's deployment. This flexibility also allows the mission to make use of other equipment from previous missions, like the electronic modules and antenna from SOLEX. Figure 6.16 shows a sketch of how the Cargo Bay could be used for other mission purposes.

## 6.6 Final Lander Design

This section presents the final results of the thesis development. Figure 6.17 shows all the equipment installed in the Lander frame, integrating necessary systems such as the Sample Stowage Device, TINA arm, Tray, and Cargo Bay. To protect the mechanisms and enhance the Lander's appearance, metallic covers were installed. The Lander with these covers can be seen in Figure 6.17.



*Figure 6.17: On the left: Lander with the integration of Sample Stowage Device, TINA, Cargo Bay and Tray. On the right: Lander with the equipments and the metallic cover.*

Many applications require local computers to operate, so it was necessary to dedicate a space for them in the Lander. To avoid sacrificing space in the cargo bay and to provide quick access to the electronics, an Electronics Bay was created. All electronics and power systems are installed beneath the Lander, as shown in Figure 6.18. The cover of this bay is metallic gold, mimicking the appearance of space blankets commonly used in Space Landers.

The validation of the Lander was performed during the dry runs of Surface Avatar, as seen in Figure 6.18. Protocols 1 and 2 were extensively tested, ensuring that the Lander met all the requirements for mission execution. The Sample Return protocol correctly used the Sample Stowage Device, while TINA successfully transferred the Sample Tube from the Hands-on Tray to storage and vice-versa. The Seismometer protocol was also well executed, with the Cargo Bay providing ample space for handling maneuvers. TINA was able to place the seismometer on the Tray for Justin to pick it up.



*Figure 6.18: On the left: representation of the Lander with the Electronics Bay in metallic gold. On the right: The Lander during the execution of the Seismometer protocol.*

Some functionalities still need to be fully implemented. The tray is mounted in its rail guide, but the motor and integration with the mission commands are missing. The new TINA position, which is an output from the Particle Swarm Optimization, also needs to be implemented.

---

## 7 Discussion

The final Lander design offers flexibility by using standard profiles, allowing for the easy addition of new features. For Protocol 1 (Section XX), a mechanized tray can be installed inside the Cargo Bay to hold more Seismometers. If needed, a box can be created to secure Bert inside the Lander, and TINA can remove this box using linear guides and place it on the Hands-on Tray for deployment. Equipment like an antenna can also be installed on other parts of the Lander. A protocol can be established for replacing this equipment by following a procedure involving TINA, the Tray, and possibly other robots.

During the first Prime Session, the Lander was extensively used to execute the two protocols mentioned in Section XX. Both protocols demonstrated the Lander's versatility with a robotic arm for handling and manipulating objects, along with the tray, which provides a space for robots to transfer and manipulate items. The Sample Return task can be seamlessly executed with TINA, the Hands-on Tray, the Sample Tube, and the Sample Stowage Device working together under mission control coordination.

Adding an active tray increases the possibilities for object handling and interaction between robots, enhancing the Lander's flexibility beyond just adding new features. The ability to adjust the Tray's height allows the Lander to adapt during operation based on the object being handled and the robots operating the protocols. For example, if the Interact Rover is handling a large object, it may struggle to place it on a fixed-height Tray. Mission control can then command the Tray to move to a position suitable for the Interact Rover.

For standard objects, the mission can use April Tags to identify each object being handled and automatically adjust the Tray's height. A command can trigger the Tray movement, or the system can be designed to start the Tray adaptation procedure when a standard object is near the Lander.

Overall, the Lander can pose challenges to robot teleoperation by offering various levels of operational complexity. This can range from a simple command to retrieve a seismometer to a manipulation challenge with the Sample Tube in teleoperation mode to complete a Sample Return task. Additionally, it is ready for future modifications due to its flexible design. Most importantly, with the implementation of the Hands-on Tray, it can adapt during protocol execution, offering a higher level of operational complexity and posing greater challenges to teleoperation procedures.

### 8 Conclusion

Surface Avatar is an important mission for the research and development of robotic teleoperation. It provides a deep understanding of the conditions under which a robotic team performs complex tasks. Like many other analog missions, Surface Avatar uses a physical space called MUSA, where equipment is built to mimic possible real missions to the Moon or Mars. One key part of MUSA is the robotic Lander, the topic of this thesis. It directly interacts with Rollin' Justin, Interact Rover, and Bert. These four robots form the Surface Avatar robotic team.

The Lander, created using product development methods, has many functionalities, such as a Sample Stowage Device that, with the Sample Tube, supports a sample return protocol, which is common in space missions. Manipulating the Sample Tube is challenging, especially when done by Justin's hands. Furthermore, the Sample Stowage Device provides a sequence of procedures that, combined with the handling complexity of the Sample Tube, helps assess teleoperation challenges.

The addition of the TINA robotic arm, placed in an optimal position regarding its workspace and installation robustness, and the Hands-on Tray provides flexibility beyond just adding new functionalities in the future. They enable the Lander to be flexible during the execution of protocols by adapting to better fit the requirements of the handled object and the robots involved.

In conclusion, this thesis provides a deep understanding of the development of a mockup lander for an analog mission, resulting in a robotic Lander that fulfills the Surface Avatar requirements. At the same time, it is flexible enough to be modified in the future and adapt during operation, advancing lander technology for analog mission, and helping enhance the research and development of robotic teleoperation missions.

---

## Bibliography

- Azmi, W., S. N. Azmi, H. Nobanee, and P. A. Hamil (2024). “Out-of-this-world returns: How did the market value India’s successful moon mission?” In: *Economics Letters* 234, p. 111490. DOI: <https://doi.org/10.1016/j.econlet.2023.111490>. URL: <https://www.sciencedirect.com/science/article/pii/S0165176523005165>.
- Banks, A., J. Vincent, and C. Anyakoha (Dec. 2007). “A review of particle swarm optimization. Part I: background and development”. In: *Natural Computing* 6.4, pp. 467–484. DOI: 10.1007/s11047-007-9049-5. URL: <https://doi.org/10.1007/s11047-007-9049-5>.
- Bayer, R., P. Schmaus, M. Pfau, B. Pleintinger, D. Leidner, F. Wappler, A. Maier, T. Krueger, et al. (Oct. 2019). “Deployment of the SOLEX Environment for Analog Space Telerobotics Validation”. In.
- Boeder, P. A. and C. E. Soares (2020). “Mars 2020: mission, science objectives and build”. In: *Systems Contamination: Prediction, Control, and Performance 2020*. Ed. by C. E. Soares, E. M. Wooldridge, and B. A. Matheson. Vol. 11489. International Society for Optics and Photonics. SPIE, p. 1148903. DOI: 10.1117/12.2569650. URL: <https://doi.org/10.1117/12.2569650>.
- Bonitz, R., L. Shiraishi, M. Robinson, J. Carsten, R. Volpe, A. Trebi-Ollenu, R. E. Arvidson, P. C. Chu, et al. (2009). “The Phoenix Mars Lander Robotic Arm”. In: *2009 IEEE Aerospace conference*, pp. 1–12. DOI: 10.1109/AERO.2009.4839306.
- Bonitz, R. G., L. Shiraishi, M. Robinson, R. E. Arvidson, P. C. Chu, J. J. Wilson, K. R. Davis, G. Paulsen, et al. (2008). “NASA Mars 2007 Phoenix Lander Robotic Arm and Icy Soil Acquisition Device”. In: *Journal of Geophysical Research: Planets* 113.E3. DOI: <https://doi.org/10.1029/2007JE003030>. eprint: <https://agupubs.onlinelibrary.wiley.com/doi/pdf/10.1029/2007JE003030>. URL: <https://agupubs.onlinelibrary.wiley.com/doi/abs/10.1029/2007JE003030>.
- Borst, C., T. Wimbock, F. Schmidt, M. Fuchs, B. Brunner, F. Zacharias, P. R. Giordano, R. Konietschke, et al. (2009). “Rollin’ Justin - Mobile platform with variable base”. In: *2009 IEEE International Conference on Robotics and Automation*, pp. 1597–1598. DOI: 10.1109/ROBOT.2009.5152586.
- Butterfass, J., M. Grebenstein, H. Liu, and G. Hirzinger (2001). “DLR-Hand II: next generation of a dextrous robot hand”. In: *Proceedings 2001 ICRA. IEEE International Conference on Robotics and Automation (Cat. No.01CH37164)*. Vol. 1, 109–114 vol.1. DOI: 10.1109/ROBOT.2001.932538.

- Cardone, M., C. Laroque, M. Sarkarati, K. Nergaard, P. Steele, and S. Martin (2016). “The METERON Operations Environment and Robotic Services, a plug-and-play system infrastructure for Robotic experiments”. In: *SpaceOps 2016 Conference*. DOI: 10.2514/6.2016-2474. eprint: <https://arc.aiaa.org/doi/pdf/10.2514/6.2016-2474>. URL: <https://arc.aiaa.org/doi/abs/10.2514/6.2016-2474>.
- Carey, W., T. Krueger, A. Wedler, K. Wormnes, J. Grenouilleau, E. Ferreira, K. Nergaard, L. Hann, et al. (Sept. 2022). “METERON Analog-1: A Touch Remote”. In.
- Carey, W., K. Nergaard, F. Frescheville, J. Grenouilleau, and A. Schiele (Nov. 2012). “METERON: A Mission Concept Proposal for Preparation of Human-Robotic Exploration”. In.
- Chavers, G., L. Watson-Morgan, M. Smith, N. Suzuki, and T. Polsgrove (2020). “NASA’s Human Landing System: The Strategy for the 2024 Mission and Future Sustainability”. In: *2020 IEEE Aerospace Conference*, pp. 1–9. DOI: 10.1109/AERO47225.2020.9172599.
- Ehrenfried, M. v. (2020). *The artemis lunar program returning people to the Moon*. Springer.
- Fonseca Prince, A., B. Voder Mayer, B. Pleintinger, A. Kolb, G. Franchini, E. Staudinger, E. Dietz, S. Schröder, et al. (Aug. 2023). “Modular Mechatronics Infrastructure for robotic planetary exploration assets in a field operation scenario”. In: *Acta Astronautica*. Elsevier Acta Astronautica 212. The research has been supported by the Helmholtz Association, Germany project ARCHES (contract number ZT-0033)., pp. 160–176. URL: <https://elib.dlr.de/198082/>.
- Fonseca Prince, A., B. Voder Mayer, B. Pleintinger, A. Kolb, E. Staudinger, E. Dietz, S. Schröder, S. Frohmann, et al. (Oct. 2021). “Design and Implementation of a Modular Mechatronics Infrastructure for Robotic Planetary Exploration Assets”. In: *Proceedings of the International Astronautical Congress, IAC*. URL: <https://elib.dlr.de/145167/>.
- Fuchs, M., C. Borst, P. Robuffo Giordano, A. Baumann, E. Kraemer, J. Langwald, R. Gruber, N. Seitz, et al. (2009). “Rollin’ Justin - Design considerations and realization of a mobile platform for a humanoid upper body”. In: *2009 IEEE International Conference on Robotics and Automation*, pp. 4131–4137. DOI: 10.1109/ROBOT.2009.5152464.
- Fuller, S., E. Lehnhardt, C. Zaid, and K. Halloran (2022). “Gateway program status and overview”. In: *Journal of Space Safety Engineering* 9.4, pp. 625–628. DOI: <https://doi.org/10.1016/j.jsse.2022.07.008>. URL: <https://www.sciencedirect.com/science/article/pii/S2468896722000763>.
- George, A. J. (2024). “A Short Review on India’s Interplanetary Missions”. In: *Acceleron Aerospace Journal* 2.1, pp. 138–147. DOI: 10.61359/11.2106-2403. URL: <https://acceleron.org.in/index.php/aaaj/article/view/AAJ.11.2106-2403>.

- 
- Gingras, D., T. Lamarche, P. Allard, N. Jackson, S. Gemme, M. Taylor, C. Taylor, C. Dubois, et al. (2020). “LUNAR EXPLORATION ANALOGUE DEPLOYMENT (LEAD): OVERVIEW OF THE 2017-2019 ROBOTIC SAMPLE RETURN MISSION SIMULATIONS”. In: URL: <https://api.semanticscholar.org/CorpusID:245999553>.
- Gisler, M. and D. Sornette (2009). “Exuberant Innovations: The Apollo Program”. In: *Society* 46.1, pp. 55–68. DOI: 10.1007/s12115-008-9163-8. URL: <https://doi.org/10.1007/s12115-008-9163-8>.
- Golombek, M. P., R. C. Anderson, J. R. Barnes, J. F. Bell III, N. T. Bridges, D. T. Britt, J. Brückner, R. A. Cook, et al. (1999). “Overview of the Mars Pathfinder Mission: Launch through landing, surface operations, data sets, and science results”. In: *Journal of Geophysical Research: Planets* 104.E4, pp. 8523–8553. DOI: <https://doi.org/10.1029/98JE02554>. eprint: <https://agupubs.onlinelibrary.wiley.com/doi/pdf/10.1029/98JE02554>. URL: <https://agupubs.onlinelibrary.wiley.com/doi/abs/10.1029/98JE02554>.
- Goswami, J. (2010). “An Overview of the Chandrayaan-1 Mission”. In: *41st Annual Lunar and Planetary Science Conference*. Lunar and Planetary Science Conference, p. 1591.
- Helmholtz (2018). URL: <https://www.arches-projekt.de/en/project-arches/>.
- Hirzinger, G., N. Sporer, A. Albu-Schaffer, M. Hahnle, R. Krenn, A. Pascucci, and M. Schedl (2002). “DLR’s torque-controlled light weight robot III—are we reaching the technological limits now?” In: *Proceedings 2002 IEEE International Conference on Robotics and Automation (Cat. No.02CH37292)*. Vol. 2, 1710–1716 vol.2. DOI: 10.1109/ROBOT.2002.1014788.
- Honeycutt, J. H., C. Cianciola, and J. Blevins (2020). “NASA’s Space Launch System: Progress Toward Launch”. In: *ASCEND 2020*. DOI: 10.2514/6.2020-4037. eprint: <https://arc.aiaa.org/doi/pdf/10.2514/6.2020-4037>. URL: <https://arc.aiaa.org/doi/abs/10.2514/6.2020-4037>.
- Hoshino, T., S. Wakabayashi, M. Ohtake, Y. Karouji, T. Hayashi, H. Morimoto, H. Shiraishi, T. Shimada, et al. (2020). “Lunar polar exploration mission for water prospection - JAXA’s current status of joint study with ISRO”. In: *Acta Astronautica* 176, pp. 52–58. DOI: <https://doi.org/10.1016/j.actaastro.2020.05.054>. URL: <https://www.sciencedirect.com/science/article/pii/S0094576520303374>.
- ISRO, I. S. R. O. (2024). *Chandrayaan-3*. URL: [https://www.isro.gov.in/Chandrayaan3\\_Details.html](https://www.isro.gov.in/Chandrayaan3_Details.html).
- Jones, E. M. (1995). *Apollo 17 image library*. URL: <https://www.nasa.gov/history/alsj/a17/images17.html>.
- Jones, E. M. and K. Glover (1995). *Apollo 11 image library*. URL: <https://www.nasa.gov/history/alsj/a11/images11.html>.

- Kanu, N. J., E. Gupta, and G. C. Verma (2024). “An insight into India’s Moon mission – Chandrayan-3: The first nation to land on the southernmost polar region of the Moon”. In: *Planetary and Space Science* 242, p. 105864. DOI: <https://doi.org/10.1016/j.pss.2024.105864>. URL: <https://www.sciencedirect.com/science/article/pii/S003206332400028X>.
- Kessler, P., T. Prater, T. Nickens, and D. Harris (2022). “Artemis Deep Space Habitation: Enabling a Sustained Human Presence on the Moon and Beyond”. In: *2022 IEEE Aerospace Conference (AERO)*, pp. 01–12. DOI: 10.1109/AERO53065.2022.9843393.
- Kloman, E. (1972). *Unmanned Space Project Management: Surveyor and Lunar Orbiter*. NASA SP. Scientific, Technical Information Office, National Aeronautics, and Space Administration. URL: <https://books.google.de/books?id=XN8gAAAAIAAJ>.
- Krueger, T., E. Ferreira, A. Gherghescu, L. Hann, E. Exter, F. van der Hulst, L. Gerdes, L. Cencetti, et al. (Oct. 2020a). “Designing and Testing a Robotic Avatar for Space-to-Ground Teleoperation: the Developers’ Insights”. In.
- Krueger, T., F. van der Hulst, E. Ferreira, K. Wormnes, E. den Exter, A. Gherghescu, L. Gerdes, L. Hann, et al. (Oct. 2020b). “A Newcomer’s Guide to the Challenges of a Complex Space-to-Ground Experiment, With Lessons from Analog-1”. In: *International Symposium on Artificial Intelligence, Robotics and Automation in Space (I-SAIRAS) 2020*. URL: <https://elib.dlr.de/148182/>.
- Lamarche, T., N. Jackson, P. Allard, S. Gemme, D. Gingras, G. Faubert, and M. Picard (2020). “SAMPLE HANDLING SUBSYSTEM (SHS): CONCEPT DEMONSTRATION FOR A LUNAR SAMPLE RETURN MISSION”. In: URL: <https://api.semanticscholar.org/CorpusID:246000552>.
- Lehnhardt, E. and D. Connell (2023). “The Gateway Program as Part of NASA’s Plans for Human Exploration Beyond Low Earth Orbit”. In: *IEEE Space Computing Conference*. URL: <https://ntrs.nasa.gov/api/citations/20230014342/downloads/IEEE%20-%20Gateway%20Overview%20FINAL%20100223.pdf>.
- Leidner, D. S. (2019). “Fundamentals”. In: *Cognitive Reasoning for Compliant Robot Manipulation*. Cham: Springer International Publishing, pp. 25–35. DOI: 10.1007/978-3-030-04858-7\_2. URL: [https://doi.org/10.1007/978-3-030-04858-7\\_2](https://doi.org/10.1007/978-3-030-04858-7_2).
- Li, C., J. Liu, X. Ren, W. Zuo, X. Tan, W. Wen, H. Li, L. Mu, et al. (2015). “The Chang’e 3 Mission Overview”. In: *Space Science Reviews* 190.1, pp. 85–101. DOI: 10.1007/s11214-014-0134-7. URL: <https://doi.org/10.1007/s11214-014-0134-7>.
- Li, C., W. Zuo, W. Wen, X. Zeng, X. Gao, Y. Liu, Q. Fu, Z. Zhang, et al. (2021). “Overview of the Chang’e-4 Mission: Opening the Frontier of Scientific Exploration of the Lunar Far Side”. In: *Space Science Reviews* 217.2, p. 35. DOI: 10.1007/s11214-021-00793-z. URL: <https://doi.org/10.1007/s11214-021-00793-z>.



- 
- Lii, N. Y., D. Leidner, P. Birkenkamp, B. Pleintinger, R. Bayer, and T. Krueger (June 2017). “Toward scalable intuitive telecommand of robots for space deployment with METERON SUPVIS Justin”. In: *The 14th Symposium on Advanced Space Technologies for Robotics and Automation (ASTRA)*. European Space Agency. URL: <https://elib.dlr.de/113125/>.
- Lii, N. Y.-S., P. Schmaus, D. Leidner, T. Krueger, J. Grenouilleau, A. Pereira, A. Giuliano, A. S. Bauer, et al. (Sept. 2022). “Introduction to Surface Avatar: the First Heterogeneous Robotic Team to be Commanded with Scalable Autonomy from the ISS”. In: *Proceedings of the International Astronautical Congress, IAC*. Vol. IAC-22. International Astronautical Federation, IAF. URL: <https://elib.dlr.de/189618/>.
- M. Shami, T., A. El-Saleh, M. Alswaitti, Q. Al-Tashi, A. Summakieh, and S. Mirjalili (Jan. 2022). “Particle Swarm Optimization: A Comprehensive Survey”. In: *IEEE Access* PP, pp. 1–1. DOI: 10.1109/ACCESS.2022.3142859.
- Maier, M., M. Chalon, M. Pfanne, R. Bayer, M. Mascarenhas, H.-J. Sedlmayr, and A. Shu (Jan. 2019). “TINA: small torque controlled robotic arm for exploration and small satellites”. In.
- Miranda, L. J. (2018). “PySwarms: a research toolkit for Particle Swarm Optimization in Python”. In: *Journal of Open Source Software* 3.21, p. 433. DOI: 10.21105/joss.00433. URL: <https://doi.org/10.21105/joss.00433>.
- Moeller, R. C., L. Jandura, K. Rosette, M. Robinson, J. Samuels, M. Silverman, K. Brown, E. Duffy, et al. (Dec. 2020). “The Sampling and Caching Subsystem (SCS) for the Scientific Exploration of Jezero Crater by the Mars 2020 Perseverance Rover”. In: *Space Science Reviews* 217.1, p. 5. DOI: 10.1007/s11214-020-00783-7. URL: <https://doi.org/10.1007/s11214-020-00783-7>.
- NASA (May 2024). URL: <https://www.nasa.gov/analog-missions/#:~:text=What%20are%20Analog%20Missions%3F,they%20are%20used%20in%20space..>
- National Air and Space Museum (1975). URL: [https://airandspace.si.edu/collection-objects/drive-tube-apollo/nasm\\_A19810876000](https://airandspace.si.edu/collection-objects/drive-tube-apollo/nasm_A19810876000).
- Osinski, G. R., M. Battler, C. M. Caudill, R. Francis, T. Haltigin, V. J. Hipkin, M. Kerrigan, E. A. Pilles, et al. (2019). “The CanMars Mars Sample Return analogue mission”. In: *Planetary and Space Science* 166, pp. 110–130. DOI: <https://doi.org/10.1016/j.pss.2018.07.011>. URL: <https://www.sciencedirect.com/science/article/pii/S0032063318300047>.
- Ott, C., O. Eiberger, W. Friedl, B. Bauml, U. Hillenbrand, C. Borst, A. Albu-Schaffer, B. Brunner, et al. (2006). “A Humanoid Two-Arm System for Dexterous Manipulation”. In: *2006 6th IEEE-RAS International Conference on Humanoid Robots*, pp. 276–283. DOI: 10.1109/ICHR.2006.321397.

- Pahl, G., W. Beitz, J. Feldhusen, and K. Grote (2006). *Engineering design : A systematic approach*. London: Springer.
- Poli, R., J. Kennedy, and T. Blackwell (June 2007). “Particle swarm optimization”. In: *Swarm Intelligence* 1.1, pp. 33–57. DOI: 10.1007/s11721-007-0002-0. URL: <https://doi.org/10.1007/s11721-007-0002-0>.
- Raffin, A., D. Seidel, J. Kober, A. Albu-Schäffer, J. Silvério, and F. Stulp (2023). *Learning to Exploit Elastic Actuators for Quadruped Locomotion*. arXiv: 2209.07171 [id='cs.RO' full\_name='Robotics' is\_active=True alt\_name=None in\_archive='cs' is\_general=False description='Roughly includes material in ACM Subject Class I.2.9.'].
- Reagan, M., B. Janoiko, J. Johnson, P. Steven Chappell, and A. Abercromby (2012). “NASA’s Analog Missions: Driving Exploration Through Innovative Testing”. In: *AIAA SPACE 2012 Conference & Exposition*. DOI: 10.2514/6.2012-5238. eprint: <https://arc.aiaa.org/doi/pdf/10.2514/6.2012-5238>. URL: <https://arc.aiaa.org/doi/abs/10.2514/6.2012-5238>.
- Sánchez-Lavega, A., T. del Rio-Gaztelurrutia, R. Hueso, M. d. I. T. Juárez, G. M. Martínez, A.-M. Harri, M. Genzer, M. Hieta, et al. (2023). “Mars 2020 Perseverance Rover Studies of the Martian Atmosphere Over Jezero From Pressure Measurements”. In: *Journal of Geophysical Research: Planets* 128.1. e2022JE007480 2022JE007480, e2022JE007480. DOI: <https://doi.org/10.1029/2022JE007480>. eprint: <https://agupubs.onlinelibrary.wiley.com/doi/pdf/10.1029/2022JE007480>. URL: <https://agupubs.onlinelibrary.wiley.com/doi/abs/10.1029/2022JE007480>.
- Schmaus, P., D. Leidner, T. Krueger, J. Grenouilleau, A. Pereira, A. S. Bauer, N. Bechtel, S. Gomez, et al. (Sept. 2022). “On Realizing Multi-Robot Command through Extending the Knowledge Driven Teleoperation Approach”. In.
- Schmaus, P., D. Leidner, T. Krüger, A. Schiele, B. Pleintinger, R. Bayer, and N. Y. Lii (2018). “Preliminary Insights From the METERON SUPVIS Justin Space-Robotics Experiment”. In: *IEEE Robotics and Automation Letters* 3.4, pp. 3836–3843. DOI: 10.1109/LRA.2018.2856906.
- Schuster, M. J., M. G. Müller, S. G. Brunner, H. Lehner, P. Lehner, R. Sakagami, A. Dömel, L. Meyer, et al. (2020). “The ARCHES Space-Analogue Demonstration Mission: Towards Heterogeneous Teams of Autonomous Robots for Collaborative Scientific Sampling in Planetary Exploration”. In: *IEEE Robotics and Automation Letters* 5.4, pp. 5315–5322. DOI: 10.1109/LRA.2020.3007468.

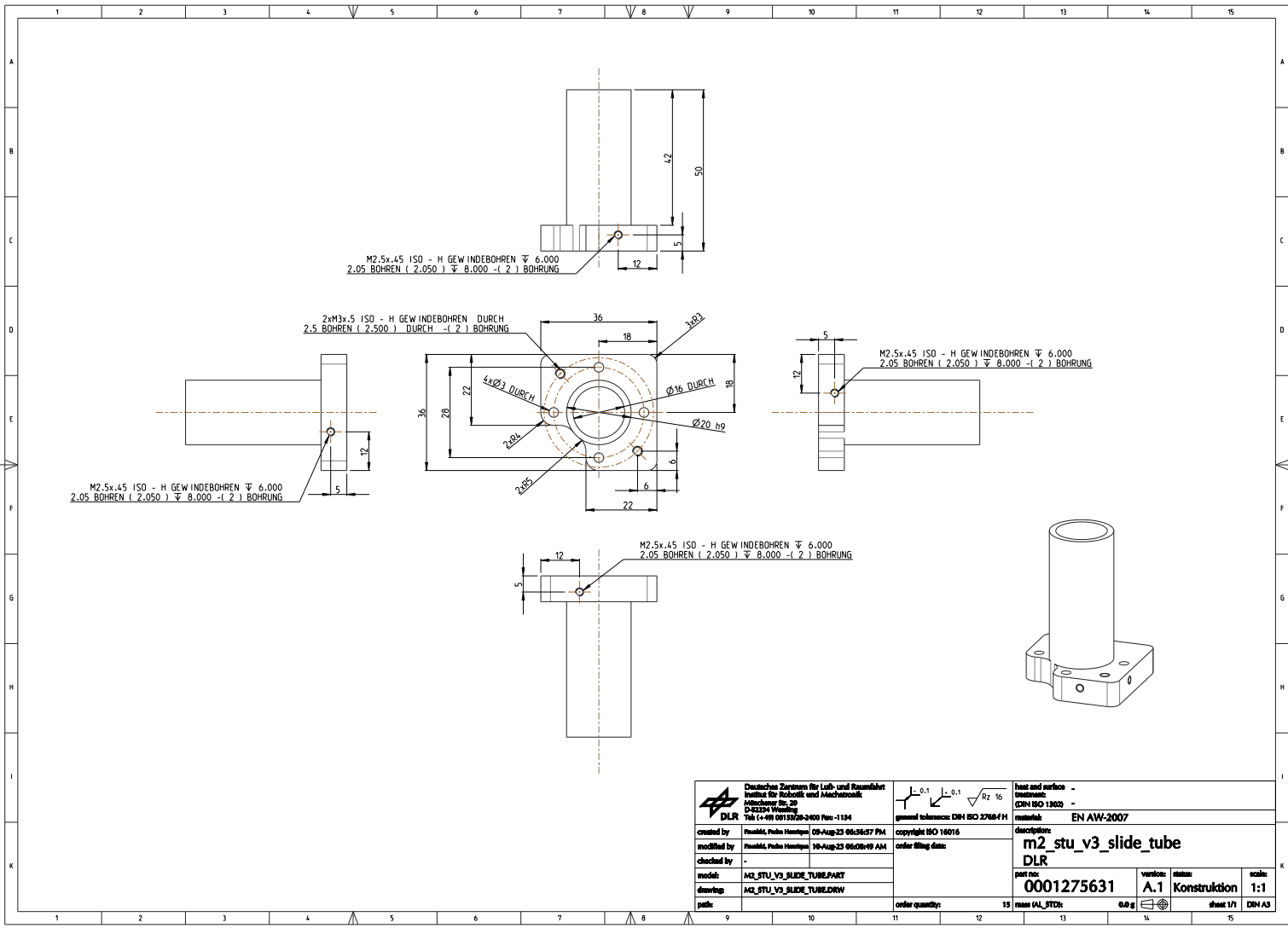
- 
- Seidel, D., M. Hermann, T. Gumpert, F. C. Loeffl, and A. Albu-Schäffer (2020). “Using Elastically Actuated Legged Robots in Rough Terrain: Experiments with DLR Quadruped bert”. In: *2020 IEEE Aerospace Conference*, pp. 1–8. DOI: 10.1109/AERO47225.2020.9172301.
- Shotwell, R. (2005). “Phoenix—the first Mars Scout mission”. In: *Acta Astronautica 57.2. Infinite Possibilities Global Realities, Selected Proceedings of the 55th International Astronautical Federation Congress, Vancouver, Canada, 4-8 October 2004*, pp. 121–134. DOI: <https://doi.org/10.1016/j.actaastro.2005.03.038>. URL: <https://www.sciencedirect.com/science/article/pii/S0094576505001190>.
- Slyuta, E. (2021). “CHAPTER 3 - The Luna program”. In: *Sample Return Missions*. Ed. by A. Longobardo. Elsevier, pp. 37–78. DOI: <https://doi.org/10.1016/B978-0-12-818330-4.00003-3>. URL: <https://www.sciencedirect.com/science/article/pii/B9780128183304000033>.
- Smith, M., D. Craig, N. Herrmann, E. Mahoney, J. Krezel, N. McIntyre, and K. Goodliff (2020). “The Artemis Program: An Overview of NASA’s Activities to Return Humans to the Moon”. In: *2020 IEEE Aerospace Conference*, pp. 1–10. DOI: 10.1109/AERO47225.2020.9172323.
- Soffen, G. A. and C. W. Snyder (1976). “The First Viking Mission to Mars”. In: *Science* 193.4255, pp. 759–766. DOI: 10.1126/science.193.4255.759. eprint: <https://www.science.org/doi/pdf/10.1126/science.193.4255.759>. URL: <https://www.science.org/doi/abs/10.1126/science.193.4255.759>.
- Sundararajan, V. (2018). “Overview and Technical Architecture of India’s Chandrayaan-2 Mission to the Moon”. In: *2018 AIAA Aerospace Sciences Meeting*. DOI: 10.2514/6.2018-2178. eprint: <https://arc.aiaa.org/doi/pdf/10.2514/6.2018-2178>. URL: <https://arc.aiaa.org/doi/abs/10.2514/6.2018-2178>.
- Tzanetos, T., M. Aung, J. Balaram, H. F. Grip, J. T. Karras, T. K. Canham, G. Kubiak, J. Anderson, et al. (2022). “Ingenuity Mars Helicopter: From Technology Demonstration to Extraterrestrial Scout”. In: *2022 IEEE Aerospace Conference (AERO)*, pp. 01–19. DOI: 10.1109/AERO53065.2022.9843428.
- Watson-Morgan, L., K. Chojnacki, L. Gagliano, S. Holcomb, L. Means, R. Ortega, T. Percy, T. Polsgrove, et al. (2023). In: *NASA’s Human Landing System: A Sustaining Presence on the Moon*.
- Wedler, A., M. G. Müller, M. Schuster, M. Durner, P. Lehner, A. Dömel, F. Steidle, M. Vayugundla, et al. (Sept. 2022). “Finally! Insights into the ARCHES Lunar Planetary Exploration Analogue Campaign on Etna in summer 2022”. In: *73rd International Astronautical Congress, IAC 2022*. URL: <https://elib.dlr.de/191389/>.

- Williamson, M. (2006). *Lunar lander - the development of the Apollo Lunar Module*. DOI: 10.1049/PBHT033E\_ch9. URL: [https://digital-library.theiet.org/content/books/10.1049/pbht033e\\_ch9](https://digital-library.theiet.org/content/books/10.1049/pbht033e_ch9).
- Witze, A. (Nov. 2022). *Lift off! Artemis Moon rocket launch kicks off New Era of Human Exploration*. URL: <https://www.nature.com/articles/d41586-022-02310-w>.
- Wormnes, K., W. Carey, T. Krueger, L. Cencetti, E. den Exter, S. Ennis, E. Ferreira, A. Fortunato, et al. (2022). In: *Open Astronomy* 31.1, pp. 5–14. DOI: doi:10.1515/astro-2022-0002. URL: <https://doi.org/10.1515/astro-2022-0002>.
- Xiao, L., Y. Qian, Q. Wang, and Q. Wang (2021). “CHAPTER 9 - The Chang’e-5 mission”. In: *Sample Return Missions*. Ed. by A. Longobardo. Elsevier, pp. 195–206. DOI: <https://doi.org/10.1016/B978-0-12-818330-4.00009-4>. URL: <https://www.sciencedirect.com/science/article/pii/B9780128183304000094>.
- Xin, L. (Jan. 2024). *Japan’s successful Moon landing was the most precise ever*. URL: <https://www.nature.com/articles/d41586-024-00151-3>.
- Zhou, C., Y. Jia, J. Liu, H. Li, Y. Fan, Z. Zhang, Y. Liu, Y. Jiang, et al. (2022). “Scientific objectives and payloads of the lunar sample return mission—Chang’E-5”. In: *Advances in Space Research* 69.1, pp. 823–836. DOI: <https://doi.org/10.1016/j.asr.2021.09.001>. URL: <https://www.sciencedirect.com/science/article/pii/S0273117721006931>.

# Appendix

## **A Sample Tube**

Here you can find the specifications for the Sample Tube. Due to the complexity of representing the 3D printed parts, this section presents just the core of the Sample Tube, which guarantees the rigidity of the entire equipment.

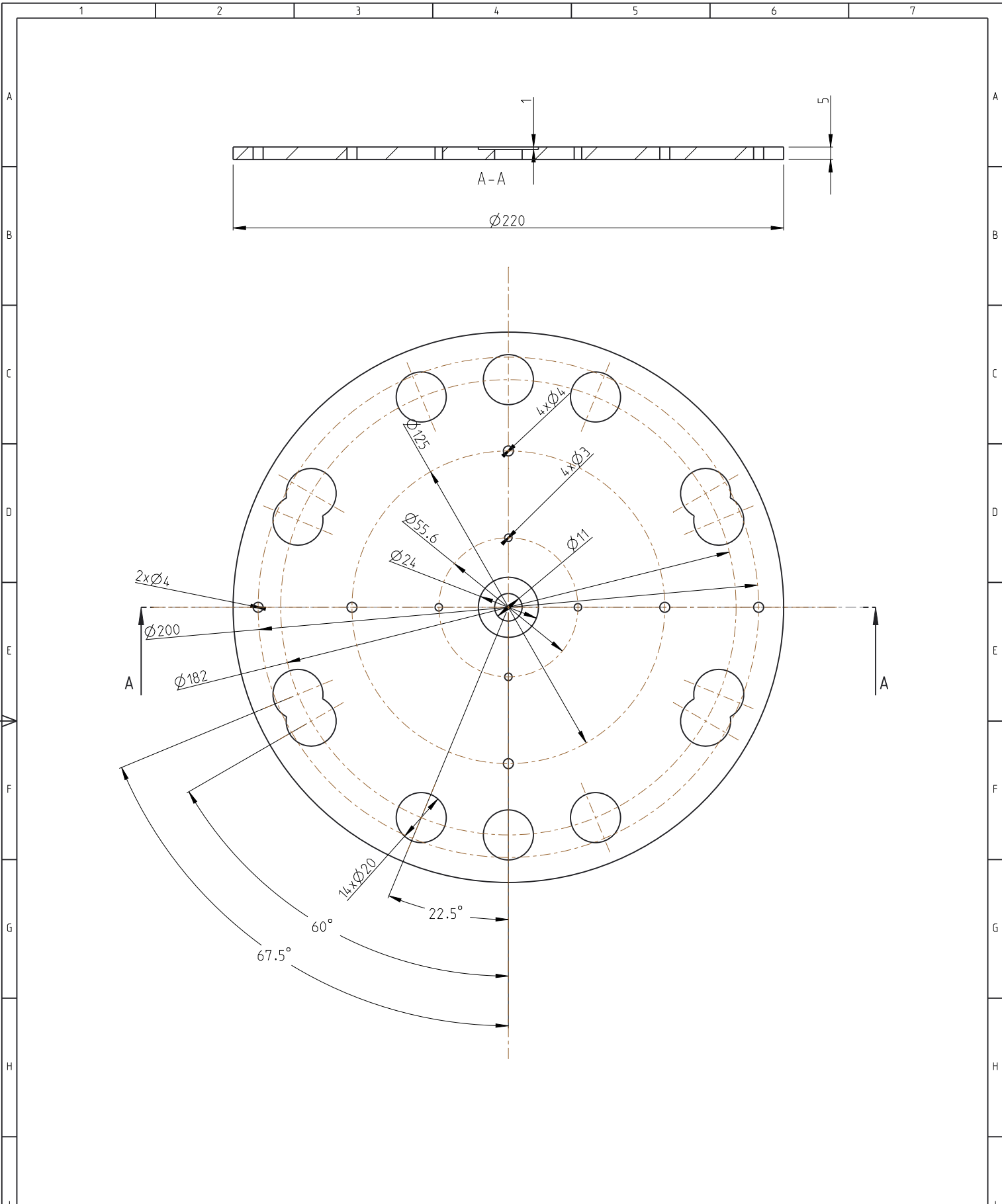



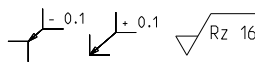
Deutsches Zentrum für Luft- und Raumfahrt Institut für Robotik und Mechatronik Airbus Nr. 20 D-22334 Wessling Tel: (+49) 0211 930-2400 Fax: -1134		heat and surface treatment: - material: EN AW-2007
created by: Frank, Peter Henning 09-Aug-23 06:56:37 PM modified by: Frank, Peter Henning 30-Aug-23 06:09:49 AM checked by: - model: M2_STU_V3_SLIDE_TUBE.PART drawing: M2_STU_V3_SLIDE_TUBE.DRW title:	copyright: ISO 14016 order filing date: order quantity: 15 mass (M_STU): 0.0 g	description: m2_stu_v3_slide_tube DLR part no: 0001275631 version: A.1 status: Konstruktion scale: 1:1 sheet 1/1 DIN A3

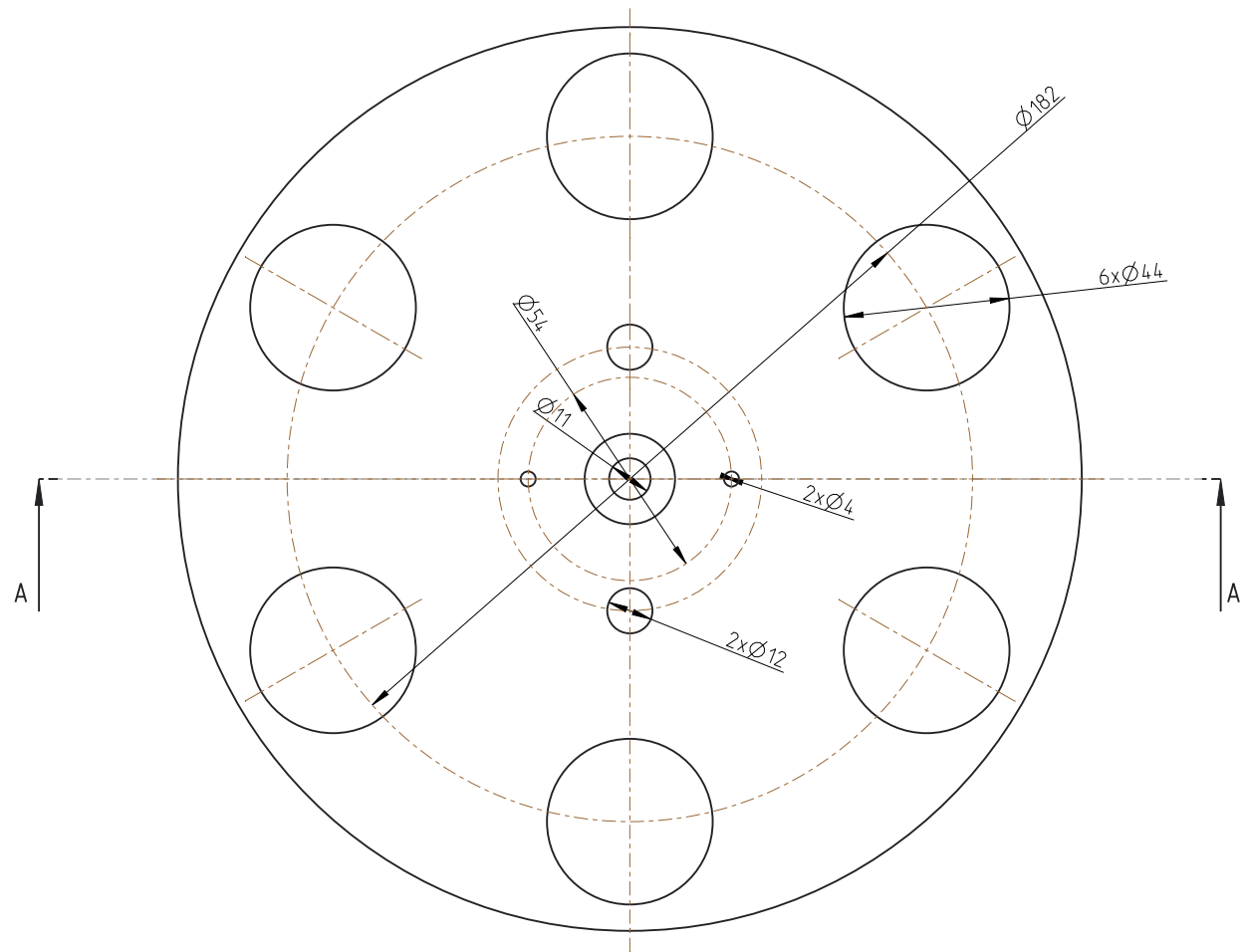
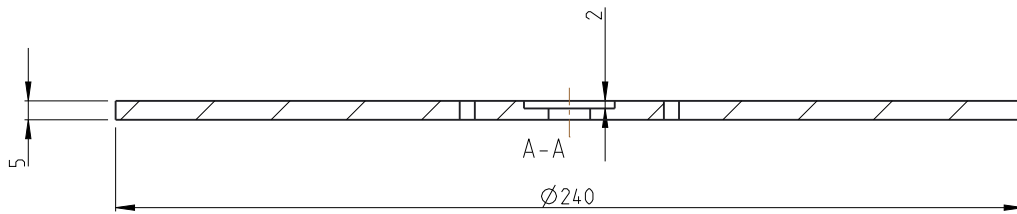
## **B Rotational Stowage Device**


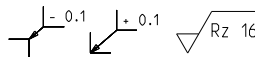
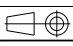
Here you can find the custom parts for the Rotational Stowage Device.

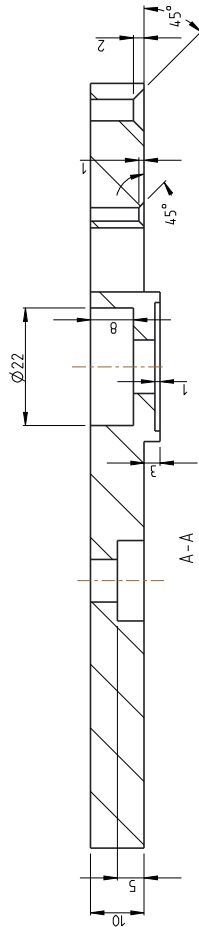
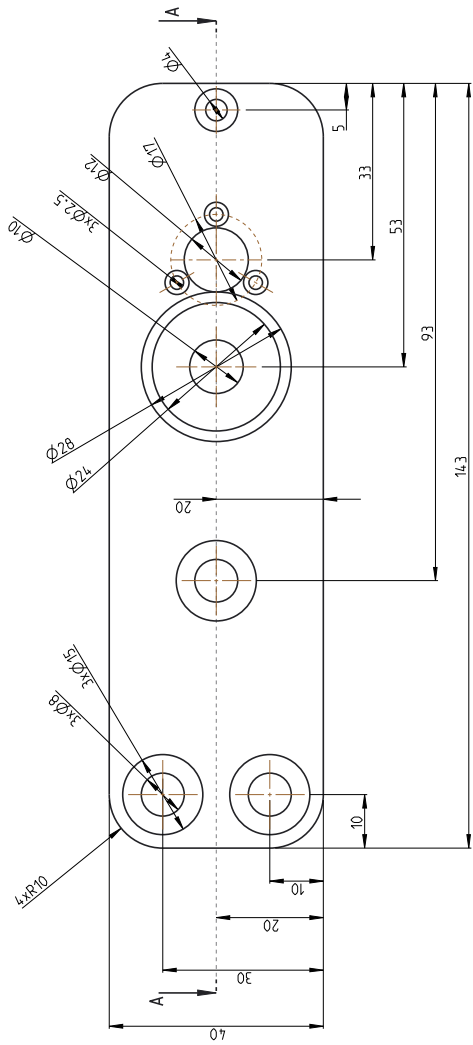





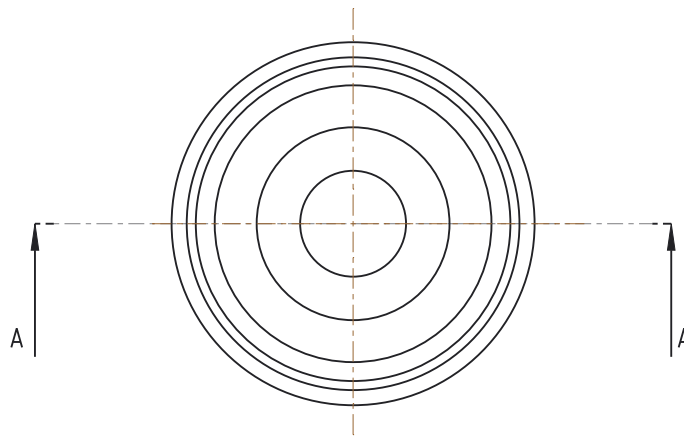
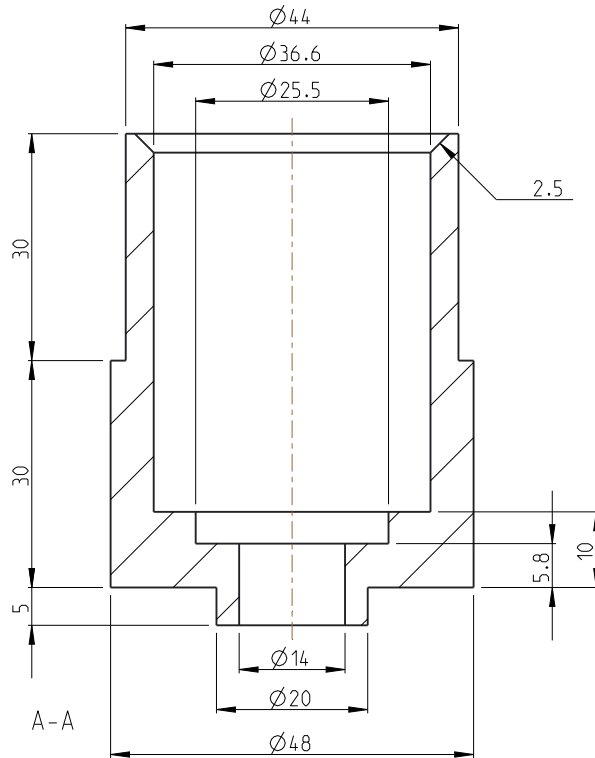
 <b>Deutsches Zentrum für Luft- und Raumfahrt</b> Institut für Robotik und Mechatronik Münchener Str. 20 D-82234 Weßling Tel: (+49) 08153/28-2400 Fax: -1134	 general tolerance: DIN ISO 2768-f H		heat and surface treatment: - (DIN ISO 1302) - material: EN AW-2007		
	created by: Pavelski, Pedro Henrique 15-Nov-22 11:37:56 AM modified by: Pavelski, Pedro Henrique 15-Nov-22 05:02:25 PM checked by: - model: M2_RSU_S_BASE_BOTTOM_V2.PART drawing: M2_RSU_S_BASE_BOTTOM_V2.DRW path: /Produkte/Marc-II/Marc-II Revolving Storage Unit	copyright ISO 16016 order filing date:		description: <b>m2_rsu_s_base_bottom_v2.prt</b> <b>DLR</b> part no: <b>0001202614</b> mass (AL_STD): <b>0.0 g</b>	
		order quantity: <b>3</b>	version: <b>A.2</b> status: <b>Konstruktion</b> sheet 1/1	scale: <b>1:2</b> DIN A4	



 <b>Deutsches Zentrum für Luft- und Raumfahrt</b> Institut für Robotik und Mechatronik Münchener Str. 20 D-82234 Wessling Tel: (+49) 08153/28-2400 Fax: -1134	 general tolerance: DIN ISO 2768-f H		heat and surface treatment: - (DIN ISO 1302) -	
	created by: Pavelski, Pedro Henrique 15-Nov-22 01:13:19 PM modified by: Pavelski, Pedro Henrique 24-Jan-23 02:20:25 PM checked by: - model: M2_RSU_S_BASE_UPPER_6_V2.PART drawing: M2_RSU_S_BASE_UPPER_6_V2.DRW path: /Produkte/Marc-II/Marc-II Revolving Storage Unit		material: EN AW-2007 description: m2_rsu_s_base_upper_6_v2.prt DLR	
copyright ISO 16016 order filing date:		part no: 0001202626 mass (AL_STD): 0.0 g		version: A.2 status: Konstruktion sheet 1/1
order quantity: 3		 scale: 1:2 DIN A4		



 Deutsches Zentrum für Luft- und Raumfahrt Institut für Robotik und Mechatronik München, Str. 20 85375 Freising, Germany Tel: (+49) 89 1883326-2400 Fax: -1134		heat and surface treatment: (DIN ISO 1302) -	
created by: Pevicki, Pedro Henrique 15-Nov-22 11:37:56 AM modified by: Pevicki, Pedro Henrique 23-Jan-23 04:25:52 PM checked by: -		description: EN AW-2007	
model: M2_RSU_S_BASE_MOUNTING_V2.PART drawing: M2_RSU_S_BASE_MOUNTING_V2.DRW path: /Produkt/Mech/Ansch-1/Revolving Storage Unit		material: m2_rsu_s_base_mounting_v2.prt DLR	
order filling date:		part no.: 0001202611	
copyright: ISO 16016		version: A.1 Konstruktion 1:1	
order quantity: 3		mass (AL_STD): 0.0 g	
sheet 22		DIN A3	



Deutsches Zentrum für Luft- und Raumfahrt  
 Institut für Robotik und Mechatronik  
 Münchener Str. 20  
 D-82234 Weßling  
 Tel: (+49) 08153/28-2400 Fax: -1134

$\begin{matrix} \text{---} & -0.1 \\ \text{---} & +0.1 \end{matrix}$ 
 $\sqrt{Rz\ 16}$   
 general tolerance: DIN ISO 2768-f H

heat and surface treatment: -  
 (DIN ISO 1302) -

material: POM

created by	Pavelski, Pedro	29-Nov-22 05:18:30 PM
modified by	Pavelski, Pedro	23-Jan-23 12:43:18 PM
checked by	-	
model:	M2_RSU_S_PROBE_SUPPORT_V2.PART	
drawing:	M2_RSU_S_PROBE_SUPPORT_V2.DRW	
path:	/Produkte/Marc-II	

copyright ISO 16016
order filing date:
order quantity: 14

description: m2_rsu_s_probe_support_v2.prt DLR			
part no: 0001205024	version: A.1	status: Konstruktion	scale: 1:1
mass (POM): 0.0 g	sheet 1/1		DIN A4

---

## **C Extended Reachability Mechanism**

Here you can find the custom made components for the ERM, part of the Sample Stowage Device.

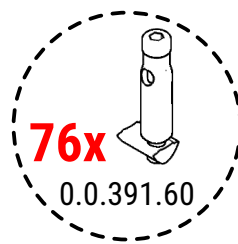
### **C.1 Case for the Rotational Stowage Device**

The case was built using the standard construction profile of 20mm. Below, you can find the part counting and the assembled drawing.

## Stückliste

Position	Artikelbezeichnung	Artikel-Nr.	Seite	Anzahl
1	Profil 5 20x20, natur, Länge: 28mm	0.0.370.03	2	4
2	Profil 5 20x20, natur, Länge: 145mm	0.0.370.03	2	2
3	Profil 5 20x20, natur, Länge: 240mm	0.0.370.03	2	15
4	Profil 5 20x20, natur, Länge: 270mm	0.0.370.03	2	4
5	Automatik-Verbindungssatz 5, verzinkt	0.0.391.60	-	76

### Verbindungstechnik ( gesamt )



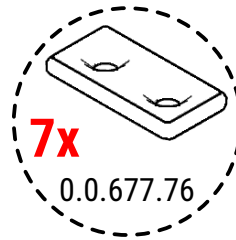
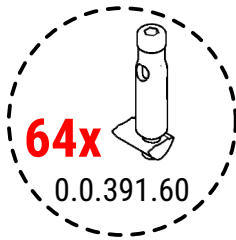
## **C.2 ERM frame**

The frame holds both RSUs, the electronics and provides structure to connect the Sample Stowage Device to the Lander.

## Stückliste

Position	Artikelbezeichnung	Artikel-Nr.	Seite	Anzahl
1	Profil 5 20x20, natur, Länge: 47mm	0.0.370.03	2	6
2	Profil 5 20x20, natur, Länge: 67mm	0.0.370.03	2	2
3	Profil 5 20x20, natur, Länge: 106mm	0.0.370.03	2	2
4	Profil 5 20x20, natur, Länge: 160mm	0.0.370.03	2	3
5	Profil 5 20x20, natur, Länge: 280mm	0.0.370.03	2	2
6	Profil 5 20x20, natur, Länge: 294mm	0.0.370.03	2	1
7	Profil 5 20x20, natur, Länge: 300mm	0.0.370.03	3	4
8	Profil 5 20x20, natur, Länge: 700mm	0.0.370.03	3	6
9	Automatik-Verbindungssatz 5, verzinkt	0.0.391.60	-	64
10	Winkelsatz 5 20x20	0.0.425.02	-	6
11	Lasche 5 20, weißaluminium ähnlich RAL 9006	0.0.677.76	-	7
12	Befestigungssatz 5 2-4mm mit Senkschraube M5	0.0.680.92	-	14

### Verbindungstechnik ( gesamt )





---

## D Particle Swarm Optimization

### D.1 Main File

the main file contains all the options and parameters to run the optimization as well as the command to run the PySwarms (Miranda 2018) algorithm.

```
1 import numpy as np
2 from arm_position_functions import objective_function as
  objective_function
3 from arm_position_functions import plane_from_point_normal as
  plane_from_point_normal
4 import pyswarms as ps
5 from functools import partial
6 import pickle
7
8
9 if __name__ == "__main__":
10
11 # Set the bounds for the variables
12 bounds = (np.array([0.448, -0.705, 0.460]), np.array([0.748,
  -0.425, 1.165]))
13 normalization_factor = bounds[1][0] - bounds[0][0]
14
15 box_bounds = {
16     "xmin": -0.800,
17     "xmax": 1.200,
18     "ymin": -0.600,
19     "ymax": 0.900,
20     "zmin": -1.085,
21     "zmax": 1.165
22 }
23
24 step_factors = {
25     'polar_angle1' : 0.5,
26     'azimuthal_angle1' : 0.5,
27     'polar_angle2' : 0.5,
28     'azimuthal_angle2' : 1.0
29 }
30
```

```
31 angle_min = {
32     'polar_angle1' : 0,
33     'azimuthal_angle1' : -np.pi/4,
34     'polar_angle2' : 0,
35     'azimuthal_angle2' : 0
36 }
37
38 angle_max = {
39     'polar_angle1' : np.pi,
40     'azimuthal_angle1' : 5*np.pi/4,
41     'polar_angle2' : np.pi,
42     'azimuthal_angle2' : 2*np.pi
43 }
44
45 point = np.array([-0.065, -0.4, 0.0])
46 normal = np.array([np.cos(np.pi/4), -np.cos(np.pi/4), 0.0])
47 attachment_plane = plane_from_point_normal(point, normal)
48 lenght_1 = 1.0
49 lenght_2 = 1.0
50 stl_file = 'base_opt/m2_ldr_simple_model_view.stl'
51
52 n_particles = 100
53 iters = 20
54 step = 20
55
56 workspace_weight = 0.8
57 distance_weight = 1.0 - workspace_weight
58 distance_weight = round(distance_weight,1)
59
60 options_objective_function = {
61     'step' : int(step),
62     'stl_file' : 'base_opt/m2_ldr_simple_model_view.stl',
63     'workspace_weight' : workspace_weight,
64     'distance_weight' : distance_weight,
65     'box_bounds' : box_bounds,
66     'attachment_plane' : attachment_plane,
67     'normalization_factor' : normalization_factor,
68     'angle_min' : angle_min,
69     'angle_max' : angle_max,
70     'length1' : lenght_1,
71     'length2' : lenght_2,
72     'step_factors' : step_factors
```

```
73     }
74
75     objective_function_options = partial(objective_function,
76         options_objective_function=options_objective_function)
77
78     # Initialize the optimizer
79     c1, c2, w = 0.5, 0.3, 0.9
80     options = {'c1': c1, 'c2': c2, 'w': w}
81     optimizer = ps.single.GlobalBestPSO(n_particles=n_particles,
82         dimensions=3, options=options, bounds=bounds)
83
84     # Perform optimization
85     best_cost, best_pos = optimizer.optimize(
86         objective_function_options, iters=iters)
87
88     pos_history = optimizer.pos_history
89     cost_history = optimizer.cost_history
90
91     # Save to a file
92
93     #file_name = f"base_opt/results/
94         optimizer_results_workspace_weight_{workspace_weight}_options_
95         {step}_{n_particles}_{iters}_{c1}_{c2}_{w}.pkl"
96     file_name = f"base_opt/results/
97         optimizer_results_workspace_weight_final.pkl"
98
99     with open(file_name, 'wb') as f:
100         pickle.dump({
101             'best_cost': best_cost,
102             'best_pos': best_pos,
103             'pos_history': pos_history,
104             'cost_history': cost_history
105         }, f)
```

## D.2 Objective Function

It contains the calculation to determine the score given a point in space. This part of the code is also adapted for parallel computing.

```
1 import numpy as np
```

```
2 import trimesh
3 from stl import mesh
4 import matplotlib.pyplot as plt
5 from mpl_toolkits.mplot3d import art3d
6 import math
7 import time
8 from multiprocessing import Pool, cpu_count
9
10 def objective_function(start_points1, options_objective_function):
11
12     start_time = time.time()
13
14     start_points1 = rotate_z(start_points1, -math.pi/4)
15
16     # Load options
17     stl_file = options_objective_function['stl_file']
18     attachment_plane = options_objective_function['attachment_plane']
19     distance_weight = options_objective_function['distance_weight']
20     workspace_weight = options_objective_function['workspace_weight']
21     step = options_objective_function['step']
22     normalization_factor = options_objective_function['
23         normalization_factor']
24     step_factors = options_objective_function['step_factors']
25     angle_min = options_objective_function['angle_min']
26     angle_max = options_objective_function['angle_max']
27     length1, length2 = options_objective_function['length1'],
28         options_objective_function['length2']
29
30     score = np.zeros(len(start_points1))
31     i = 0
32
33     for start_point1 in start_points1:
34         collisions = 0
35         tasks = []
36         for polar_angle1 in np.linspace(angle_min['polar_angle1'],
37             angle_max['polar_angle1'], int(step * step_factors['
38                 polar_angle1']))):
39             for azimuthal_angle1 in np.linspace(angle_min['azimuthal_angle1'],
40                 angle_max['azimuthal_angle1'], int(step * step_factors['
41                     azimuthal_angle1']))):
```

```

36 for polar_angle2 in np.linspace(angle_min['polar_angle2'],
    angle_max['polar_angle2'], int(step * step_factors['
    polar_angle2'])):
37 for azimuthal_angle2 in np.linspace(angle_min['azimuthal_angle2'],
    angle_max['azimuthal_angle2'], int(step * step_factors['
    azimuthal_angle2'])):
38 tasks.append((polar_angle1, azimuthal_angle1, polar_angle2,
    azimuthal_angle2, start_point1, length1, length2,
    options_objective_function['box_bounds']))
39
40 with Pool(initializer=init_worker, initargs=(stl_file,),
    processes=cpu_count()) as pool:
41 results = pool.starmap(check_collisions_for_angles, tasks)
42
43 collisions = sum(results)
44 collision_rate = collisions / (step ** 4 * step_factors['
    polar_angle1'] * step_factors['azimuthal_angle1'] *
    step_factors['polar_angle2'] * step_factors['azimuthal_angle2'
    ])
45
46 distance = distance_to_plane(attachment_plane, start_point1) /
    normalization_factor
47
48 score[i] = collision_rate * workspace_weight + distance *
    distance_weight
49 i += 1
50 end_time = time.time()
51 execution_time = end_time - start_time
52 print(f"\nExecution time: {execution_time:.2f} seconds")
53 # print(f"Function Value: {score}")
54 return score

```

## D.3 Support Functions

This section contains all the functions that support the Objective Function and Main File codes.

```

1 import numpy as np
2 import trimesh
3 from stl import mesh
4 import matplotlib.pyplot as plt

```

```
5 from mpl_toolkits.mplot3d import art3d
6 import math
7 import time
8 from multiprocessing import Pool, cpu_count
9
10 def distance_to_plane(plane_coefficients, points):
11
12     A, B, C, D = plane_coefficients
13     x0, y0, z0 = points
14
15     numerator = np.abs(A*x0 + B*y0 + C*z0 + D)
16     denominator = np.sqrt(A**2 + B**2 + C**2)
17
18     distance = numerator / denominator
19
20     return distance
21
22 def plane_from_point_normal(point, normal):
23     x0, y0, z0 = point
24     nx, ny, nz = normal
25
26     # Coefficients A, B, C are the components of the normal vector
27     A, B, C = nx, ny, nz
28
29     # Determine D using the point on the plane
30     D = - (A*x0 + B*y0 + C*z0)
31
32     return (np.array([A, B, C, D]))
33
34 def distance_between_points(point1, point2):
35
36     point1 = np.array(point1)
37     point2 = np.array(point2)
38
39     distance = np.linalg.norm(point2 - point1)
40
41     return distance
42
43 def rotate_z(vector, angle):
44
45     rotation_matrix = np.array([[math.cos(angle), -1*math.sin(angle),
46                                 0],
```

```
46     [math.sin(angle), math.cos(angle), 0],
47     [0, 0, 1]])
48     vector_out = np.dot(rotation_matrix, np.transpose(vector))
49     vector_out = np.transpose(vector_out)
50
51     return vector_out
52
53     def spherical_to_cartesian(polar_angle, azimuthal_angle, length):
54
55         # Calculate coordinates of the end point
56         x_end = length * np.cos(azimuthal_angle) * np.sin(polar_angle)
57         y_end = length * np.sin(azimuthal_angle) * np.sin(polar_angle)
58         z_end = length * np.cos(polar_angle)
59
60         return (x_end, y_end, z_end)
61
62     def start_and_end_points(polar_angle1, start_point1,
63                             azimuthal_angle1, length1, polar_angle2, azimuthal_angle2,
64                             length2):
65
66         end_point1 = start_point1 + spherical_to_cartesian(polar_angle1,
67                                                             azimuthal_angle1, length1)
68
69         # Compute coordinates for Line 2
70         start_point2 = end_point1 # Start Line 2 where Line 1 ends
71         end_point2 = (start_point2[0] + length2 * np.cos(azimuthal_angle2)
72                      ) * np.sin(polar_angle2),
73         start_point2[1] + length2 * np.sin(azimuthal_angle2) * np.sin(
74             polar_angle2),
75         start_point2[2] + length2 * np.cos(polar_angle2))
76
77         return end_point1, start_point2, end_point2
78
79     def plot_simple(stl_file, start_point1, polar_angle1,
80                   azimuthal_angle1, length_1, polar_angle2, azimuthal_angle2,
81                   length_2, particle_bound, workspace_bound):
82
83         end_point1, start_point2, end_point2 = start_and_end_points(
84             polar_angle1, start_point1, azimuthal_angle1, length_1,
85             polar_angle2, azimuthal_angle2, length_2)
86
87         fig = plt.figure()
```

```
79 axes = fig.add_subplot(111, projection='3d')
80
81 # Load the STL files and add the vectors to the plot
82 my_mesh = mesh.Mesh.from_file(stl_file)
83
84 poly3d = art3d.Poly3DCollection(my_mesh.vectors, alpha=0.2,
85     edgecolors='none', facecolors=(0.6, 0.6, 0.6, 0.1))
86 axes.add_collection3d(poly3d)
87
88 xlim = [-0.8, 1.5]
89 ylim = [-1.5, 1.5]
90 zlim = [-1.085, 2.5]
91
92 axes.set_xlim(xlim) # Specify the limits for the x-axis
93 axes.set_ylim(ylim) # Specify the limits for the y-axis
94 axes.set_zlim(zlim) # Specify the limits for the z-axis
95
96 # Customize axes labels
97 axes.set_xlabel('X [m]')
98 axes.set_ylabel('Y [m]')
99 axes.set_zlabel('Z [m]')
100
101 x_aspect = 1
102 y_aspect = (ylim[1] - ylim[0]) / (xlim[1] - xlim[0])
103 z_aspect = (zlim[1] - zlim[0]) / (xlim[1] - xlim[0])
104 axes.set_box_aspect([x_aspect, y_aspect, z_aspect])
105
106 x1, y1, z1 = start_point1
107 x2, y2, z2 = end_point1
108
109 # Plot the line
110 axes.plot([x1, x2], [y1, y2], [z1, z2], marker='o', color='r')
111
112 x1, y1, z1 = start_point2
113 x2, y2, z2 = end_point2
114
115 # Plot the line
116 axes.plot([x1, x2], [y1, y2], [z1, z2], marker='o', color='b')
117
118 min_x, max_x = particle_bound[0][0], particle_bound[1][0]
119 min_y, max_y = particle_bound[0][1], particle_bound[1][1]
```



```
120 min_z, max_z = particle_bound[0][2], particle_bound[1][2]
121
122 # Define the vertices for the boundary box
123 vertices = np.array([[min_x, min_y, min_z],
124 [max_x, min_y, min_z],
125 [max_x, max_y, min_z],
126 [min_x, max_y, min_z],
127 [min_x, min_y, max_z],
128 [max_x, min_y, max_z],
129 [max_x, max_y, max_z],
130 [min_x, max_y, max_z]])
131
132 vertices = rotate_z(vertices, -math.pi/4)
133 #print(vertices[2])
134
135 # Define the edges for the box
136 edges = [[vertices[0], vertices[1], vertices[2], vertices[3],
137 vertices[0]],
138 [vertices[4], vertices[5], vertices[6], vertices[7], vertices[4]],
139 [vertices[0], vertices[4]],
140 [vertices[1], vertices[5]],
141 [vertices[2], vertices[6]],
142 [vertices[3], vertices[7]]]
143
144 for edge in edges:
145     x, y, z = zip(*edge) # Unzip the coordinates
146     axes.plot3D(x, y, z, color='b') # Plot the edges
147
148 min_x, max_x = workspace_bound['xmin'], workspace_bound['xmax']
149 min_y, max_y = workspace_bound['ymin'], workspace_bound['ymax']
150 min_z, max_z = workspace_bound['zmin'], workspace_bound['zmax']
151
152 # Define the vertices for the boundary box
153 vertices = np.array([[min_x, min_y, min_z],
154 [max_x, min_y, min_z],
155 [max_x, max_y, min_z],
156 [min_x, max_y, min_z],
157 [min_x, min_y, max_z],
158 [max_x, min_y, max_z],
159 [max_x, max_y, max_z],
160 [min_x, max_y, max_z]])
```

```
160
161
162 # Define the edges for the box
163 edges = [[vertices[0], vertices[1], vertices[2], vertices[3],
164           vertices[0]],
165           [vertices[4], vertices[5], vertices[6], vertices[7], vertices[4]],
166           [vertices[0], vertices[4]],
167           [vertices[1], vertices[5]],
168           [vertices[2], vertices[6]],
169           [vertices[3], vertices[7]]]
170
171 for edge in edges:
172     x, y, z = zip(*edge) # Unzip the coordinates
173     axes.plot3D(x, y, z, color='r') # Plot the edges
174
175 #axes.view_init(elev=15, azimuth=30) #iso
176 axes.view_init(elev=0, azimuth=-90)
177 axes.set_proj_type('ortho')
178 plt.show()
179
180 def plot_cost(cost_history):
181     # Number of iterations
182     iterations = range(len(cost_history))
183
184     # Plotting the cost function
185     plt.plot(iterations, cost_history, marker='o', linestyle='--',
186             color='black')
187     plt.title('Cost Function vs. Iterations')
188     plt.xlabel('Iterations')
189     plt.ylabel('Cost')
190     plt.grid(True)
191     plt.show()
192
193 def init_worker(mesh_file):
194     global mesh
195     mesh = trimesh.load(mesh_file)
196
197 def collision_with_STL(line_start, line_end):
198     def distance_between_points(point1, point2):
199         return np.linalg.norm(np.array(point2) - np.array(point1))
```

```
199 ray_origin = line_start
200 ray_direction = line_end - line_start
201 ray_direction /= np.linalg.norm(ray_direction) # Normalize the
        direction
202
203 locations, index_ray, index_tri = mesh.ray.intersects_location(
204 ray_origins=[ray_origin],
205 ray_directions=[ray_direction]
206 )
207
208 collision = False
209 if len(locations) > 0:
210 closest_distance = min(distance_between_points(loc, ray_origin)
        for loc in locations)
211 if closest_distance < 1.0:
212 collision = True
213
214 return collision
215
216 def is_within_box(point, bounds):
217 x, y, z = point
218 return (bounds["xmin"] <= x <= bounds["xmax"] and
219 bounds["ymin"] <= y <= bounds["ymax"] and
220 bounds["zmin"] <= z <= bounds["zmax"])
221
222 def check_collisions_for_angles(polar_angle1, azimuthal_angle1,
        polar_angle2, azimuthal_angle2, start_point1, length1, length2,
        box_bounds):
223 end_point1, start_point2, end_point2 = start_and_end_points(
        polar_angle1, start_point1, azimuthal_angle1, length1,
        polar_angle2, azimuthal_angle2, length2)
224
225 # Check if end_point2 is within the box
226 if not is_within_box(end_point2, box_bounds):
227 return True
228
229 is_intersecting_1 = collision_with_STL(start_point1, end_point1)
230 is_intersecting_2 = collision_with_STL(start_point2, end_point2)
231 return is_intersecting_1 or is_intersecting_2
```

## D.4 Plotting Results

This code plots the Lander STL model with the box of interest and the boundaries. The Arm is plotted as two segments of a line.

```
1  import pickle
2  import numpy as np
3  from arm_position_functions import plot_simple as plot_simple
4  from arm_position_functions import rotate_z as rotate_z
5  from arm_position_functions import plot_cost as plot_cost
6  import matplotlib.pyplot as plt
7
8  workspace_weight = 0.8
9  # distance_weight = 1.0 - workspace_weight
10
11  n_particles = 10
12  box_bounds = {
13      "xmin": -0.800,
14      "xmax": 1.200,
15      "ymin": -0.600,
16      "ymax": 0.900,
17      "zmin": -1.085,
18      "zmax": 1.165
19  }
20  lenght_1 = 1.0
21  lenght_2 = 1.0
22  stl_file = 'base_opt/m2_ldr_simple_model_view.stl'
23  n_particles = 50
24  iters = 20
25  step = 20
26
27  bounds = (np.array([0.448, -0.705, 0.460]), np.array([0.748,
28      -0.425, 1.165]))
29
30  best_cost_list = []
31
32  #with open(f'base_opt/results/optimizer_results_workspace_weight_
33      {workspace_weight}_options_{step}_{n_particles}_{iters}.pkl', '
34      rb') as f:
```

```

34
35 best_cost = data['best_cost']
36 best_pos = data['best_pos']
37 pos_history = data['pos_history']
38 cost_history = data['cost_history']
39
40 best_cost_list.append(best_cost)
41
42 # Define the arm configuration for plot
43 start_point1 = best_pos
44 start_point1 = rotate_z(start_point1, -np.pi/4)
45
46 polar_angle1 = np.radians(90) # min = 0; max = 180
47 polar_angle2 = np.radians(135) # min = 0; max = 180
48 azimuthal_angle1 = np.radians(45) # min = -45; max = 135
49 azimuthal_angle2 = np.radians(135) # min = 0; max = 360
50
51 plot_simple(stl_file, start_point1, polar_angle1,
52            azimuthal_angle1, lenght_1, polar_angle2, azimuthal_angle2,
53            lenght_2, bounds, box_bounds)
54 plot_cost(cost_history)
55 print(best_cost)
56 print(best_pos)

```

## D.5 Plotting the Cost

The cost along the iterations is plotted using the following code.

```

1  import pickle
2  import numpy as np
3  from decimal import Decimal
4
5
6  n_particles = 50
7  iters = 15
8  step = 20
9
10 workspace_weight = 1.0
11
12 c1_list = [0.2, 0.5, 0.8]

```

## D Particle Swarm Optimization

---

```
13 w_list = [0.1, 0.3, 0.5, 0.7, 0.9]
14
15 best_cost_all = 1.0
16
17 for c1 in c1_list:
18     for w in w_list:
19         c2 = 1.0 - c1
20         c2 = round(c2,1)
21         with open(f'base_opt/results/optimizer_results_workspace_weight_{
                workspace_weight}_options_{step}_{n_particles}_{iters}_{c1}_{
                c2}_{w}.pkl', 'rb') as f:
22             data = pickle.load(f)
23
24             best_cost = data['best_cost']
25             best_pos = data['best_pos']
26
27             if best_cost < best_cost_all:
28                 best_cost_all = best_cost
29                 c1_best = c1
30                 c2_best = c2
31                 w_best = w
32
33             print(f"\nFor c1 = {c1}, c2 = {c2}, w = {w}, best cost = {
                best_cost}")
34             print(f"Best case: c1 = {c1_best}, c2 = {c2_best}, w = {w_best},
                best cost = {best_cost_all}")
```

### D.6 Discretization Impact

The code bellow was used to measure the impact of the discretization on the optimization results.

```
1 import numpy as np
2 from arm_position_functions import objective_function as
  objective_function
3 from arm_position_functions import plane_from_point_normal as
  plane_from_point_normal
4 import pickle
5
6 if __name__ == "__main__":
7
```

```
8 # Set the bounds for the variables
9 bounds = (np.array([0.448, -0.705, 0.460]), np.array([0.748,
10             -0.425, 1.165]))
11 normalization_factor = bounds[1][0] - bounds[0][0]
12
13 # Define the bounds
14 lower_bound = np.array([0.448, -0.705, 0.460])
15 upper_bound = np.array([0.748, -0.425, 1.165])
16
17 # Function to generate random coordinates within bounds
18 def generate_coordinates(num_points, lower_bound, upper_bound):
19     return np.random.uniform(lower_bound, upper_bound, (num_points,
20         len(lower_bound)))
21
22 # Generate a list of 10 coordinates
23 num_points = 5
24 #coordinates = generate_coordinates(num_points, lower_bound,
25     upper_bound)
26 file_name = f"base_opt/results/step_test_coordinates.pkl"
27 #with open(file_name, 'wb') as f:
28 #    pickle.dump(coordinates, f)
29
30 with open(file_name, 'rb') as f:
31     coordinates = pickle.load(f)
32
33 box_bounds = {
34     "xmin": -0.800,
35     "xmax": 1.200,
36     "ymin": -0.600,
37     "ymax": 0.900,
38     "zmin": -1.085,
39     "zmax": 1.165
40 }
41
42 step_factors = {
43     'polar_angle1' : 0.5,
44     'azimuthal_angle1' : 0.5,
45     'polar_angle2' : 0.5,
46     'azimuthal_angle2' : 1.0
47 }
48
49 angle_min = {
```

```
47     'polar_angle1' : 0,
48     'azimuthal_angle1' : -np.pi/4,
49     'polar_angle2' : 0,
50     'azimuthal_angle2' : 0
51 }
52
53 angle_max = {
54     'polar_angle1' : np.pi,
55     'azimuthal_angle1' : 5*np.pi/4,
56     'polar_angle2' : np.pi,
57     'azimuthal_angle2' : 2*np.pi
58 }
59
60 point = np.array([-0.065, -0.4, 0.0])
61 normal = np.array([np.cos(np.pi/4), -np.cos(np.pi/4), 0.0])
62 attachment_plane = plane_from_point_normal(point, normal)
63 lenght_1 = 1.0
64 lenght_2 = 1.0
65 stl_file = 'base_opt/m2_ldr_simple_model_view.stl'
66
67 step_list = np.linspace(64,124,11)
68
69 n_particles = 50
70 iters = 10
71 workspace_weight = 0.8
72 distance_weight = 1.0 - workspace_weight
73 distance_weight = round(distance_weight,1)
74
75 for step in step_list:
76     step = int(step)
77     print(f"Computing Objective Function for step = {step}.")
78
79     options_objective_function = {
80         'step' : step,
81         'stl_file' : 'base_opt/m2_ldr_simple_model_view.stl',
82         'workspace_weight' : workspace_weight,
83         'distance_weight' : distance_weight,
84         'box_bounds' : box_bounds,
85         'attachment_plane' : attachment_plane,
86         'normalization_factor' : normalization_factor,
87         'angle_min' : angle_min,
88         'angle_max' : angle_max,
```



```

89     'length1' : lenght_1,
90     'length2' : lenght_2,
91     'step_factors' : step_factors
92 }
93
94 costs = objective_function(coordinates,
95                             options_objective_function)
96
97 file_name = f"base_opt/results/step_test_{step}.pkl"
98 with open(file_name, 'wb') as f:
99     pickle.dump(costs, f)

```

```

1  import numpy as np
2  import pickle
3  import matplotlib.pyplot as plt
4
5  step_list = np.linspace(20, 96, 20)
6  #print(step_list)
7  cost_1_list = []
8  cost_2_list = []
9  cost_3_list = []
10
11 for step in step_list:
12     step = int(step)
13     file_name = f"base_opt/results/step_test_{step}.pkl"
14     with open(file_name, 'rb') as f:
15         costs = pickle.load(f)
16         #print(f"For step {step}: costs = {costs}")
17
18     cost_1_list.append(costs[0])
19     cost_2_list.append(costs[1])
20     cost_3_list.append(costs[2])
21
22     cost_1_mean = round(np.mean(cost_1_list), 3)
23     cost_2_mean = round(np.mean(cost_2_list), 3)
24     cost_3_mean = round(np.mean(cost_3_list), 3)
25     cost_1_std = round(np.std(cost_1_list), 3)
26     cost_2_std = round(np.std(cost_2_list), 3)
27     cost_3_std = round(np.std(cost_3_list), 3)
28
29     plt.plot(step_list, cost_1_list, label=rf'Base position 1; mean:
30             ${cost_1_mean} \pm {cost_1_std} $', color='black', marker='o')

```

## D Particle Swarm Optimization

---

```
30 plt.plot(step_list, cost_2_list, label=rf'Base position 2; mean:
    ${cost_2_mean} \pm {cost_2_std} $', color='black', marker='s')
31 plt.plot(step_list, cost_3_list, label=rf'Base position 3; mean:
    ${cost_3_mean} \pm {cost_3_std} $', color='black', marker='^')
32
33 plt.grid()
34 plt.legend()
35 plt.ylim([0.875, 0.97])
36 #plt.legend(bbox_to_anchor=(1.05, 1), loc='upper left')
37 #plt.tight_layout(rect=[0, 0, 0.75, 1])
38 #plt.title('Cost of function for three different bas')
39 plt.xlabel('Discretization')
40 plt.ylabel('Cost')
41
42 plt.show()
```

---

## E Height and Force for Hands-on Tray

This python code calculated the height and forces involved in the Hands-on Tray operation given the geometrical characteristics of the model.

```
1  import numpy as np
2  import matplotlib.pyplot as plt
3
4  # Define the function h
5  def h(l):
6  return 1.050 - np.sqrt((0.770 + l)**2 - (0.400 + 0.276)**2) +
7      0.120
8  def f_x(h):
9  h = h - 0.120
10 return (0.400 + 0.276) * 100 / (1.050 - h)
11 def f(f_x):
12 return np.sqrt(np.square(f_x) + 10000)
13 def f_y(l):
14 return np.full(len(l), 100)
15
16 # Define the range for l
17 l_values = np.linspace(0.000, 0.480, 500)
18
19 # Calculate h values
20 h_values = h(l_values)
21 f_x_values = f_x(h_values)
22 f_y_values = f_y(l_values)
23 f_values = f(f_x_values)
24
25 # Create the plot
26 fig, ax1 = plt.subplots(figsize=(10, 6))
27
28 # Plot h(l) on the primary y-axis
29 ax1.plot(l_values, h_values, color='k', label=r'$h = 1.050 - \sqrt{\{ (0.770+l)^2 - (0.400 + 0.276)^2 + 0.120\}}$')
30 ax1.set_xlabel('l')
31 ax1.set_ylabel('Tray height [m]')
32
33 # Create a secondary y-axis for F_x(h)
34 ax2 = ax1.twinx()
```

## E Height and Force for Hands-on Tray

---

```
35 ax2.plot(l_values, f_x_values, linestyle = '--', color='k', label
    =r'$F_x(h) = \frac{(0.400 + 0.420)100}{1.050-h}$')
36 ax2.plot(l_values, f_y_values, linestyle = '-.', color='k', label
    =r'$F_y = 100$')
37 ax2.plot(l_values, f_values, linestyle = ':', color='k', label=r'
    $F(h) = \sqrt{ F_x^2 + F_y^2 }$')
38 ax2.set_ylabel('Force [N]')
39
40 # Add legends
41 ax1.legend(loc='lower left')
42 ax2.legend(loc='upper right')
43
44 # Add grid
45 ax1.grid(True)
46
47 # Add titles
48 plt.title('Plot of height and Forces')
49
50 # Show plot
51 plt.show()
```

---

## **F Hands-on Tray Components**

### **F.1 Motor Specification**

The motor selected for the Tray operation is QKX00AF0B0502. The data sheet is bellow. The back of the motor is attached to the Lander via the Swivel flange, and the tip of the motor is connected to the Tray by the Clevis accessory.

## Electric cylinder LZ 60 P

# Technical data

### General information/operating conditions

Type	LZ 60 P external control	Custom
Design	Linear cylinder with integrated DC motor	
Guide	Double bearing via POM bushes	
Installation position	Any position/without shear forces/hanging only with drop protection provided by the customer	
Push force	Up to 4000 N	
Pull force	Up to 4000 N	
Self-locking	Yes	
Max. travel speed	Up to 50 mm/s	
Max. Hub	600 mm	1200 mm
Installation dimension	Stroke + 168,5 mm or Stroke + 184 mm	1383 mm
Voltage	24 to 36 V DC	
Current output	3 A or 4 A	
Protection class	IP 54	
Ambient temperature	+5°C to +40°C	
Displacement during synchronous operation	0 to 2 mm	
Duty cycle (Operation mode S3)	At nominal load, 15% (1,5 min operating time, 8,5 mins rest time)	
Repeatability	0,5 mm	
Stroke tolerances	+0,5 mm / -2,5 mm	

**Note:** RK Rose+Krieger GmbH cylinders are only designed for centric loads.

Drive	Push force [N]	Travel speed [mm/s]	Number of assigned motor channels			
			1	2	3	4
LZ 60 P	2000	11	✓	✓	each 1300 N	each 1000 N
LZ 60 P	3000	5,5	✓	✓	each 2100 N	each 1500 N
LZ 60 P	4000	3	✓	✓	each 3100 N	each 2500 N
			MultiControl II duo		MultiControl II quadro	

**Note:**

If more than 2 drives are to be operated synchronously at nominal load, BUS communication between two or more MultiControl II duo controllers is required.

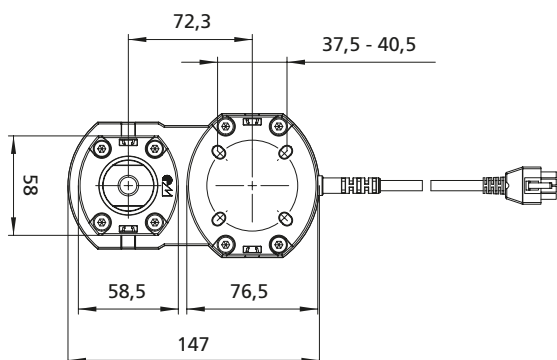
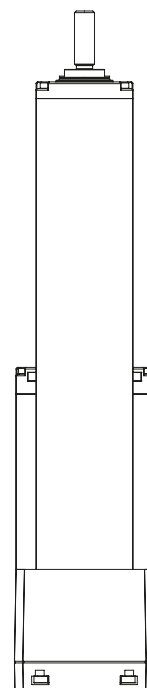
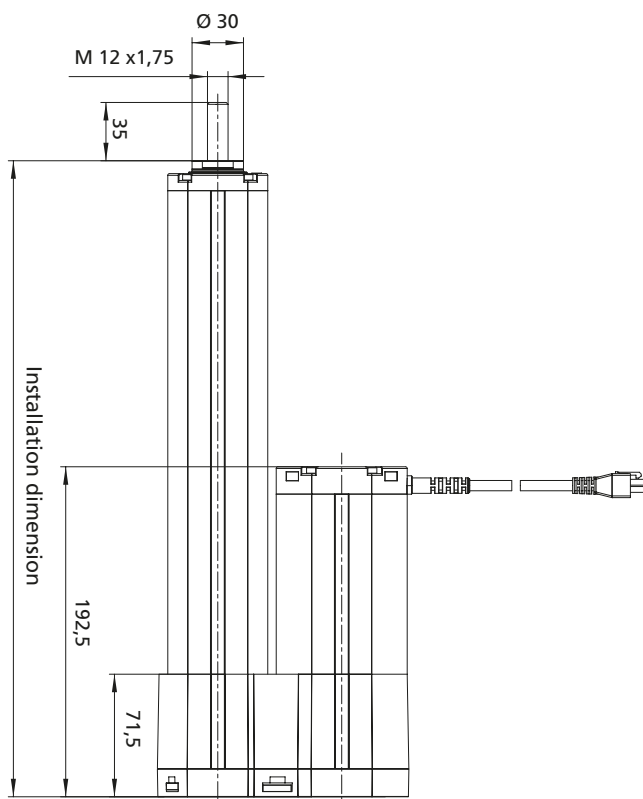
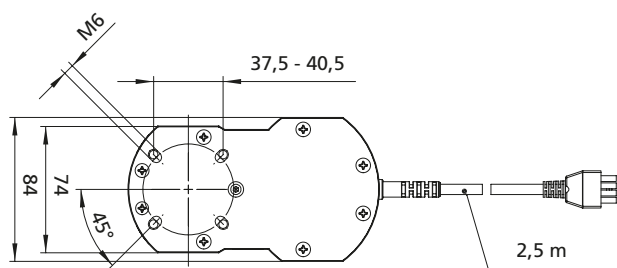
The necessary accessories can be found on page 172.

The procedure for setting up BUS communication is described in detail in the operating manual.





### LZ 60 P – Version



## Electric cylinder LZ 60 P

# Technical data

### LZ 60 S linear cylinder – highly versatile use

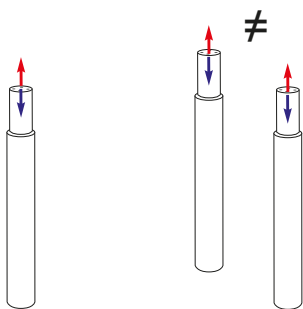
The LZ 60 series does not just impress with high functionality and high power density, but also with its attractive design. The side slots and the versatile accessories facilitate simple connection in accordance with the customer's requirements. The maximum stroke is 600 mm with a maximum lifting force of up to 4000 N per drive.



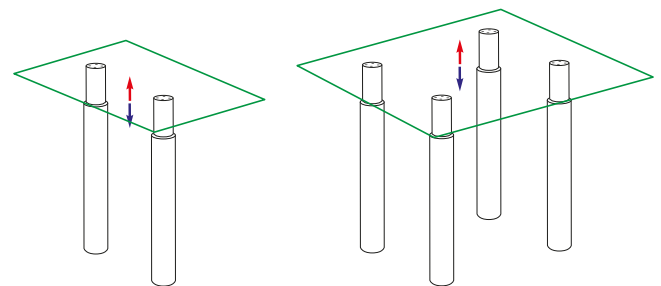
- Special features:
- High functionality
- High power density
- Attractive design

#### Ideal areas of application:

- Precise industrial applications with compact design which require a high power density



1-2 LZ 60 in single or parallel operation



2-4 LZ 60 in synchronous operation

### Parallel operation

The premium version of the MultiControl II quadro has drive group management. Alongside synchronous and stand-alone operation, this also allows the following drive combinations to run parallel (1+1, 1+2, 2+1, 2+2).

### Synchronous operation

Synchronous operation of two or more drives. In conjunction with the integrated sensors, the control (see page 122) ensures synchronisation, and thus constant alignment of all the drives in both directions of travel, even if subject to different loads. The synchronous operation tolerance depends on the lifting speed and is max. 1.5 mm for the 8 mm/s version and max. 3 mm for the 25/32 mm version.

A memory function is also available.



**Version for external control with open motor cable / incremental position sensor / limit switch**

Code No.	Type	Max. force F [N]	max. travel speed [mm/s] 24 V DC	max. travel speed [mm/s] 36 V DC
QKX00AC0B0_ _ _	LZ 60 P	1000	40	50
QKX00AB0B0_ _ _	LZ 60 P	2000	22	28
QKX00AE0B0_ _ _	LZ 60 P	3000	12	15
QKX00AF0B0	LZ 60 P	4000	6	9

e.g. stroke [mm] = **2 0 2**

Stroke* [mm]	Installation dimension [mm]	Weight [kg]
105	273.5	3.7
150	318.5	3.8
202	371.0	4.0
255	423.5	4.2
300	468.5	4.4
352	536.0	4.5
405	588.5	4.7
450	633.5	4.9
502	686.0	5.1
555	738.5	5.2
600	783.5	5.4

**Version for external MultiControl II synchronous control**

Code No.	Type	Max. force F [N]	max. travel speed [mm/s] 28 V DC
QKX00AC0E0_ _ _	LZ 60 P	1000	22,5
QKX00AB0E0_ _ _	LZ 60 P	2000	11
QKX00AE0E0_ _ _	LZ 60 P	3000	5,5
QKX00AF0E0	LZ 60 P	4000	3

e.g. stroke [mm] = **6 0 0**

\*Tolerance: +0.5mm / -2.5mm

**System components**

Code No.	Accessories
<b>Controls</b>	
QST30H12AA000	MultiControl II duo - Basic
QST30H12AA022	MultiControl II duo - Premium
QST30H14AA000	MultiControl II quadro - Basic
QST30H14AA022	MultiControl II quadro - Premium
<b>Hand switches</b>	
QZB11G07AV041	Hand switch with 6 function keys and display – 1 m cable length
QZB11G07AB041	Hand switch with 2 function keys – 1 m cable length
QZD000074	Hand switch drawer for hand switch with 6 and 2 function keys
<b>IEC connector</b>	
QZD070618	IEC cable (Europe version, earthed plug)

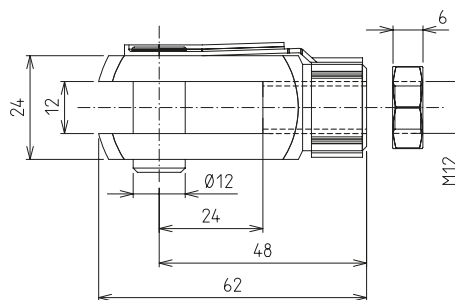
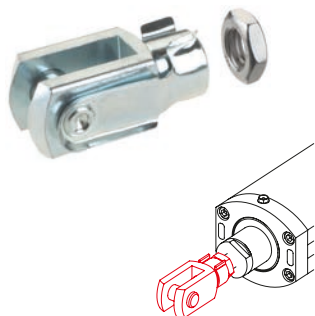
**Note:**

Further accessories (hand switches, connecting cables etc.) can be found in the chapter „Controls and accessories“ starting on page 152

## Electric cylinder LZ 60 P

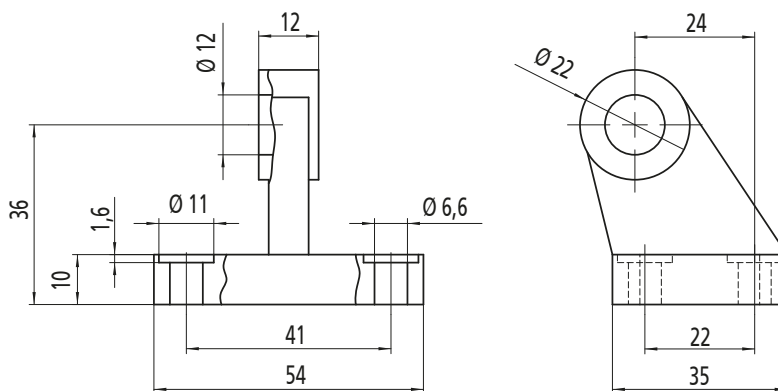
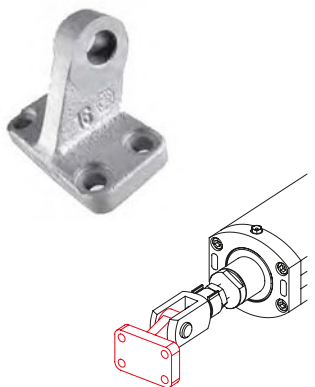
# Accessories

### Clevis



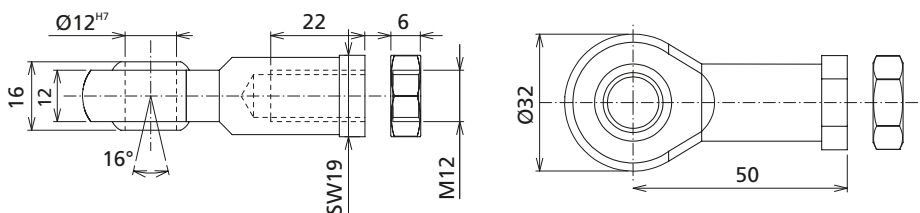
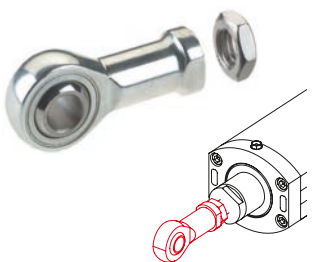
Code No.	Type
QZD050570	Clevis M12

### Bearing block for clevis



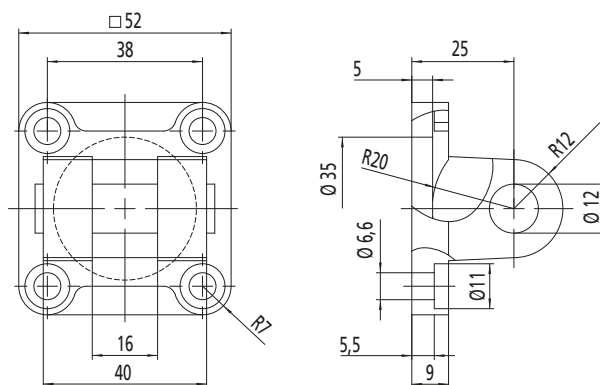
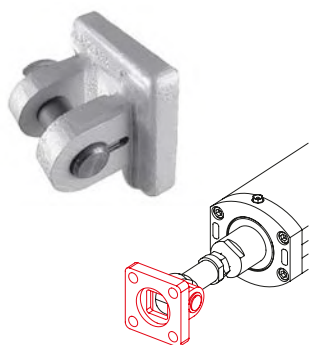
Code No.	Type
QZD050572	LZ 60 Bearing block Ø 12

### Swivel head



Code No.	Type
QZD050574	Swivel head M12

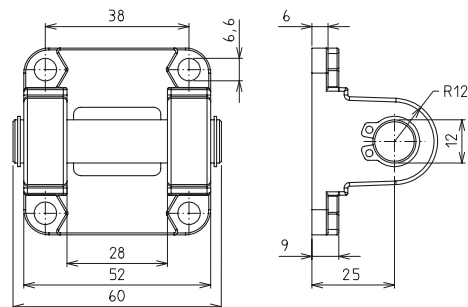
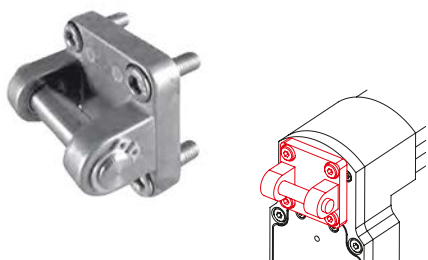
### Clevis mounting for swivel head



Code No.	Type
QZD050576	LZ 60 Clevis mounting Ø 12

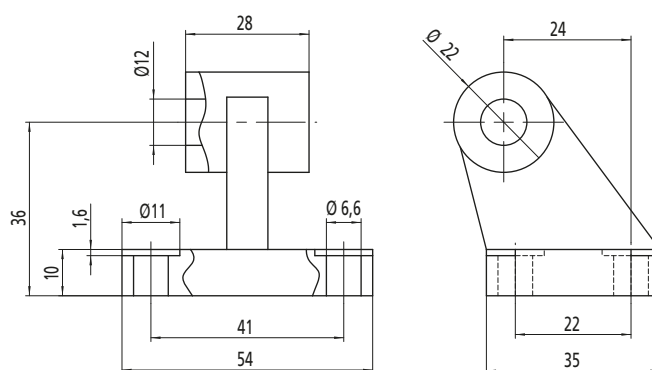
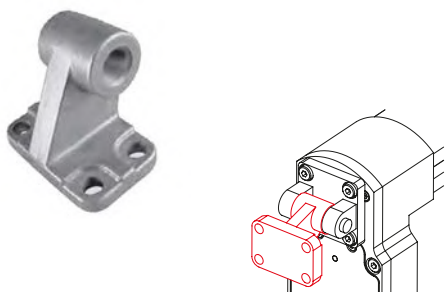


### Swivel flange



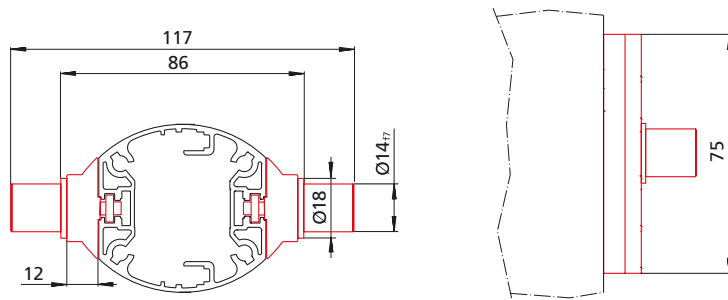
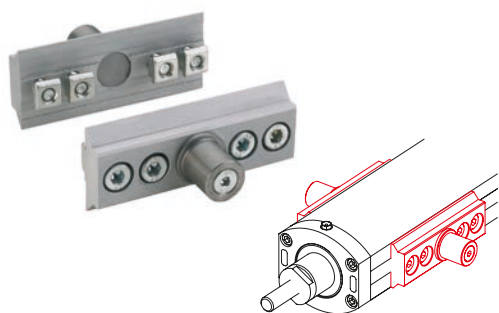
Code No.	Type
QZD050578	Swivel flange Ø 12

### Bearing block for swivel flange



Code No.	Type
QZD050583	LZ 60 Bearing block Ø 12

### Trunnion support blocks



Code No.	Type
QZD050586	Trunnion support blocks LZ 60

### Order instruction square nut:

- Purchase only in lot sizes and a multiple of that, see product table below

### Square nut

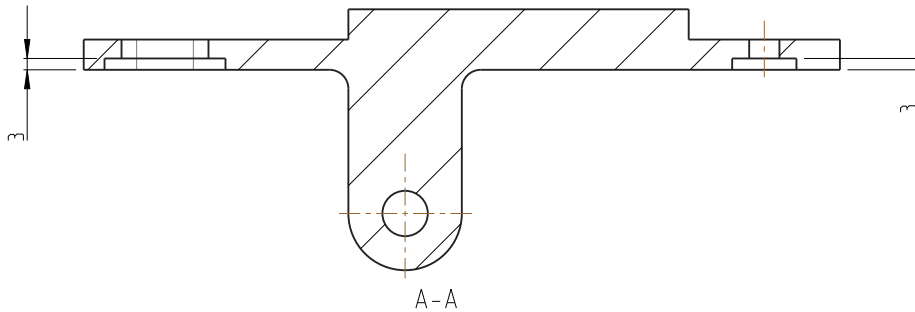
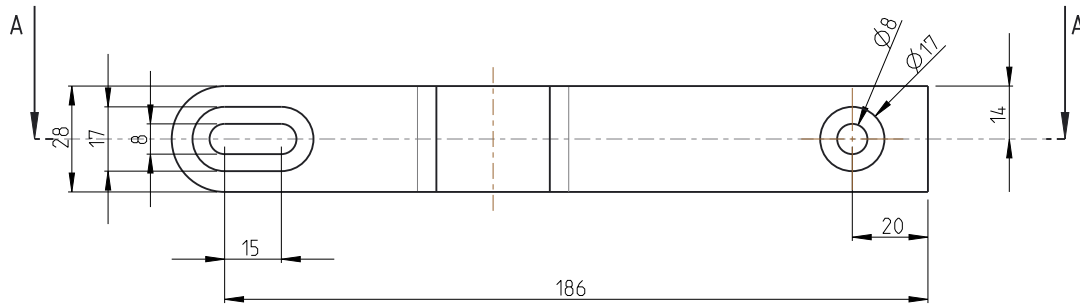
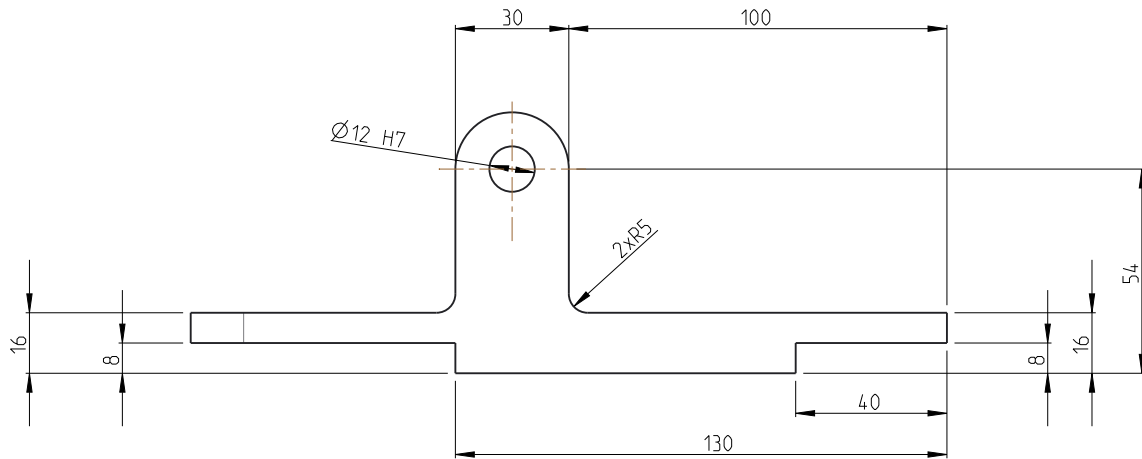


● The square nut enables the the attachment of fittings to the cylinder. Nuts can be slid into the lateral slots for this purpose.

Code No.	lot sizes	Type
QZD0505971	10, 20, 30... pcs	Square nut M6, DIN562

## **F.2 Mounting points for the Motor**

The motor uses accessories to be mounted to the Lander and Tray frames. Thus, this section shows the technical drawing of the parts that connects these accessories to the Lander and Tray. The fixed joint is secured by M8 bolts and construction profile nuts.



Deutsches Zentrum für Luft- und Raumfahrt  
 Institut für Robotik und Mechatronik  
 Münchener Str. 20  
 D-82234 Wessling  
 Tel: (+49) 08153/28-2400 Fax: -1134

general tolerance: DIN ISO 2768-f H  
 surface texture:  $\sqrt{Rz} 16$   
 dimensions:  $\begin{matrix} -0.1 \\ +0.1 \end{matrix}$

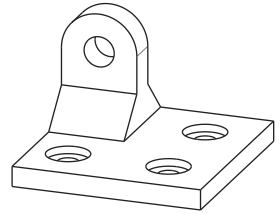
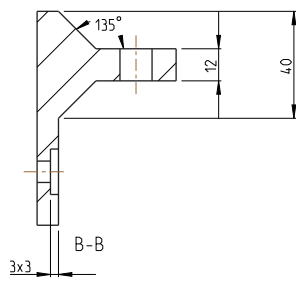
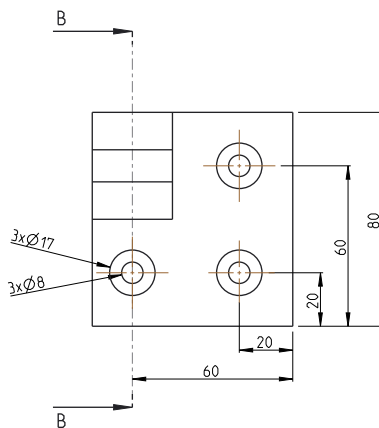
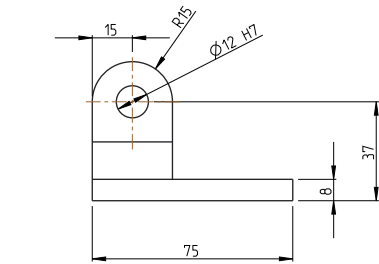
heat and surface treatment:  
 (DIN ISO 1302) -


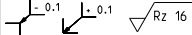
material: EN AW-2007

created by	Pavelski, Pedro Henrique	14-Mar-24 03:10:10 PM	copyright ISO 16016
modified by	Pavelski, Pedro Henrique	14-Mar-24 05:14:25 PM	order filing date:
checked by	-		
model:	M2_LDR_TRAY_ACTUATOR_MOUNT_TOP.PART		
drawing:	M2_LDR_TRAY_ACTUATOR_MOUNT_TOP.DRW		
path:		order quantity:	2

description:  
**m2\_ldr\_tray\_actuator\_mount\_top**  
 DLR

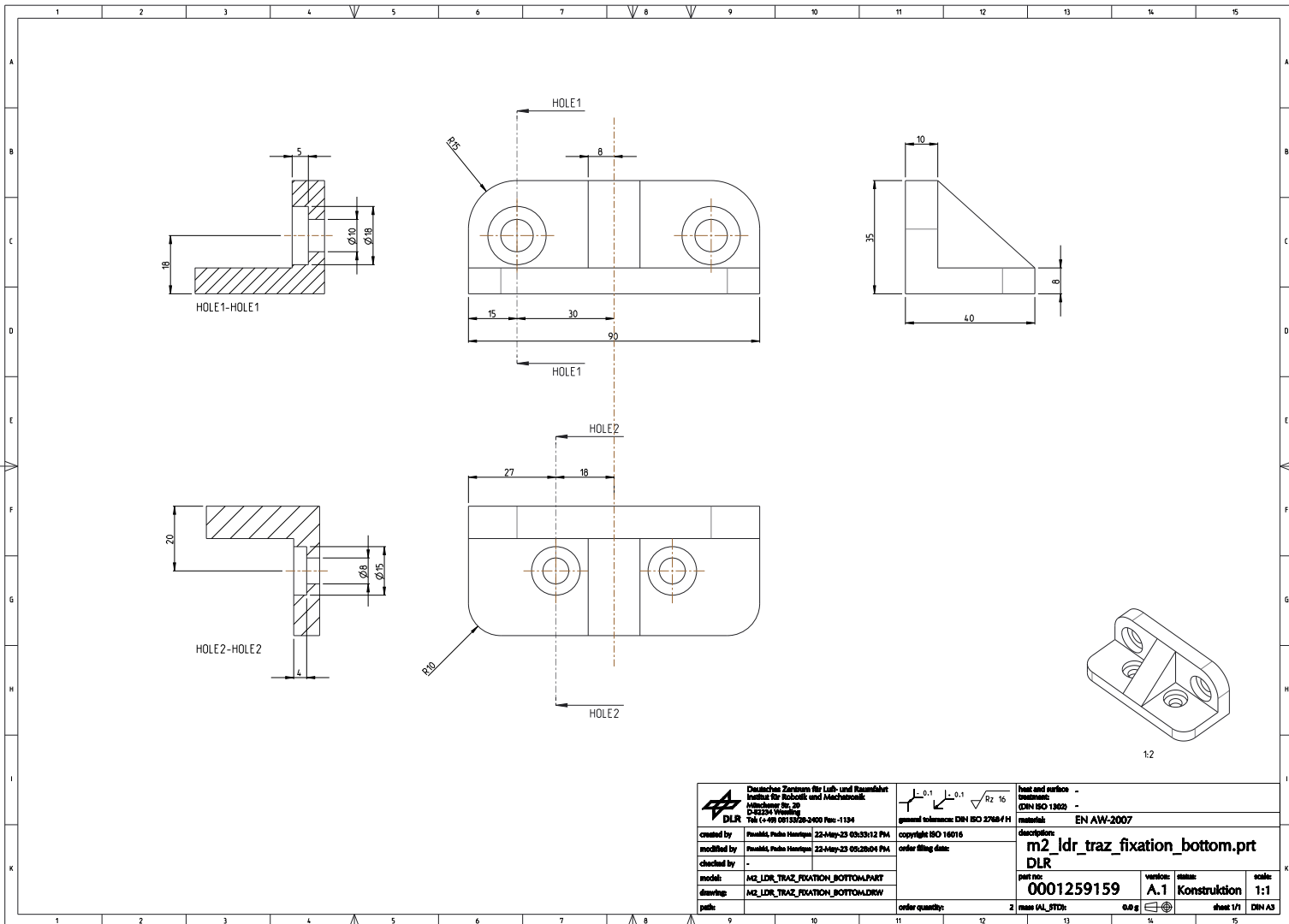
part no:	0001372076	version:	A.1	status:	Konstruktion	scale:	1:2
mass (AL_STD):	0.0 g			sheet 1/1	DIN A4		



 <b>Deutsches Zentrum für Luft- und Raumfahrt</b> Institut für Robotik und Mechatronik Münchenstr. 20 D-82234 Weßling Tel: (+49) 08153728-2400 Fax: -1134		 general tolerance: DIN ISO 2768-fH	heat and surface treatment: (DIN ISO 1302) - material: EN AW-2007
created by: Pavelčík, Pedro Henrique modified by: Pavelčík, Pedro Henrique checked by: -	14-Mar-24 03:28:37 PM 14-Mar-24 04:58:54 PM	copyright ISO 16016 order filling date:	description: <b>m2_ldr_tray_actuator_mount_down</b> <b>DLR</b>
model: M2_LDR_TRAY_ACTUATOR_MOUNT_DOWN.PART drawing: M2_LDR_TRAY_ACTUATOR_MOUNT_DOWN.DRW path:	order quantity: 0	mass (AL_STD): 0.0 g	part no: <b>0001372084</b> version: <b>A.1</b> status: <b>Konstruktion</b> scale: <b>1:2</b> sheet 1/1 DIN A4

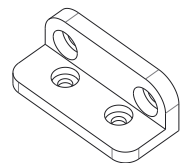
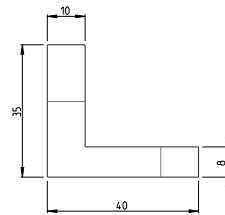
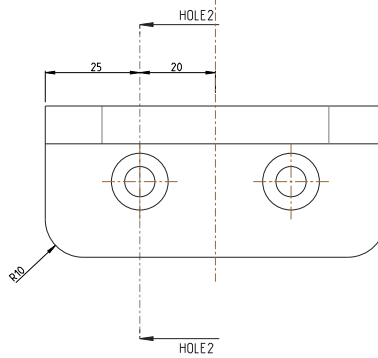
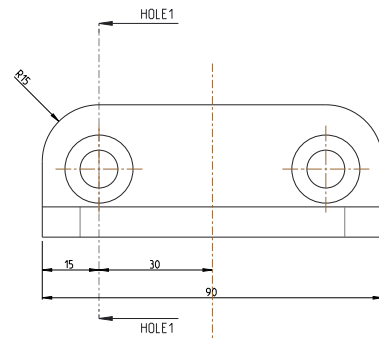
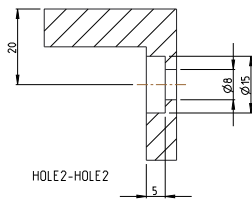
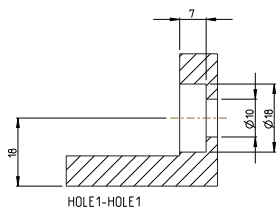
### **F.3 Mounting points for the Tray**

The tray is connected to the linear guide via the components bellow. The connection is secured by M8 bolts and construction profile nuts.



Deutsches Zentrum für Luft- und Raumfahrt Institut für Robotik und Mechatronik D-22524 Neerling Tel: (+49) 04103 200-2400 Fax: -1134		heat and surface treatment: - material: EN AW-2007
created by: Frenkel, Peter Henning 22-May-23 09:55:12 PM modified by: Frenkel, Peter Henning 22-May-23 09:28:04 PM checked by: - model: M2_LDR_TRAZ_FIXATION_BOTTOM.PART drawing: M2_LDR_TRAZ_FIXATION_BOTTOM.DRW title:	copyright: ISO 14816 order filing date: order quantity: 2 mass (M_STE): 6.0 g	general tolerance: DIN ISO 2768-4 H surface finish: $\sqrt{Rz} \ 16$ description: m2_ldr_traz_fixation_bottom.prt DLR part no: 0001259159 version: A.1 status: Konstruktion scale: 1:1 sheet 1/1 DIN A3





Deutsches Zentrum für Luft- und Raumfahrt Institut für Robotik und Mechatronik DLR D-22334 Wessling Tel: (+49) 05125 220-2400 Fax: -1134		L 0.1 L 0.3 Rz 16 general tolerance: DIN ISO 2768-M	heat and surface treatment: - material: EN AW-2007
created by: Frenkel, Peter Henning 22-Aug-23 09:27:20 PM modified by: Frenkel, Peter Henning 22-Aug-23 09:12:15 PM checked by: - model: M2_LDR_TRAZ_FIXATION_UPPER.PART drawing: M2_LDR_TRAZ_FIXATION_UPPER.DRW title:	copyright: ISO 147016 order filing date:	description: <b>m2_ldr_traz_fixation_upper</b> <b>DLR</b> part no: <b>0001259156</b> version: <b>A.1</b> name: <b>Konstruktion</b> scale: <b>1:1</b>	
order quantity: 2		mass (M_STE): 0.0 g	sheet 1/1 DIN A3